Radiat. Phys. Chem. Vol. 41, No. 4/5, pp. 579–630, 1993
Printed in Great Britain.

0146-5724/93 $6.00 + 0.00

POLARIZATION EFFECTS ON MULTIPLE SCATTERING GAMMA TRANSPORT

J. E. FERNÁNDEZ,[1]† J. H. HUBBELL,[2] A. L. HANSON[3] and L. V. SPENCER[2]

[1]Laboratorio di Ingegneria Nucleare di Montecuccolino, Università degli Studi di Bologna, via dei Colli 16, 40136 Bologna, Italy, [2]National Institute of Standards and Technology, Gaithersburg, MD 20899, U.S.A. and [3]Brookhaven National Laboratory, Upton, NY 11973, U.S.A.

(Received 8 December 1992; accepted 12 December 1992)

Abstract—The scattering of X-rays and γ-rays are events that have strong dependencies on the polarization of the incident and scattered photons. Because of this, scattering problems that can be solved without explicit reference to the state of polarization of the incident and scattered radiation are exceptional. This article reviews available information on polarization effects arising when photons in the X-ray and γ-ray regime undergo photoelectric effect, coherent (Rayleigh) scattering and incoherent (Compton) scattering by atomic electrons. In addition to descriptions and discussion of these effects, we study the backscattering of γ-rays from an infinite thickness target excited with a plane slant monodirectional and monochromatic source, using the Boltzmann transport theory and the mathematical representation of polarization introduced by Stokes. Results from this model, for both unpolarized and polarized γ-ray sources, are compared with computations performed neglecting or averaging polarization effects, showing the limitations of such approximations.

1. INTRODUCTION

X- and γ-ray photons interact with matter producing secondary radiation that carries useful information about the atoms comprising the target. Since X-rays are penetrating, it is very probable that their secondary radiation may suffer successive interactions with other atoms before leaving the specimen. This fact leads to the definition of a "thin" sample as having a thickness thin enough that we witness no more than one interaction. Because of this a multiple scattering scheme seems to be necessary to study in detail the backscattering of X-rays in a dense material excited with a monochromatic and monodirectional source. In a recent work, Fernández and Molinari (1991) showed that multiple scattering contributions due to the three prevailing processes in the X-ray regime (the photoelectric, the Rayleigh and the Compton effects) can appreciably modify the more intense first-order intensities by contributing a background or "multiple scattering spectrum". This background is formed by the overlapping of many single contributions—i.e. the possible combinations of the three types of processes for each number of collisions. Individually, each process can be more or less probable depending on the energy and the geometry involved in the scatterings. However, when they are combined they become a consistent contribution. Our knowledge on the whole background spectrum has been built, as a mosaic, by studying the contributions from certain sequences of collisions, or chains: the continuous background due to multiple Rayleigh and Compton scattering events (having the classic differential cross-sections depending on averaged polarization states) overlapping the Compton peak (Fernández, 1991; Fernández and Sumini, 1992); Compton and Rayleigh scattering contributions to the characteristic photo-peaks (Fernández *et al.*, 1990; Fernández, 1992; Fernández and Molinari, 1992), and higher-order purely photoelectric interactions (Fernández, 1989; Fernández and Molinari, 1990). The addition of all the contributions of up to two (and selected ones of up to three) orders-of-scattering obtained with an analytical solution to the Boltzmann transport equation for photons, allowed the build-up of theoretical X-ray spectra matching well experimental data (Fernández and Sumini, 1991). These results confirmed the validity of this approach to get refined solutions in X-ray spectrometry. However, the mentioned equations of transport do not include, rigorously, the state of polarization in the description of the radiation field, although an average polarization state is present in the Rayleigh and Compton kernels.

In Roentgen's 1895 "discovery" paper (Roentgen, 1895) he conjectured that his newly-revealed radiation (now called "X-rays") might be ultraviolet light, in which case it should meet a list of four criteria including: "It cannot be polarized by any ordinary polarizing media." However, in the years following, several attempts were made to find polarization effects in X-rays, as the notions of electromagnetic radiation were still in the early stages of development, with the "ether" still a popular medium

†On leave of absence from the Faculty of Mathematics, Astronomy and Physics (FaMAF), University of Córdoba, Argentina. Fellow of CONICET, Buenos Aires, Argentina.

for its propagation. In 1905, Barkla's scattering measurements (Barkla, 1905) indicated a weak polarization of the primary X-ray beam, and in 1906 Barkla (1906) added a second carbon-block scatterer to his experimental arrangement. The tertiary scattered beam indeed exhibited large azimuthal variations in intensity when recorded in a detector rotated about the second carbon-block scatterer in a plane perpendicular to the direction of the secondary (first-scattered) X-ray beam. This confirmed the plane-polarization of the scattered X-ray beam, and hence the kinship of X-rays to visible and to ultraviolet light, despite Roentgen's above criterion in his conjecture.

Barkla's (1906) results were quickly confirmed by Haga (1907) and others. These were followed by similar-geometry measurements reported in 1924 by Compton and Hagenow (1924) whose observations included not only 100% polarization in the 90° first-scattered beam, but also a modified (lowered energy) scattered component. This energy modification is a major characteristic of the photon interaction process soon to become well-known as "Compton scattering". Further measurements extended the range of primary photon energies into the "hard X-ray" region, including the 1936 work of Rodgers (1936) who studied the polarization of 80–800 kV primary X rays Compton scattered into 90°.

With the exception of two papers by Spencer and co-workers (Spencer, 1948; Spencer and Wolff, 1953) and the seminal work by Fano *et al.* (1959), radiation transport calculations including the effects of polarization on radiation scattering processes appear to be non-existent until two recent papers by Fernández and co-workers (Fernández and Molinari, 1993; Fernandez, 1993a). Also polarization effects on the differential (in angle) scattering cross sections have been recently studied by Hanson and co-workers (Hanson, 1986a, b, c, 1988a, b, 1990; Hanson and Meron, 1988) for synchrotron light applications. However, in other recent transport calculations, mostly using the Monte Carlo technique, these polarization effects have been universally ignored. Hence it is of interest to investigate or find reference to the magnitude of the error introduced into present transport calculations resulting from the omission of polarization effects, and to determine if it would be worth-while to try to include such effects in future calculations.

The accounting for polarization effects presents many interesting points that need elucidation. Four parameters are necessary to fully describe the state of polarization, of a beam of X-rays (Stokes, 1852; Chandrasekhar, 1950; McMaster, 1954, 1961; Fano *et al.*, 1959; Pomraning, 1973). Further, the state of polarization, and hence these parameters, changes every time the photon undergoes a scattering event. Accordingly, a proper description of photon transport including polarization effects involves four coupled equations of transfer. The well-known equation of transport can be considered as the result of approximating this set of four equations over all final polarization states, assuming the incident X-rays are unpolarized. This approximation, however, introduces an error that can be corrected by formulating the radiative transfer equations with proper account of the state of polarization. The events mentioned above can exhibit significant differences in their interaction probabilities depending on the polarization of the incident photons. In contrast, the photoelectric effect has much lower sensitivity. These different behaviours have suggested that the continuous background intensity (due to the Compton and Rayleigh scattering) in an X-ray spectrum could be reduced by using a source of appropriately polarized photons, and/or choosing appropriate (collimated) directions for excitation and detection. Spectral background reduction resulting from the use of polarized photons has led to techniques of adding polarizers to the beam (Christoffersson and Mattson, 1983; Wobrauschek and Aiginger, 1983; Wielopolski *et al.*, 1989) or using

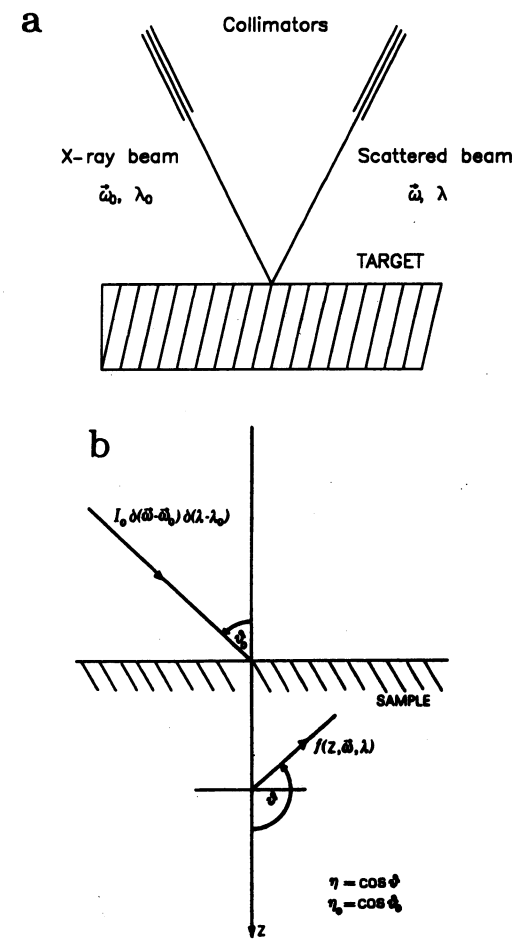

Fig. 1. (a) Irradiation scheme of an homogeneous specimen of infinite thickness excited with a collimated monochromatic X-ray source. (b) The magnitudes represented in the photon transport equation (10).

Table 1. Notations used by Chandrasekhar (1950); Spencer and Wolff (1953), Fano *et al.* (1959) and McMaster (1961); and this work for Stokes intensities

Chandrasekhar	Spencer	This work
I	I_0	I_I
Q	I_1	I_Q
U	I_2	I_U
V	I_3	I_V

We prefer to denote the intensity with capital I as usual, with the explicit mention of the Stokes components with subscripts. This allows us to modify easily the notation for representing the intensity in others reference systems as, for instance, $I_\parallel$ and $I_\perp$ in the (L) system.

X-rays from electron synchrotron storage rings (Sparks *et al.*, 1977, 1978; Hanson *et al.*, 1983, 1987; Iida *et al.*, 1985; Jacklevic *et al.*, 1985; Knöchel *et al.*, 1985; Prins *et al.*, 1985).

In this article we shall discuss the influence of the various parameters defining the polarization state, with recourse to some recent results already mentioned, which lead to detailed descriptions of the multiple-scattering contributions from different interactions (such as the photoelectric effect, and Compton and Rayleigh scattering by atomic electrons). We shall discuss the four-component Stokes vector approach which represents the polarized intensity of a low energy γ-ray spectrum. We shall emphasize a transport model for an infinite thickness target excited with a plane source of highly collimated, monochromatic radiation having an arbitrary state of polarization [see Fig. 1(a)] for which extensive calculations are available (Fernández and Sumini, 1991; Fernández, 1993a). With recourse to a recursive solution (Fernández and Molinari, 1993) to the resulting set of equations, valid with all the interactions of interest, we shall study the effect of polarization on single chains of collisions capable of contributing separately to the X-ray background. The results for unpolarized γ-ray sources will be compared with the analogous intensity terms calculated with those in the unpublished paper by Spencer (1948) and with the scalar equation. The scalar equation averages polarization effects which introduces limitations in the approximations. The results for polarized γ-ray sources will be compared with the studies on scattering cross sections by Hanson and co-workers (Hanson, 1986a, b, c, 1988a, b, 1990; Hanson and Meron, 1988).

2. THE REPRESENTATION OF POLARIZED RADIATION (THE STOKES PARAMETERS)

The polarization of γ-rays, a net wave effect, needs four parameters to be represented. The intensity of the beam clearly constitutes one parameter. It is the only parameter taken into account in scalar representations of radiation transport, the "usual" modeling in Monte Carlo simulations (Cashwell and Everett, 1959; Carter and Cashwell, 1975). In addition, at each space point and for a given wavelength and direction of propagation, the most general beam of γ-rays can be regarded as a mixture of an elliptically polarized fraction and a fraction of unpolarized γ-rays. The fraction of the photons that are polarized (the degree of polarization) constitutes the second parameter. The remaining two parameters are necessary to describe the ellipse associated with the elliptically polarized component. One of these parameters specifies the orientation of the ellipse, i.e. the angle between the major (or minor) axis of the ellipse and a fixed coordinate axis in the space. This is generally referred to as a specification of the orientation of the ellipse of polarization. The final parameter is the ellipticity of the ellipse, i.e. the ratio of the two axes of the ellipse. Because of the diverse nature of these four quantities, it is convenient to use an equivalent set of quantities, introduced by Sir George Stokes (1852), which contains all the physical information about the polarization state of the γ-ray beam. In this way, radiative transfer can be described using four-component parametrization obeying a vector transport equation (e.g. Chandrasekhar, 1950; Spencer and Wolff, 1953; Fano *et al.*, 1959; Pomraning, 1973).

In summary, a polarized photon beam of γ-rays needs four parameters I_I, I_Q, I_U and I_V—the Stokes parameters (or set S) each having the dimension of an intensity—to specify the intensity, the degree of polarization, the orientation of the ellipse of polarization and the ellipticity at each point of the space and in any given direction (see Table 1 for an equivalence with other notations). Actually, a more convenient set of parameters $I_\parallel$, $I_\perp$, I_U and I_V can be used. This set, named L, is related to the former through the relationships:

$$I_I = I_\parallel + I_\perp \tag{1a}$$

$$I_Q = I_\parallel - I_\perp, \tag{1b}$$

$$I_U, I_V. \tag{1c}$$

Photons possess electric field vectors $\mathscr{E}$ (perpendicular to the propagation vectors) directions define the plane of polarization. If a beam of photons is polarized, there is a net alignment of the $\mathscr{E}$ vectors. The plane that is made of the propagation vector and this net of the $\mathscr{E}$ vectors is sometimes called erroneously the plane of polarization. The plane defined by the propagation directions $\hat{k}$ of the photon beam before and after the collision is known as scattering plane. $I_\parallel$ is the fraction of photons whose projections of $\mathscr{E}$ vectors are in the plane of scattering. $I_\perp$ is the fraction of photons whose projections are perpendicular to this plane. Since the electric vector associated with the beam of γ-ray lies in a plane perpendicular to $\hat{k}$, it can be resolved in such directions:

$$\mathscr{E} = \hat{\epsilon}_\perp \mathscr{E}_\perp + \hat{\epsilon}_\parallel \mathscr{E}_\parallel, \tag{1d}$$

$$\hat{k} = \hat{\epsilon}_1 \times \hat{\epsilon}_2, \tag{1e}$$

$$|\mathscr{E}_\perp|^2 = I_\perp, \tag{1f}$$

$$|\mathscr{E}_\parallel|^2 = I_\parallel. \tag{1g}$$

Following Pomraning (1973) we can express the set S—intensities with subindices (I, Q, U, V)—in terms of the angles χ (rotation of the major axis of the polarization ellipse about $\hat{\epsilon}_\parallel$) and β (related to the major-to-minor axes ratio or ellipticity). The meanings of these parameters become apparent from the relationships:

$$I_Q = I_I \cos 2\beta \cos 2\chi, \tag{2a}$$

$$I_U = I_I \cos 2\beta \sin 2\chi, \tag{2b}$$

$$I_V = I_I \sin 2\beta. \tag{2c}$$

For *elliptically* polarized γ-rays we note that

$$\sin 2\beta = \frac{I_V}{I_I}, \tag{3a}$$

$$\tan 2\chi = \frac{I_U}{I_Q}, \tag{3b}$$

and the Stokes parameters verify the relation

$$I_I^2 = I_Q^2 + I_U^2 + I_V^2. \tag{3c}$$

Consequently, only three of these four parameters are independent.

Table 2 shows some common states of polarization represented using both sets of parameters, S and L.

For *partially polarized* γ-rays (i.e. a mixture of unpolarized and elliptically polarized γ-rays), the four parameters are necessary and the following relation holds

$$I_I^2 \geqslant I_Q^2 + I_U^2 + I_V^2. \tag{4}$$

It is clear that the total intensity I_I and the additional parameters I_Q, I_U and I_V, completely determine, from an experimental point of view, the characteristics of an arbitrary beam. That is, two beams with the same Stokes parameters, are optically equivalent since experimentally they cannot be distinguished.

From these relations Chandrasekhar (1950) has shown that an *unpolarized beam* of γ-rays can be expressed as a mixture of two independent elliptically polarized beams of equal intensity, having similar ellipses of polarization with their major axes perpendicular to each other ($\chi_1 - \chi_2 = \pm\pi/2$), and sense of polarization of one beam contrary to that of the other ($\beta_1 = -\beta_2$). These two beams are said to be oppositely polarized. It should be emphasized that, besides the relationship with χ_2 and β_2, χ_1 and β_1 are arbitrary. Hence an unpolarized γ-ray beam is equivalent to a mixture of two independent oppositely polarized beams of equal intensity.

In a similar way, a *general beam* of γ-rays can be represented by two independent elliptically polarized beams with intensities and states of polarization given by

$$I_1 = \tfrac{1}{2}[I_I - (I_Q^2 + I_U^2 + I_V^2)^{1/2}], \quad (-\beta, \chi \pm \pi/2); \tag{5a}$$

$$I_2 = \tfrac{1}{2}[I_I + (I_Q^2 + I_U^2 + I_V^2)^{1/2}], \quad (\beta, \chi); \tag{5b}$$

where β and χ are given by the relationships

$$\sin 2\beta = \frac{I_V}{(I_Q^2 + I_U^2 + I_V^2)^{1/2}}, \tag{5c}$$

$$\tan 2\chi = \frac{I_U}{I_Q}. \tag{5d}$$

It is customary to define the *degree of polarization* P as the fraction of polarized (scattered) radiation after the collision, which in terms of the Stokes intensities is given by the dimensionless ratio

$$P = \frac{(I_Q^2 + I_U^2 + I_V^2)^{1/2}}{I_I}. \tag{5e}$$

For the case of plane polarized photons $\beta = 0°$ so I_V, the ellipticity, is zero. The unpolarized photons can actually be thought of as being a subset of the polarized photons and have the criteria $I_\parallel = I_\perp = \frac{1}{2}I_I$. This fact can be used to simplify calculations in certain cases.

3. THE TRANSPORT EQUATION FOR POLARIZED PHOTONS

The flow of γ-rays is completely determined as the solution of a transport equation describing the balance between the number of photons of given energy and direction entering and leaving an infinitesimal volume element. This balance may be formulated for conditions where the γ-ray source is constant in time (steady-state problem) and, therefore, also the photon flow in the medium. In what follows we shall, firstly, build up the scalar integro-differential Boltzmann transport equation for

Table 2. Some characteristic states of polarization are shown using both sets of parameters, S and L, normalized to an unitary total intensity

Polarization	Set S (I, Q, U, V)	Set L $(\perp, \parallel, U, V)$
Unpolarized	(1, 0, 0, 0)	$(\frac{1}{2}, \frac{1}{2}, 0, 0)$
Linear (generic)	(1, cos 2χ, sin 2χ, 0)	$\frac{1}{2}$(1 + cos 2χ, 1 − cos 2χ, 2 sin 2χ, 0)
Linear (∥) (parallel)	(1, 1, 0, 0)	(0, 1, 0, 0)
Linear (⊥) (perpendicular)	(1, −1, 0, 0)	(1, 0, 0, 0)
Linear (45°)	(1, 0, 1, 0)	$(\frac{1}{2}, \frac{1}{2}, 1, 0)$
Circular	(1, 0, 0, 1)	$(\frac{1}{2}, \frac{1}{2}, 0, 1)$

χ denotes the orientation of the line of polarization about the intersection of the polarization plane with the scattering plane.

photons in an infinite medium; secondly, adapt the scalar equation to the simple set-up model of backscattering from an infinite target; and thirdly, convert this scalar equation into a four-vector equation maintaining all of the information about the polarization state of the interacting radiation.

3.1. The scalar photon transport equation for an infinite medium

Let us consider a point $\mathbf{r}$ and an infinitesimal right cylinder with a base area dA centered at $\mathbf{r}$ and with a height $d\ell$, whose lateral surface is parallel to a direction ω. We define the flux $f(\mathbf{r}, \omega, \lambda)\, d\lambda\, d\omega$ as the number of photons with wavelengths between λ and $\lambda + d\lambda$, and with directions between ω and $\omega + d\omega$, which cross a unit area of the base of the infinitesimal cylinder per unit time.

We shall use the wavelength λ in place of the energy E because it is more convenient to describe the above interactions, although the use of E is entirely equivalent, $E = hc/\lambda$. This choice will also allow us to maintain close compatibility with previous results. We should not forget that crystallographic and spectroscopic techniques evolved much earlier in the wavelength domain than in the energy domain. It is always possible to convert the results from the wavelength to the energy domain with an appropriate transformation.

The net number of photons with specified direction and energy leaving the infinitesimal cylinder per unit time is represented by the quantity

$$f(\mathbf{r} + \omega\, d\ell, \omega, \lambda)\, dA - f(\mathbf{r}, \omega, \lambda)\, dA, \qquad (6)$$

which can be expressed in differential form

$$\omega \cdot \nabla f(\mathbf{r}, \omega, \lambda)\, dA\, d\ell. \qquad (7)$$

Three factors contribute to this net outflow:

(i) The *narrow-beam linear attenuation in the whole volume of the cylinder*, which amounts to $-\mu(\lambda)\, d\ell f(\mathbf{r}, \omega, \lambda)\, dA$: Narrow-beam attenuation is ruled by the known one-dimensional Beer–Lambert attenuation law. $\mu(\lambda)$ is the specimen's total mass attenuation coefficient, and is strongly wavelength (energy)-dependent, but it is independent of geometry, because measurements of narrow-beam attenuation coefficients are performed with the classic experiment of intensity attenuation by thin absorber foils. $\mu(\lambda)$ is considered to be "linear" since it is assumed that each interaction removes the photon from the beam.

(ii) The *scattering of photons* with direction ω' and wavelength λ' into ω and λ: If the scattering happens anywhere within the cylinder volume $dA\, d\ell$, it contributes a positive outflow from the cylinder. This term depends on the flow $f(\mathbf{r}, \omega, \lambda)$ times the probability density function $\mathcal{k}(\omega, \lambda, \omega', \lambda')$ of photon scattering into ω and λ from ω' and λ' (per unit path through the medium and per unit $d\omega$ and $d\lambda$). The product must be integrated over all incident directions ω' and wavelengths λ' to give the whole scattering contribution.

The word "scattering" denotes some generic process capable of transmuting a photon of some energy and direction into another photon with different (or equal) energy and direction, and does not strictly mean a scattering process. In this sense, the radiative photoeffect responsible of XRF emission may be considered a scattering process.

(iii) The *source*, if any, introduces photons with a given energy and direction within the cylinder.

If the photons are produced with a source density $\mathcal{S}(\mathbf{r}, \omega, \lambda)$, per unit volume, per unit time, per steradian and per unit λ, the corresponding excess flow out of the cylinder will be $dA\, d\ell \mathcal{S}(\mathbf{r}, \omega, \lambda)$, per unit time, per steradian and per unit λ.

Equating the difference (7) to the sum of the above three factors and factoring out the arbitrary cylindrical volume $dA\, d\ell$, we obtain the scalar transport equation for photons in an homogeneous medium

$$\omega \cdot \nabla f(\mathbf{r}, \omega, \lambda) = -\mu(\lambda) f(\mathbf{r}, \omega, \lambda) + \int_0^\infty d\lambda' \int_{4\pi} d\omega' \times \mathcal{k}(\omega, \lambda, \omega', \lambda') f(\mathbf{r}, \omega', \lambda') + \mathcal{S}(\mathbf{r}, \omega, \lambda). \qquad (8)$$

Although equation (8) is quite general, it corresponds to an infinite geometry. In general, the functions μ, $\mathcal{k}$ and $\mathcal{S}$ will depend on the medium composition, the interactions, the geometry of interest, and the excitation source. The integro–differential equation (8) is an extremely difficult equation to solve. Analytical solutions usually require a high degree of approximation. Even then there are only a few specific sets of μ, $\mathcal{k}$ and $\mathcal{S}$ that allow us to analytically solve equation (8). Therefore for most real experimental conditions, numerical methods are used to describe the system.

3.2. Set-up model: backscattering from an infinite thickness target of homogeneous composition

We shall adapt equation (8) to represent the scattering of a monochromatic and collimated γ-ray beam in a thick homogeneous target. Following Fano *et al.* (1959), the transport equation for an incident beam of parallel rays with flight direction ω_0 hitting the infinite sample surface, reduces to a one-dimensional spatial equation. The monochromatic beam of wavelength λ_0 is represented by a Dirac δ-function $\delta(\lambda - \lambda_0)$ and the collimation in the direction ω_0 by $\delta(\omega - \omega_0)$. Since a plane through the point $\mathbf{r}_0$ and perpendicular to $\mathbf{u}$ (a unit vector) has the equation

$\mathbf{u}\cdot\mathbf{r}=\mathbf{u}\cdot\mathbf{r}_0$, a source of I_0 uniformly distributed photons $cm^{-2}s^{-1}$ on this plane is represented by the function $I_0\,\delta(\mathbf{u}\cdot\mathbf{r}-\mathbf{u}\cdot\mathbf{r}_0)$. Then, the complete source term can be written as

$$\mathcal{S}(\mathbf{r},\omega,\lambda)=I_0\,\delta(\mathbf{u}\cdot\mathbf{r}-\mathbf{u}\cdot\mathbf{r}_0)\,\delta(\omega-\omega_0)\,\delta(\lambda-\lambda_0). \tag{9}$$

The flux calculation is easier when the medium is infinite and homogeneous, that is, when the coefficients μ and k take the same values through all the space. Under this assumption, if the source function depends spatially on the component of $\mathbf{r}$ along $\boldsymbol{\Omega}$ ($\boldsymbol{\Omega}$ being some arbitrary direction), the flux distribution has the same plane of symmetry, i.e. it depends on the single space coordinate $\mathbf{r}\cdot\boldsymbol{\Omega}$. Therefore, we can eliminate two spatial variables in the transport equation (8) by choosing the point $\mathbf{r}_0$ as the origin of coordinates and the direction $\mathbf{u}$ as the z-axis. In this way the spatial flux distribution will depend only on z and $\boldsymbol{\omega}\cdot\nabla f$ will reduce to $\omega_z(\partial f/\partial z)$.

The transport equation can also be adapted, preserving the above conditions, to describe the diffusion in a semi-infinite medium. To this end, we assume the source is just placed along the plane interface between two infinite semi-spaces: an infinite empty region over the infinite target. A sketch of the geometrical arrangement is shown in Fig. 1 (a and b).

So far, as we are concerned with photons interacting in the target (positive z), we can assume that the photons escaping towards the upper side may suffer absorption but cannot be backscattered into the target. This model (Fernández *et al.*, 1989) represents the behaviour of radiation in two semi-infinite media of different density (the density in the sample being much greater than the density in the surrounding empty space or air).

Such a model can be well represented replacing the kernel $k(\omega,\lambda,\omega',\lambda')$ by a new one including explicitly this spatial dependence. The new kernel should take the value zero for negative z (because photons in the upper semi-space have zero probability of being scattered) while it should match the old kernel in the lower semi-space. Consequently, the empty semi-space is figured in the equation through its non-restitution property, rather than by a change in the density or in the absorption coefficient. This choice preserves the mathematical shape of equation (8) while ensuring a uniform $\mu(\lambda)$.

3.3. The scalar transport equation for the model

The scalar Boltzmann equation for the model is

$$\eta\frac{\partial f(z,\omega,\lambda)}{\partial z}=-\mu(\lambda)f(z,\omega,\lambda)+\int_0^\infty d\lambda'\int_{4\pi}d\omega' k(\omega,\lambda,\omega,\lambda')\mathcal{U}(z)f(z,\omega',\lambda')+I_0\,\delta(z)\,\delta(\omega-\omega_0)\,\delta(\lambda-\lambda_0), \tag{10}$$

†"L" and "S" are sets of parameters as shown in Table 2.

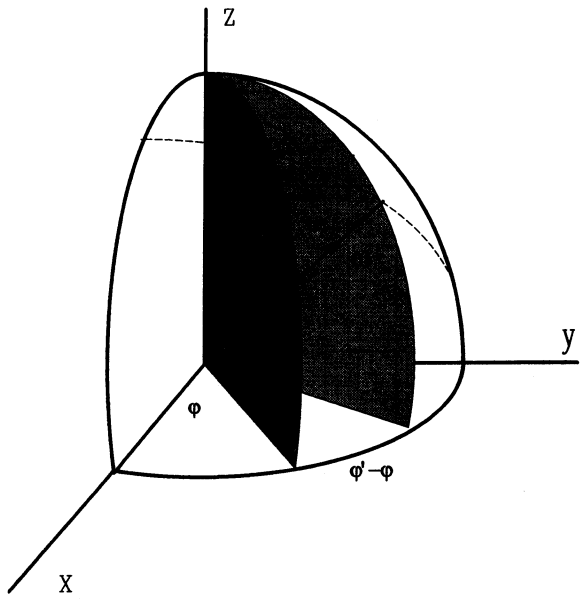

Fig. 2. Transformation between the plane of scattering and the meridian plane. Θ denotes the scattering angle.

where η denotes the directional cosine ω_z, $d\omega'=d\eta'\,d\varphi'$ the differential of solid angle in the direction of the unitary vector ω' and $\mathcal{U}(z)$ the unitary step Heaviside function. It should be noted that, although the transport equation (10) is one-dimensional in the space coordinates, the flux maintains all the angular information through its dependence on ω.

Thus far our discussion of the equation of transfer has not included rigorously the state of polarization in the description of the radiation field. However, polarization can be taken into account in the scalar kernels by defining the possible interactions between photons and matter. For instance, it is current practice to consider scattering kernels depending on an average state of polarization. This choice is valid for one single scattering of unpolarized incident radiation and/or polarization insensitive detector, but introduces an error as we shall show in the next sections.

3.4. The vector transport equation for the model

The transport equation for the fourth-vector describing the albedo flux $\mathbf{f}^{(L)}(\mathbf{r},\omega,\lambda)$† of polarized photons scattered from an infinite thickness target irradiated with a plane source at $z=0$ [components $f_\perp^{(L)}(\mathbf{r},\omega,\lambda)$, $f_\parallel^{(L)}(\mathbf{r},\omega,\lambda)$, $f_U^{(L)}(\mathbf{r},\omega,\lambda)$ and $f_V^{(L)}(\mathbf{r},\omega,\lambda)$ in the meridian plane] can be written (see e.g. Fernández and Molinari, 1993), similarly to equation (10), as

$$\eta\frac{\partial}{\partial z}\mathbf{f}^{(L)}(z,\omega,\lambda)=-\mu(\lambda)\mathbf{f}^{(L)}(z,\omega,\lambda)+\delta(z)\mathcal{S}^{(L)}(\omega,\lambda)+\mathcal{U}(z)\int_0^\infty d\lambda'\times\int_{4\pi}d\omega'\mathbb{H}^{(L)}(\omega,\lambda,\omega',\lambda')\mathbf{f}^{(L)}(z,\omega',\lambda'). \tag{11a}$$

Here

$$\mathbb{H}^{(L)}(\omega, \lambda, \omega', \lambda') = \mathbb{L}^{(L)}(\pi - \Psi) \times \mathbb{K}^{(L)}(\omega, \lambda, \omega', \lambda')\mathbb{L}^{(L)}(-\Psi'), \quad (11b)$$

is the kernel matrix in the meridian plane of reference; $\mathbb{K}^{(L)}(\omega, \lambda, \omega', \lambda')$ the scattering matrix in the scattering plane of reference; and $\mathbb{L}$ the four-by-four rotation matrix which transforms the description of the scattered flux from the scattering plane to the meridian plane or reference; $\mu(\lambda)$ is the narrow-beam attenuation coefficient independent of the state of polarization of the photon (assuming the matter is isotropic) and $\mathscr{S}^{(L)}(\omega, \lambda)$ is the source vector flux [with components $\mathscr{S}_\perp$, $\mathscr{S}_\parallel$, $\mathscr{S}_U$ and $\mathscr{S}_V$]. The rotation angles Ψ and Ψ' in equation (11b), shown in Fig. 2, are defined by the relationships

$$\cos\Psi = \frac{\eta'\sqrt{1-\eta^2} - \eta\sqrt{1-\eta'^2}\cos(\varphi - \varphi')}{(1-(\omega'\cdot\omega)^2)^{1/2}}, \quad (11c)$$

and

$$\cos\Psi' = \frac{\eta\sqrt{1-\eta'^2} - \eta'\sqrt{1-\eta^2}\cos(\varphi - \varphi')}{(1-(\omega'\cdot\omega)^2)^{1/2}}. \quad (11d)$$

For a rotation of the axes through an angle φ in the clockwise direction, the matrix $\mathbb{L}^{(L)}$ is defined as (e.g. Chandrasekhar, 1950; Pomraning, 1973)

$$\mathbb{L}^{(L)}(\varphi) = \begin{bmatrix} \cos^2\varphi & \sin^2\varphi & \frac{1}{2}\sin 2\varphi & 0 \\ \sin^2\varphi & \cos^2\varphi & -\frac{1}{2}\sin 2\varphi & 0 \\ -\sin 2\varphi & \sin 2\varphi & \cos 2\varphi & 0 \\ 0 & 0 & 0 & 1 \end{bmatrix}. \quad (12)$$

A transport equation for the Stokes components of the flux, similar to equation (11a), can be obtained by substituting L by S in equations (11a) and (11b), and using the rotation matrix $\mathbb{L}^{(S)}$ defined as

$$\mathbb{L}^{(S)}(\varphi) = \begin{bmatrix} 1 & 0 & 0 & 0 \\ 0 & \cos 2\varphi & \sin 2\varphi & 0 \\ 0 & -\sin 2\varphi & \cos 2\varphi & 0 \\ 0 & 0 & 0 & 1 \end{bmatrix}, \quad (13)$$

together with a consistent matrix kernel $\mathbb{K}^{(S)}(\omega, \lambda, \omega', \lambda')$ and vector source $\mathscr{S}^{(S)}(\omega, \lambda)$ in the system S.

From a mathematical point of view, the only apparent difference between equation (11a) and the corresponding scalar transport equation for average polarized radiation [see equation (10)] is the vectorial character of equation (11a). Equation (11a) represents a system of four integro-differential equations

$$\eta\frac{\partial}{\partial z}f_i^{(L)}(z, \omega, \lambda) = -\mu(\lambda)f_i^{(L)}(z, \omega, \lambda) + \delta(z)\mathscr{S}_i^{(L)}(\omega, \lambda) + \mathscr{U}(z)\int_0^\infty d\lambda' \int_{4\pi} d\omega' \sum_j H_{ij}^{(L)}(\omega, \lambda, \omega', \lambda') \times f_j^{(L)}(z, \omega', \lambda'), \quad (i,j = \perp, \parallel, U, V); \quad (14)$$

where $H_{ij}^{(L)}$ denotes the corresponding matrix element of $\mathbb{H}^{(L)}$. It is worth noting that the interaction term introduces coupling between the components of the angular flux as long as $\mathbb{H}^{(L)}$ is non diagonal.

3.5. *Solution of the vector transport equation*

It can be shown that equation (14) has a solution similar to that described by Fernández *et al.* (1989) for the scalar transport equation (10), in terms of the partial fluxes for once-, twice-, etc., scattered photons, i.e.

$$f_i^{(L)}(z, \omega, \lambda) = \sum_{k=0}^{\infty} f_i^{(L)(k)}(z, \omega, \lambda), \quad (15)$$

with

$$f_i^{(L)(0)}(z, \omega, \lambda) = \frac{1}{2|\eta|}\mathscr{S}_i^{(L)}(\omega, \lambda) \times \exp\left[-\frac{\mu|z|}{|\eta|}\right](1 + \operatorname{sgn}\eta \operatorname{sgn} z), \quad (16)$$

and

$$f_i^{(L)(n)}(z, \omega, \lambda) = \frac{1}{2|\eta|}\int_0^\infty d\tau \exp\left(-\frac{|z-\tau|\mu}{|\eta|}\right) \times (1 + \operatorname{sgn}\eta \operatorname{sgn}(z-\tau))\int_0^\infty d\lambda' \int_{4\pi} d\omega' \times \sum_j H_{ij}^{(L)}(\omega, \lambda, \omega', \lambda')f_j^{(L)(n-1)}(\tau, \omega', \lambda'), \quad (17a)$$

where $(i, j = \perp, \parallel, U, V)$. Equation (17a) is valid for $n > 0$. It is worth noting that no assumption was made as to the kernel shape, which renders the solution very general.

It is customary to employ an equivalent expression to equation (17a) where the integral over z is divided into two parts, according to the sign of $(z - \tau)$. The solution for *positive* z is

$$f_i^{(L)(n)}(z, \omega, \lambda) = \frac{1}{|\eta|}\left\{\frac{(1+\operatorname{sgn}\eta)}{2}\exp\left(-\frac{z\mu}{|\eta|}\right)\int_0^z d\tau \times \exp\left(\frac{\tau\mu}{|\eta|}\right)\int_0^\infty d\lambda' \int_{4\pi} d\omega' \sum_j H_{ij}^{(L)}(\omega, \lambda, \omega', \lambda') \times f_j^{(L)(n-1)}(\tau, \omega', \lambda') + \frac{(1-\operatorname{sgn}\eta)}{2}\int_0^\infty d\tau \times \exp\left(-\frac{\tau\mu}{|\eta|}\right)\int_0^\infty d\lambda' \int_{4\pi} d\omega' \sum_j H_{ij}^{(L)}(\omega, \lambda, \omega', \lambda') \times f_j^{(L)(n-1)}(\tau + z, \omega', \lambda')\right\}. \quad (17b)$$

The coupling of all the components of the $(n-1)$th-order in every component of the (n)th-order is apparent in equations (17a) and (17b).

The iterative scheme of equations (16) and (17), as does the scalar model, produces an analytical Monte Carlo-like solution which is very useful for studying multiple scattering processes with the insertion of the appropriate interaction kernels. The sum of equation (15) converges in a

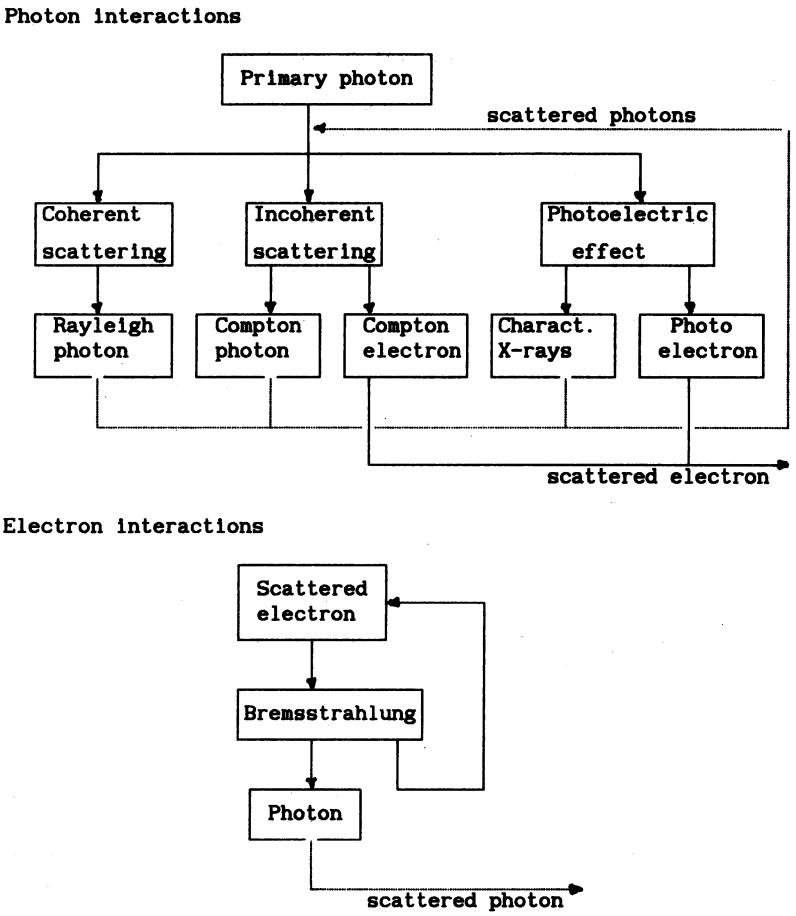

Fig. 3. Principal mechanisms of photon and electron scattering in the low energy γ-ray regime. Scattered electrons feedback new photons into the photon interactions cycle, and, therefore, the full transport problem should be solved with two coupled systems of transport equations, one for polarized photons and one for polarized electrons. The photon transport equation (14), which neglects the electron interactions, is an excellent approximation when the probability for bremsstrahlung is low, i.e. for low energies of the scattered electrons.

few terms because the interaction kernels for photons are less than unity. As equation (17) was derived by considering only pure photonic transport, we can only iterate over the photon–photon lines of the photon–electron shower represented in Fig. 3. However, this approach remains valid since these processes are responsible for the generation of the majority of the new photons. In other words, the neglected electron–photon chains have a sufficiently low probability to modify the results obtained with this theory as long as the excitation energy E_0 is not much greater than 100 keV. The bremsstrahlung radiation has an energy distribution from the electron energy down to zero.

3.6. *First- and second-order scattering intensities*

The albedo partial fluxes and the scattered partial intensities are related through the relationships

$$I_i^{(L)(n)}(\omega, \lambda) = |\eta| f_i^{(L)(n)}(0, \omega, \lambda), \quad n = 1, 2, \ldots . \quad (18)$$

The higher the order of emission the lower the corresponding intensity. This renders the addition of the first two orders—one and two collisions, respectively—in most of the cases responsible for the main part of the total emission for almost all the target materials within a wide range of excitation energies.

From equations (17) and (18), we obtain the L components of both the first-order intensity

$$I_{(a)i}^{(L)(1)}(\omega, \lambda) = \frac{(1 - \operatorname{sgn}\eta)}{2} \int_0^\infty d\lambda' \int_{4\pi} d\omega' \times \frac{(1 + \operatorname{sgn}\eta')}{2} \frac{1}{|\eta'|} \frac{1}{\dfrac{\mu}{|\eta|} + \dfrac{\mu'}{|\eta'|}} \times \sum_j H_{(a)ij}^{(L)}(\omega, \lambda, \omega', \lambda') \mathscr{S}_j^{(L)}(\omega', \lambda'), \quad (19)$$

a	Photoelectric effect	Coherent scattering (Rayleigh)	Incoherent scattering (Compton)
	(P) Characteristic lines (Discrete) [U,L,C]Eqn (51)	(R) Rayleigh peak (Discrete) [U,C] Eqn (58) [L] Eqn (73e)	(C) Compton peak (Discrete) [U,C] Eqn (59) [L] Eqn (74f)

a \ b	Photoelectric effect	Coherent scattering (Rayleigh)	Incoherent scattering (Compton)
Photo-electric effect	(P,P) Secondary XRF intensity. (Discrete) [U,L,C]Eqn (52)	(P,R) XRF photons Rayleigh scattered towards the detector. (Discrete) [U,L,C] Eqn (55)	(P,C) XRF photons Compton scattered towards the detector. Modifies the XRF line shape. (Continuous) [U,L,C] Eqn (57)
Coherent scattering (Rayleigh)	(R,P) XRF due to photoelectric absorption of Rayleigh scattering. (Discrete) [U,C] Eqn (53) [L] Eqn (71a)	(R,R) Modifies the Rayleigh peak. (Discrete) [U,C] Eqn (60a) [L] Eqn (75a)	(R,C) Modifies the Compton peak. (Continuous) [U,C] Eqn (62a) [L] Eqn (77a)
Incoherent scattering (Compton)	(C,P) XRF due to photoelectric absorption of Compton scattering. (Discrete) [U,C] Eqn (56) [L] Eqn (72a)	(C,R) Modifies the Compton peak. (Continuous) [U,C] Eqn (63a) [L] Eqn (78a)	(C,C) Modifies the Compton peak. (Continuous) [U,C] Eqn (61a) [L] Eqn (76a)

Fig. 4. Physical meaning of the single and double scattering chains involving the photoelectric effect, and Rayleigh and Compton scattering. For each chain are indicated the equation numbers for the computation of the corresponding intensity term. Y, L and C denote the kind of source (unpolarized, linearly polarized and circularly polarized, respectively) used to deduce the relationship.

and the second-order one

$$I^{(L)(2)}_{(\alpha,\delta)i}(\omega,\lambda)=\frac{(1-\operatorname{sgn}\eta)}{2}\int_0^\infty d\lambda'\int_{4\pi}d\omega'\frac{1}{|\eta'|}\sum_j\sum_k$$

$$\times\left\{\frac{(1+\operatorname{sgn}\eta')}{2}\int_0^\infty d\lambda''\int_{4\pi}d\omega''\frac{(1+\operatorname{sgn}\eta'')}{2}\frac{H^{(L)}_{(\delta)ij}(\omega,\lambda,\omega',\lambda')H^{(L)}_{(\alpha)jk}(\omega',\lambda',\omega'',\lambda'')\mathscr{P}^{(L)}_k(\omega'',\lambda'')}{|\eta''|\left(\frac{\mu}{|\eta|}+\frac{\mu'}{|\eta'|}\right)\left(\frac{\mu}{|\eta|}+\frac{\mu''}{|\eta''|}\right)}\right.$$

$$\left.+\frac{(1-\operatorname{sgn}\eta')}{2}\int_0^\infty d\lambda''\int_{4\pi}d\omega''\frac{(1+\operatorname{sgn}\eta'')}{2}\frac{H^{(L)}_{(\delta)ij}(\omega,\lambda,\omega',\lambda')H^{(L)}_{(\alpha)jk}(\omega',\lambda',\omega'',\lambda'')\mathscr{P}^{(L)}_k(\omega'',\lambda'')}{|\eta''|\left(\frac{\mu''}{|\eta''|}+\frac{\mu'}{|\eta'|}\right)\left(\frac{\mu}{|\eta|}+\frac{\mu''}{|\eta''|}\right)}\right\}. \quad (20)$$

Equations (19) and (20) are the expressions (Fernández and Molinari, 1993) for calculating the intensity contributions (at the direction ω, and as a function of wavelength λ) for a one-collision chain

$$(\omega', \lambda') \xrightarrow{a} (\omega, \lambda),$$

and for a two-collision chain

$$(\omega'', \lambda'') \xrightarrow{a} (\omega', \lambda') \xrightarrow{b} (\omega, \lambda),$$

respectively. The lower indices a and b represent valid (probabilistically independent) photon–photon interactions in the low energy γ-ray regime as, for instance, the photoelectric, the Rayleigh and the Compton effects, whose contributions to the photon cycle are shown in Fig. 3. Figure 4 lists the nine ways of combining these three processes to produce the two-collision chains which contribute the second-order intensities whose L components can be calculated with equation (20).

4. THE EFFECT OF POLARIZATION ON THE PREVAILING INTERACTIONS IN THE LOW ENERGY γ-RAY REGIME

Photons can interact in different ways depending on their energy (e.g. Compton and Alison, 1935; Evans, 1955; Jauch and Rohrlich, 1976; Agarwal, 1991). The photons in the low energy γ-ray regime interact with the electron shells which surround the nucleus. The nucleus itself does not contribute to the scattering or absorption of photons.

The interaction of a photon of energy $h\nu$ with an isolated atom A has the effect of changing the atom's state from $|i\rangle$ to $|f\rangle$, which can be expressed as

$$A_i + h\nu_i \rightarrow A_f + h\nu_f. \tag{21}$$

Equation (21) denotes the type of photon–atom interaction of interest in this work, having one initial photon and only one resulting photon. A_f denotes the atom plus all the non-photonic particles (such as electrons) produced in the reaction.

There are three major photon–atom processes† whose influence prevail in the low energy γ-ray regime (Davisson and Evans, 1952; Hubbell *et al.*, 1974; Creagh, 1987): the *photoelectric effect* in which the photon causes the ejection of an electron leaving a hole in the atom which, when the vacancy is filled by an electron from another level, emits a fluorescence photon having the energy difference between the two levels; the *unmodified* or *Rayleigh scattering* in which the photon transfers momentum to the atom but not energy; and the *modified* or *Compton scattering* in which both momentum and energy are transferred to the electrons comprising the atom.

What we call an interaction may not be strictly a single process. Any sequence of physical processes in rapid succession, originated by a photon and producing another (other) photon(s), can be statistically considered as a unique interaction, as occurring for example with the photoelectric effect (see Fig. 3).

The resulting (or secondary) photon from an interaction may collide in turn with another atom, starting a multiple chain of events that we want (and need) to study. However, not only photons are produced in the photon–atom interactions. The photoelectric effect and the modified scattering cause electrons to be ejected from the atom which in turn can produce new lower energy photons. Since these contributions render the transport problem far more complicated we shall neglect this work bremsstrahlung (braking radiation) from Compton and photoelectrons (May and Wick, 1951; Olsen and Maximon, 1958, 1959; Olsen, 1968; Tseng and Pratt, 1973; Alexandropoulos *et al.*, 1988); photoionization due to Auger electrons (Bishop and Riviere, 1969), photoelectrons (Ebel *et al.*, 1971) and Compton electrons (Stoev, 1992); and also other photon sources such pair production–annihilation (Fano, 1949b; Wick, 1951; Olsen and Maximon, 1958, 1959; McMaster, 1960; Olsen, 1968; Maximon and Olsen, 1962; Kel'ner, 1969; Tseng and Pratt, 1974).

The single-process scalar kernels play an important role in transport theory. They represent the probability density—by unit wavelength, by unit solid angle and by unit path—that the process may change the phase-space variables from (ω', λ') to (ω, λ). Therefore, the scalar kernel is directly related to the double-differential scattering coefficient of the interaction. Thus, the scattering coefficient for the process T can be obtained from the kernel $\mathcal{k}_T(\omega, \lambda, \omega', \lambda')$ using the relationship

$$\sigma_T(\lambda', \omega') = \int_0^\infty d\lambda \int_{4\pi} d\omega \, \mathcal{k}_T(\omega, \lambda, \omega', \lambda'), \tag{22a}$$

allowing the comparison with experimental or theoretical data. The scalar scattering kernel is usually defined for an average polarization state of the incident radiation.

Similarly, the matrix kernel $\mathbb{K}_T^{(S)}(\omega, \lambda, \omega', \lambda')$ (in the S system) satisfies the equivalent relationship

$$\begin{aligned}\sigma_T(\lambda', \omega') &= (1,0,0,0) \int_0^\infty d\lambda \int_{4\pi} d\omega \\ &\quad \times \mathbb{H}_{(T)}^{(S)}(\omega, \lambda, \omega', \lambda') \begin{bmatrix} 1 \\ 0 \\ 0 \\ 0 \end{bmatrix} \\ &= \int_0^\infty d\lambda \int_{4\pi} d\omega \, K_{T_{11}}^{(S)}(\omega, \lambda, \omega', \lambda') \\ &= \int_0^\infty d\lambda \int_{4\pi} d\omega \, \mathcal{k}_T(\omega, \lambda, \omega', \lambda'), \end{aligned} \tag{22b}$$

where $\mathbb{H}$ was defined in equation (11b), the column vector on the right side represents an incident unpolarized beam, and the row vector on the left side

†There are also "minor" processes such as X-ray resonant Raman scattering that also exist. They are observable only under specific conditions.

represents a detector insensitive to polarization. Analogously, we can write in the system L

$$\sigma_T(\lambda', \omega') = (1, 1, 0, 0) \begin{bmatrix} \sigma_{T\perp}(\lambda', \omega') \\ \sigma_{T\parallel}(\lambda', \omega') \\ 0 \\ 0 \end{bmatrix}$$

$$= \frac{1}{2}(1, 1, 0, 0) \int_0^\infty d\lambda \int_{4\pi} d\omega \times \mathbb{H}_{(T)}^{(L)}(\omega, \lambda, \omega', \lambda') \begin{bmatrix} 1 \\ 1 \\ 0 \\ 0 \end{bmatrix}$$

$$= \frac{1}{2} \sum_{i=1}^{2} \sum_{j=1}^{2} \int_0^\infty d\lambda \int_{4\pi} d\omega \times H_{(T)ij}^{(L)}(\omega, \lambda, \omega', \lambda')$$

$$= \frac{1}{2} \int_0^\infty d\lambda \int_{4\pi} d\omega \, \mathcal{k}_T(\omega, \lambda, \omega', \lambda') \times \sum_{i=1}^{2} \sum_{j=1}^{2} t_{ij}(\omega, \lambda, \omega', \lambda'). \quad (22c)$$

In the last equality of equation (22c) we defined, for convenience, the matrix kernel in the system L as

$$\mathbb{K}_T^{(L)}(\omega, \lambda, \omega', \lambda') = k_T(\omega, \lambda, \omega', \lambda') \mathbb{T}_T^{(L)}(\omega, \lambda, \omega', \lambda') \quad (23)$$

where $k_T(\omega, \lambda, \omega', \lambda')$ denotes the same scalar kernel (i.e. depending on average polarization) which appears in equations (22a) and (22b). From equations (22a) and (22c), the elements $t_{ij}(\omega, \lambda, \omega', \lambda')$ of the upper left 2×2 submatrix of $\mathbb{T}$ in equation (23) must satisfy the relationship

$$\frac{1}{2} \sum_{i=1}^{2} \sum_{j=1}^{2} t_{ij}(\omega, \lambda, \omega', \lambda') = 1, \quad (24)$$

which expresses one of the transformation rules between the matrix elements of $\mathbb{K}$ in the systems S and L. From equations (22) the analogy between the scalar kernel $\mathcal{k}_T(\omega, \lambda, \omega', \lambda')$, built for an average polarization state, and the matrix kernel $\mathbb{K}$, applied to unpolarized incident radiation and polarization independent detector, is apparent.

Additionally, we can obtain from equation (22c) the normal and parallel components [$\sigma_{T\perp}(\lambda', \omega')$ and $\sigma_{T\parallel}(\lambda', \omega')$, respectively] of the scattering coefficient (for incident unpolarized γ-rays)

$$\sigma_{T\perp}(\lambda', \omega') = \frac{1}{2} \int_0^\infty d\lambda \int_{4\pi} d\omega \times k_T(\omega, \lambda, \omega', \lambda')(t_{11} + t_{12}), \quad (25a)$$

and

$$\sigma_{T\parallel}(\lambda', \omega') = \frac{1}{2} \int_0^\infty d\lambda \int_{4\pi} d\omega \times k_T(\omega, \lambda, \omega', \lambda')(t_{21} + t_{22}). \quad (25b)$$

The cross sections for the interaction processes of interest can be calculated independently. They constitute the main part of the total attenuation coefficient (McMaster *et al.*, 1969; Storm and Israel, 1970; Veigele, 1973; Hubbell *et al.*, 1986; Saloman *et al.*, 1988; Cullen *et al.*, 1989), so we can define the total attenuation coefficient as

$$\mu = \sigma_C + \sigma_R + \tau, \quad (26)$$

where σ_C and σ_R are the Compton (incoherent) and Rayleigh (coherent) integral attenuation coefficients and τ is the photoelectric attenuation coefficient.

If we consider attenuation of photons, then at low energies the atomic photoelectric effect predominates, while at intermediate energies Compton scattering dominates. If, however, we are concerned with scattering of photons, then Rayleigh scattering dominates at low energies or forward angles, while Compton scattering dominates at higher energies or larger angles.

In what follows we shall write the atomic interaction kernels for the three dominating processes that participate in low energy γ-ray photon transport. Since our aim is to explain the contribution of multiple scattering terms, we shall use the coherent and incoherent scattering factor approximation to describe scattering cross-sections. These scattering factor approximations assume a smooth behaviour to the scattering cross-sections so they cannot explain scattering resonances (Kissel and Pratt, 1987) such as anomalous scattering (Kane *et al.*, 1986; Bui and Milazzo, 1989). The effect of the relative motion of the electrons with respect to the incident photon beam will not be addressed since it complicates the transport equation. The relative motion of the electrons does not have a significant effect on the coherent scattering. However, at least for the incoherent case, the scattering factor can be obtained with an integration of momentum profiles of single orbitals (Ribberfors and Berggren, 1982) giving a simple connection between the Compton profiles and the corresponding scattering factor. Polarization effects will be considered in detail, and will be discussed separately for every scattering process.

4.1. *Photoelectric effect*

The photoelectric effect is an indirect photon–photon process. In the photoelectric effect a photon is absorbed by an atom creating a hole in the atom with the ejection of an electron. The energy of this electron is the difference between that of the incident photon and of the binding energy of the electron. The vacancy will be spontaneously filled by means of an electron transition from a higher energy level. The deexcitation energy is carried off with the emission of a characteristic photon or Auger electrons. Statistically, the two combined processes (absorption/ejection) may be considered as a single interaction. The theory of the photoionization process has received great attention (e.g. Fano and Cooper, 1968;

Starace, 1982; Amusia, 1990), the photoelectric cross-section has been largely investigated with experiments and theoretical calculations (Scofield, 1987), and collected data are available elsewhere (Scofield, 1973; Saloman *et al.*, 1988).

The scalar kernel for the production of a characteristic line of wavelength λ_i [see Bearden (1967) for X-ray wavelengths] from a pure element target due to the photoelectric absorption of photons with wavelength λ' (Fernández, 1989) is given by

$$\mathcal{k}_{P_{\lambda_i}}(\omega, \lambda, \omega', \lambda') = \frac{1}{4\pi} Q_{\lambda_i}(\lambda')\,\delta(\lambda - \lambda_i) \times [1 - \mathcal{U}(\lambda' - \lambda_{e_i})], \quad (27)$$

The isotropy of the secondary X-rays is reflected by the kernel independence on ω and by the 4π normalization factor. The line is assumed to be monochromatic, neglecting its natural width (Krause and Oliver, 1979) that is significantly less than the instrumental width (Salem *et al.*, 1977). The XRF emission probability density $Q_{\lambda i}(\lambda')$ for the line λ_i (in [cm^{-1}]) is given by the probability relation

$$Q_{\lambda_i}(\lambda') = \tau_s(\lambda')(1 - 1/J_{\lambda_i})\omega_{\lambda_i}\Gamma_{\lambda_i}, \quad (28)$$

where $\tau_s(\lambda')$ is the photoelectric attenuation coefficient [cm^{-1}] of the emitter element s, $J_{\lambda i}$ is the absorption-edge jump (McMaster *et al.*, 1969; Scofield, 1973; Saloman *et al.*, 1988; Cullen *et al.*, 1989), $\omega_{\lambda i}$ the fluorescence yield (Fink *et al.*, 1966; Bambynek *et al.*, 1972; Salem *et al.*, 1974; Krause, 1979; Langenberg and Van Eck, 1979; Cohen, 1987; Hubbell, 1989) and $\Gamma_{\lambda i}$ the line emission probability of the line at λ_i into its own spectral series (Scofield, 1969, 1974, 1975; Hansen *et al.*, 1970; Khan and Karimi, 1980). For compilations of calculated values of $\tau_s(\lambda')$ for neutral atoms with a relativistic Hartree–Slater model (renormalized to the Hartree–Fock model for $Z = 2$–54) see Hubbell and coworkers (Hubbell *et al.*, 1974, 1980; Hubbell, 1982), and (without renormalization) Scofield (1973), Saloman *et al.*, (1988), Cullen *et al.*, (1989) and Trubey *et al.* (1989); for a discussion about the significance of the normalization see Saloman and Hubbell (1987). The line is emitted only when λ' is lower than the threshold of the absorption edge wavelength λ_{ei} (Bearden and Burr, 1967; Cullen *et al.*, 1989) of the series to which the line belongs as described in the Heaviside function $\mathcal{U}$ in equation (27).

The complete emission spectrum of the element s is obtained adding all the single line terms:

$$\mathcal{k}_P(\omega, \lambda, \omega', \lambda') = \frac{1}{4\pi} \sum_i Q_{\lambda_i}(\lambda')\,\delta(\lambda - \lambda_i) \times [1 - \mathcal{U}(\lambda' - \lambda_{e_i})]. \quad (29)$$

The photoelectric effect has low sensitivity to the polarization of the incident photon but is not completely insensitive to it. According to Flügge *et al.* (1972), after photoionization, the fluorescence X-rays originating from the vacancy states with $j = 1/2$, (K shell and L_1, L_2, M_1 and M_2 subshells, etc.) will only be isotropic and unpolarized. However, those fluorescence X-rays which are emitted from the filling of vacancy states with $j = 3/2$ (L_3, M_3 and M_4 subshells) and with $j = 5/2$, (M_5 subshell) will be anisotropic and polarized. This theoretical prediction was recently confirmed experimentally by Kahlon *et al.* (1991) supporting the hypothesis that the vacancy states with $j > 1/2$ have a nonstatistical population distribution of their magnetic substates and are aligned. The level of percentage polarization measured by these authors for the L_ℓ and L_α lines was 86 (6)% and 29 (2)% for thorium and 79 (6)% and 36 (2)% for uranium.

Assuming that photoelectric X-ray emission is independent of polarization (as is the case with the intense K lines), the matrix elements t_{ij} of the polarization kernel verify the relationship $t_{11} = t_{12} = t_{21} = t_{22}$, and we can write the matrix polarization kernel for the emission of a characteristic line of wavelength λ_i as

$$\mathbb{K}^{(L)}_{P_{\lambda_i}}(\omega, \lambda, \omega', \lambda') = k_{P_{\lambda_i}}(\omega, \lambda, \omega', \lambda') \times \begin{bmatrix} 1/2 & 1/2 & 0 & 0 \\ 1/2 & 1/2 & 0 & 0 \\ 0 & 0 & 0 & 0 \\ 0 & 0 & 0 & 0 \end{bmatrix}, \quad (30)$$

where $k_{P_{\lambda_i}}(\omega, \lambda, \omega', \lambda')$ was defined in equation (27). The complete emission spectrum can be obtained similarly as in equation (29). We get a degree of polarization $P_P \equiv 0$ for these radiative transitions.

4.2. *Rayleigh scattering*

The coherent scattering is a process where the photons change direction (momentum transfer) but not energy (Kane *et al.*, 1986). This scattering takes place with the more tightly bound electrons of the atom which behave rigidly during the interaction. The Rayleigh atomic kernel for unpolarized photons, with phase-space coordinates (ω', λ') scattered by a pure element target with atomic number Z into the coordinates (ω, λ), is (Fernández *et al.*, 1990)

$$\mathcal{k}_R(\omega, \lambda, \omega', \lambda') = \sigma\,\delta(\lambda - \lambda')(1 + (\omega \cdot \omega')^2) \times \frac{F^2(\lambda', \omega \cdot \omega', Z)}{Z}. \quad (31)$$

$\sigma = \rho N Z r_0^2/(2A)$ is a macroscopic attenuation coefficient (in [cm^{-1}]), r_0 being the classical radius of the electron, ρ the density, N Avogadro's number and A the atomic weight. The delta function stresses the monochromaticity of the scattering. The angular dependence of the kernel (31) is due to the last two factors: the Thomson angular factor representing an average polarization state, and the

square of the atomic form factor comprising the constructive interference from the whole charge distribution. The coherent form factor $F(\lambda', \omega \cdot \omega', Z)$ can explain atomic contributions that are significantly greater than Z times the contribution from one single electron. Special limits are $F(\lambda', 1, Z) = F(\infty, \omega \cdot \omega', Z) = Z$ and $F(0, \omega \cdot \omega', Z) = 0$. Experimental data tables of form factors, and references to theoretical computations for many electron atoms may be found in the classical paper of Hubbell *et al.* (1975) and in more recent works (Hubbell and Øverbø, 1979); Schaupp *et al.*, 1983; Kane *et al.*, 1986). A closed expression (Veigele *et al.*, 1966) giving approximate values for F is available. More precise values are achieved with semi-empirical formulae and fitting coefficients of theoretical calculations (Cromer and Waber, 1974). The integration of scalar kernel (29) [as described by equation (22a)] to obtain the total Rayleigh coefficient was performed numerically by McMaster *et al.* (1969), Hubbell *et al.* (1975) and analytically by Hanson (1985).

Assuming that electron binding (in many electron atoms) can be described by a polarization independent form factor (Brown and Meyers, 1956, 1957; Kane *et al.*, 1986), the matrix kernel for Rayleigh scattering of polarized radiation becomes

$$\mathbb{K}_R^{(L)}(\omega, \lambda, \omega', \lambda') = 2\sigma\,\delta(\lambda - \lambda') \begin{bmatrix} \omega \cdot \omega'^2 & 0 & 0 & 0 \\ 0 & 1 & 0 & 0 \\ 0 & 0 & \omega \cdot \omega' & 0 \\ 0 & 0 & 0 & \omega \cdot \omega' \end{bmatrix} \frac{F^2(\lambda', \omega \cdot \omega', Z)}{Z}$$

$$= \frac{\kappa_R(\omega, \lambda, \omega', \lambda')}{1 + (\omega \cdot \omega')^2} \begin{bmatrix} 2\omega \cdot \omega'^2 & 0 & 0 & 0 \\ 0 & 2 & 0 & 0 \\ 0 & 0 & 2\omega \cdot \omega' & 0 \\ 0 & 0 & 0 & 2\omega \cdot \omega' \end{bmatrix}. \quad (32)$$

From equations (25a) and (25b), and using equation (32), it is possible to compute the normal and parallel components of the total Rayleigh coefficient, as

$$\sigma_{R\perp}(\lambda', \omega') = \int_0^\infty d\lambda \int_{4\pi} d\omega\, \kappa_R(\omega, \lambda, \omega', \lambda') \times \frac{1 - (1 - \omega \cdot \omega'^2)\cos^2 \Psi}{1 + (\omega \cdot \omega')^2} \quad (33a)$$

and

$$\sigma_{R\parallel}(\lambda', \omega') = \int_0^\infty d\lambda \int_{4\pi} d\omega\, \kappa_R(\omega, \lambda, \omega', \lambda') \times \frac{\omega \cdot \omega'^2 - (1 - \omega \cdot \omega'^2)\cos^2 \Psi}{1 + (\omega \cdot \omega')^2}, \quad (33b)$$

where the angle Ψ was defined in equation (11c). Evaluated normal and parallel components of the total Rayleigh coefficient for linearly polarized incident radiation [and therefore, with different excitation conditions as those assumed in equation (25)] were calculated by Hanson (1986a, 1986b, 1986c).

As we shall show below, the degree of polarization

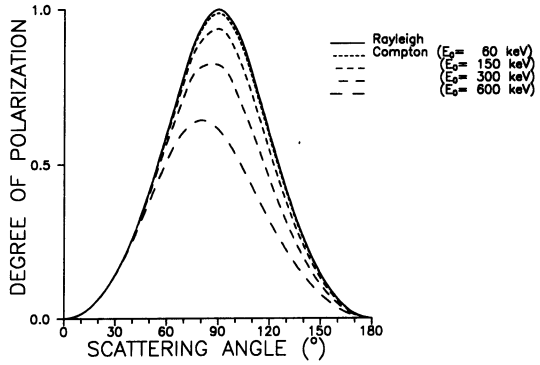

Fig. 5. Degrees of polarization for Rayleigh and Compton effects as a function of the scattering angle. The Compton degree of polarization depends on the wavelength of the incoming photon because of the relation between wavelength and scattering angle in the Compton shift. It is shown for several excitation energies from 60 to 600 keV. It is apparent that both interactions have their maxima at or near 90° scattering.

for the Rayleigh scattering is given by the relationship

$$P_R(\omega, \lambda, \omega', \lambda') = \frac{1 - (\omega \cdot \omega')^2}{1 + (\omega \cdot \omega')^2}, \quad (34)$$

plotted in Fig. 5 as a function of the scattering angle Θ between 0° and 180°. The graph shows clearly that total polarization is reached only at 90° scattering. In the other cases a partially polarized beam always remain after scattering, except at 0° and 180° where the polarized fraction vanishes. Equation (34) illustrates how scattering can be used as a polarization filter because of the $\omega \cdot \omega'$. This also illustrates that after the scattering, the degree of polarization depends on where the scattered photons are observed. Single scattering maximizes the degree of polarization. This fact has been used to produce polarized X-rays by placing scattering blocks between an X-ray tube and the sample (Wobrauschek and Aiginger, 1983; Wielopolski *et al.* 1989).

Complementary information on polarization effects in coherent scattering can be found from the following authors who have treated, either theoretically or experimentally, the problem: Brenner *et al.* (1954), Brini *et al.* (1958, 1959), Sood (1958), Bobel and Passatore (1960), Fuschini *et al.* (1960), Manuzio and Vitale (1961), Standing and Jovanovich (1962),

Cole (1963), Singh *et al.*, (1964), Anand *et al.* (1965), Williams and McNeill (1965), Somayajulu *et al.* (1968), Somayajulu and Lakshminarayana (1968b), Molak *et al.* (1971), Simon and Daniel (1977), Dwiggins (1983), Roy *et al.* (1986), Hanson (1988a, 1988b, 1990), Hanson and Meron (1988).

4.3. *Compton scattering*

In incoherent scattering, energy as well as direction is changed (Compton, 1923; Evans, 1958). This process takes place with the outer electrons of the atom. The Compton atomic kernel for incident photons, with phase-space coordinates (ω', λ') scattered by a pure specie target of atomic number Z into the coordinates (ω, λ), is (Fernández *et al.*, 1990)

$$\mathcal{K}_C(\omega, \lambda, \omega', \lambda') = \sigma K_{KN}(\lambda, \lambda') S(\lambda', \omega \cdot \omega', Z) \times \frac{1}{\lambda_C} \delta\left(1 - \omega \cdot \omega' + \frac{\lambda' - \lambda}{\lambda_C}\right). \quad (35)$$

where

$$K_{KN}(\lambda, \lambda') = \left(\frac{\lambda'}{\lambda}\right)^2 \times \left\{\frac{\lambda}{\lambda'} + \frac{\lambda'}{\lambda} + \frac{\lambda - \lambda'}{\lambda_C}\left(\frac{\lambda - \lambda'}{\lambda_C} - 2\right)\right\}, \quad (36)$$

and $\lambda_C = 0.0242631$ Å is the Compton wavelength. The $\sigma K_{KN}(\lambda, \lambda')$ factor denotes the well known Klein–Nishina differential cross section (Klein and Nishina, 1929) representing an average polarization state. The direction-wavelength delta in equation (35) fixes the integration path in the phase-space along the line $1 - \omega \cdot \omega' + (\lambda' - \lambda)/\lambda_C = 0$ [this condition does not account for the shift for bound electrons (Evans, 1958)]. $S(\lambda', \omega \cdot \omega', Z)$ is the incoherent scattering function which takes into account the electron binding. Some special limits are $S(\lambda, 1, Z) = S(\infty, \omega \cdot \omega', Z) = 0$ and $S(0, \omega \cdot \omega', Z) = 1$. Data tables and references to theoretical computations are found in the paper of Hubbell *et al.* (1975) (note that their "scattering funciton" means $S \cdot Z$ here). A closed approximate formula for S was obtained (Veigele *et al.*, 1966) with the Thomas–Fermi model. Precise values of the S factor can be computed with semi-empirical formulas and fitting coefficients to theoretical calculations (Smith *et al.*, 1975).

The pre-collision motion of the electrons has been ignored in the kernel equation (35), limiting the Compton peak to a monochromatic line. Because of the *Compton profile* (that is the projection of the electron momentum distribution on the z axis) the width due to the scattered photons is larger than the instrumental width. The more rigorous theoretical treatment associated with the Compton profile is not sufficiently tractable for extensive calculation and will not be discussed here. However, the multiple scattering effects will be better appreciated in a context of generality, independent of the state of excitation of the atom and the chemical bond to other atoms.

A Klein–Nishina polarization dependent coefficient could be written in place of equation (36) (Nishina, 1929; Evans, 1958; Stroscio, 1984), which depends on the angle between the directions of polarization of the incident (ϵ') and scattered radiation (ϵ). It shows the familiar relationship

$$K_{KN}(\lambda, \lambda') = \left(\frac{\lambda'}{\lambda}\right)^2 \left\{\frac{\lambda}{\lambda'} + \frac{\lambda'}{\lambda} + -2 + 4(\epsilon \cdot \epsilon')^2\right\}. \quad (37)$$

This statement means that the scattering cross section determines the probability for a plane polarized photon to be scattered in a certain direction and then to pass through a hypothetical filter which accepts only radiation polarized in a certain plane. Elliptical polarization is not considered in that treatment. Therefore, for a complete analysis of the polarization effects it is convenient to use the Stokes method.

Assuming that the effect of the charge distribution (in many electron atoms) contributes a polarization independent scattering function and the spin of the electron is randomly oriented before and is not observed after the scattering (Fano *et al.*, 1959), the matrix kernel for Compton scattering becomes

$$\mathbb{K}_C^{(L)}(\omega, \lambda, \omega', \lambda') = \frac{\sigma}{\lambda_C}\left(\frac{\lambda'}{\lambda}\right)^2 S(\lambda', \omega \cdot \omega', Z)\, \delta\left(1 - \omega \cdot \omega' + \frac{\lambda' - \lambda}{\lambda_C}\right) \times \begin{bmatrix} 1 + \frac{a}{2} + 2b(b-2) & \frac{a}{2} - 1 & 0 & 0 \\ \frac{a}{2} - 1 & 1 + \frac{a}{2} & 0 & 0 \\ 0 & 0 & 2(1-b) & 0 \\ 0 & 0 & 0 & a(1-b) \end{bmatrix}$$

$$= \frac{\mathcal{K}_C(\omega, \lambda, \omega', \lambda')}{a + b(b-2)} \begin{bmatrix} 1 + \frac{a}{2} + 2b(b-2) & \frac{a}{2} - 1 & 0 & 0 \\ \frac{a}{2} - 1 & 1 + \frac{a}{2} & 0 & 0 \\ 0 & 0 & 2(1-b) & 0 \\ 0 & 0 & 0 & a(1-b) \end{bmatrix}, \quad (38)$$

where we have defined the auxiliary variables

$$a=\frac{\lambda}{\lambda'}+\frac{\lambda'}{\lambda}, \quad \text{and} \quad b=\frac{\lambda-\lambda'}{\lambda_C}.$$

In the limiting case of $\lambda=\lambda'\to\infty$, we obtain the matrix of Rayleigh scattering.

Several authors have paid attention to the build-up of a much more detailed polarization matrix depending on the initial and final polarization states of both interacting photon and electron (see Franz, 1936, 1938; Fano, 1949a; Lipps and Tolhoek, 1954a, 1954b; Tolhoek, 1956; Olsen, 1968; Ewald and Franz, 1976) but this extent of detail is excessive for the scope of this paper. However, it is necessary for studying the effects of polarization on the scattering of γ-rays in a target exposed to a magnetic field (Gibbs *et al.*, 1989; Sakai *et al.*, 1989).

From equations (25a) and (25b), and using equation (38), it is possible to compute the normal and parallel components of the total Compton coefficient, as

$$\sigma_{C\perp}(\lambda',\omega')=\frac{1}{2}\int_0^\infty d\lambda\int_{4\pi}\mathrm{d}\omega\,\kappa_C(\omega,\lambda,\omega',\lambda')\times\frac{a+2b(b-2)\cos^2\Psi}{a+b(b-2)} \tag{39a}$$

and

$$\sigma_{C\parallel}(\lambda',\omega')=\frac{1}{2}\int_0^\infty d\lambda\int_{4\pi}\mathrm{d}\omega\,\kappa_C(\omega,\lambda,\omega',\lambda')\times\frac{a+2b(b-2)\sin^2\Psi}{a+b(b-2)}, \tag{39b}$$

with the angle Ψ defined by equation (11c). Evaluated normal and parallel components of the total Compton coefficient for linearly polarized incident radiation [and therefore, with different excitation conditions as the assumed in equation (25)] were also calculated by Hanson (1986a, 1986b, 1986c).

As we shall show below, the degree of polarization for Compton scattering is given by the relationship

$$P_C(\omega,\lambda,\omega',\lambda')=\frac{\dfrac{\lambda-\lambda'}{\lambda_C}\left(2-\dfrac{\lambda-\lambda'}{\lambda_C}\right)}{\dfrac{\lambda}{\lambda'}+\dfrac{\lambda'}{\lambda}+\dfrac{\lambda-\lambda'}{\lambda_C}\left(\dfrac{\lambda-\lambda'}{\lambda_C}-2\right)}. \tag{40}$$

In contrast to the degree of polarization of Rayleigh scattering [equation (34)] which does not depend on wavelength, the degree of polarization of Compton scattering depends on both, the scattering angle and the wavelength, as it is shown in Fig. 5.

Complementary information on polarization effects in incoherent scattering can be found from the following authors who have treated, either theoretically or experimentally, the problem: Wightman (1948), Spencer (1948), Spencer and Wolff (1953), Metzger and Deutsch (1950), Hoover *et al.* (1952), McMaster (1954, 1961), Frolov (1960), Miller and Wilcox (1961), Huber *et al.* (1963), Singh *et al.* (1964, 1965), Hamilton and McIntyre (1967), Alexandropoulos *et al.* (1971), Bock (1971), Milton *et al.* (1972), Tsai *et al.* (1972), Kel'ner *et al.* (1975), Ewald and Franz (1976), Leubner and Metzler (1984), Xu (1984), Hanson (1988a, 1988b, 1990), Hanson and Meron (1988).

4.4. *The total kernel*

According to our previous assumptions about the composition of the total attenuation coefficient we can write an expression, analogous to equation (26), for the total scalar kernel for photons in the low energy γ-ray regime

$$\kappa(\omega,\lambda,\omega',\lambda')=\kappa_R(\omega,\lambda,\omega',\lambda')+\kappa_C(\omega,\lambda,\omega',\lambda')+\sum_i\kappa_{P_{\lambda_i}}(\omega,\lambda,\omega',\lambda'), \tag{41a}$$

and for the total matrix kernel

$$\mathbb{K}^{(L)}(\omega,\lambda,\omega',\lambda')=\mathbb{K}_R^{(L)}(\omega,\lambda,\omega',\lambda')+\mathbb{K}_C^{(L)}(\omega,\lambda,\omega',\lambda')+\sum_i\mathbb{K}_{P_{\lambda_i}}^{(L)}(\omega,\lambda,\omega',\lambda'), \tag{41b}$$

which, integrated as in equation (22), allows us to recover the radiative part of equation (26).

Up to now, we have considered the above kernels for a target of a pure element with atomic number Z. We will now analyse how to determine attenuation coefficients for materials composed by several species of atoms. We denote by W_j the *weight fraction* of the element j which satisfies the relationship

$$\sum_j W_j=1, \tag{42}$$

The mass attenuation coefficient (in [cm^2/g]) for a composite material obeys the well known relation (Davisson and Evans, 1952; Evans *et al.*, 1955)

$$\frac{\mu}{\rho}=\sum_j W_j\left(\frac{\mu}{\rho}\right)_j, \tag{43}$$

where μ is the total attenuation coefficient given by equation (26) and $(\mu/\rho)_j$ is the total mass attenuation coefficient for the single element j. The coefficients of the single interactions follow a similar relationship.

The total kernel for a composite material is easily obtained from the kernels for the single sample components replacing all the attenuation coefficients by mass attenuation coefficients in equations (29), (31) and (35).

$$\kappa(\omega,\lambda,\omega',\lambda')=\sum_j W_j\left\{\kappa_R(\omega,\lambda,\omega',\lambda')|_j+\kappa_C(\omega,\lambda,\omega',\lambda')|_j+\sum_i\kappa_{P_{\lambda_i}}(\omega,\lambda,\omega',\lambda')|_j\right\}, \tag{44a}$$

where $\kappa_a(\omega,\lambda,\omega',\lambda')|_j$ represents the "mass" kernel for the interaction a with the specie of atoms Z_j. Analogously, matrix kernels satisfy the equivalent relationship

$$\mathbb{K}^{(L)}(\omega,\lambda,\omega',\lambda')=\sum_j W_j\left\{\mathbb{K}_R^{(L)}(\omega,\lambda,\omega',\lambda')|_j+\mathbb{K}_C^{(L)}(\omega,\lambda,\omega',\lambda')|_j+\sum_i\mathbb{K}_{P_{\lambda_i}}^{(L)}(\omega,\lambda,\omega',\lambda')|_j\right\}. \tag{44b}$$

5. EFFECTS OF POLARIZATION FOR SCATTERED RADIATION FROM UNPOLARIZED SOURCES

It has been shown in Section 3.5 that equation (8) has the general flux solution (15) similar to that described in Fernández *et al.* (1989), in terms of the partial fluxes for once-, twice-, etc., scattered photons. The components of the partial intensities can be easily derived from the components of the albedo partial fluxes (17). We are interested in the Stoke's I component (or $I_\parallel + I_\perp$ in the L system) which gives information on the number of photons carried by the wave. Particularly, we are interested in showing how much it changes our prediction of the intensity when polarization is considered rigorously as in equation (17). The other intensity components Q, U and V are related to other effects, intrinsic to polarization, and will be analysed successively.

5.1. *Multiple Scattering Intensities*

The I component of the intensity vector is equivalent to the intensity of the scalar model. Therefore, this magnitude has similar properties. The higher the order of emission the lower the corresponding intensity. This renders the addition of the first two orders—one and two collisions, respectively—responsible for the main part of the total emission for almost all target materials within a wide range of excitation energies. See Fig. 4 for the possible combinations giving second-order intensity terms.

As we have seen before, the absence of polarization in unpolarized γ-rays is mathematically expressed by means of two oppositely polarized beams (the ϵ vectors are perpendicular to each other) of the same intensity. Hence, a monochromatic and collimated source of I_0 unpolarized photons $\mathrm{cm}^{-2}\,\mathrm{s}^{-1}$ is represented by the source function

$$\mathscr{S}^{(L)}(\omega, \lambda) = \frac{I_0}{2}\delta(\omega - \omega_0)\,\delta(\lambda - \lambda_0)\begin{bmatrix}1\\1\\0\\0\end{bmatrix}. \quad (45)$$

If a represents any of the processes of interest, its corresponding matrix kernel [see equation (23)] has the reduced expression

$$\mathbb{K}_a^{(L)}(\omega, \lambda, \omega', \lambda') = k_a(\omega, \lambda, \omega', \lambda') \times \begin{bmatrix} a_{11} & a_{12} & 0 & 0\\ a_{12} & a_{22} & 0 & 0\\ 0 & 0 & a_{33} & 0\\ 0 & 0 & 0 & a_{44}\end{bmatrix}. \quad (46)$$

This matches all of the kernels of interest in Section 4 and agrees with the symmetry relations of the scattering processes (Van de Hulst, 1957). In equation (46) $k_a(\omega, \lambda, \omega', \lambda')$ is the scalar kernel depending on the average polarization, and the non-null matrix elements a_{ij} are shown explicitly. Substitution of equations (45) and (46) into the solution of the transport equation gives, for the first-order, one-collision chain

$$(\omega_0, \lambda_0) \xrightarrow{a} (\omega, \lambda)$$

$$\mathbf{I}_{(a)I}^{(1)(S)}(\omega, \lambda) = A(\eta_0, \lambda_0, \eta, \lambda) \times k_a(\omega, \lambda, \omega_0, \lambda_0) = \mathbf{I}_{(a)}^{(1)}(\omega, \lambda). \quad (47a)$$

Equation (47a) is for the generic interaction a (Fernández and Molinari, 1993) and illustrates the first-order intensities in both theories are equal. We have defined the auxiliary function A

$$A(\eta_1, \lambda_1, \eta_2, \lambda_2) = \frac{(1 + \operatorname{sgn}\eta_1)}{2}\frac{(1 - \operatorname{sgn}\eta_2)}{2} \times \frac{I_0}{|\eta_1|}\frac{1}{\dfrac{\mu_1}{|\eta_1|} + \dfrac{\mu_2}{|\eta_2|}}. \quad (47b)$$

The other Stokes components of the first order vector intensity are

$$\mathbf{I}_{(a)Q}^{(1)(S)}(\omega, \lambda) = \tfrac{1}{2}A(\eta_0, \lambda_0, \eta, \lambda)k_a(\omega, \lambda, \omega_0, \lambda_0) \times (a_{11} - a_{22})\cos 2\Psi, \quad (47c)$$

$$\mathbf{I}_{(a)U}^{(1)(S)}(\omega, \lambda) = \tfrac{1}{2}A(\eta_0, \lambda_0, \eta, \lambda)k_a(\omega, \lambda, \omega_0, \lambda_0) \times (a_{11} - a_{22})\sin 2\Psi, \quad (47d)$$

$$\mathbf{I}_{(a)V}^{(1)(S)}(\omega, \lambda) = 0, \quad (47e)$$

where Ψ is given by equation (11c) with ω_0 in place of ω'.

Equivalently, we can represent the first-order vector intensity $\mathbf{I}_{(a)}^{(1)(S)}$ decomposed into two beams, the unpolarized and the polarized fractions, given by

$$\mathbf{I}_{(a)}^{(1)(S)} = \mathbf{I}_{(a)}^{(1)(S)u} + \mathbf{I}_{(a)}^{(1)(S)p}, \quad (48a)$$

where

$$\mathbf{I}_{(a)}^{(1)(S)u} = \tfrac{1}{2}A(\eta_0, \lambda_0, \eta, \lambda)k_a(\omega, \lambda, \omega_0, \lambda_0) \times (2a_{11} + a_{12} + a_{21})\begin{bmatrix}1\\0\\0\\0\end{bmatrix}, \quad (48b)$$

$$\mathbf{I}_{(a)}^{(1)(S)p} = \tfrac{1}{2}A(\eta_0, \lambda_0, \eta, \lambda)k_a(\omega, \lambda, \omega_0, \lambda_0) \times (a_{22} - a_{11})\begin{bmatrix}1\\\cos 2\Psi\\\sin 2\Psi\\0\end{bmatrix}. \quad (48c)$$

The polarized fraction $\mathbf{I}_{(a)}^{(1)(S)p}$ represents a beam linearly polarized along a plane forming an angle ψ with the scattering plane. It is worth noting that equation

(48a) can be expressed as a function of the degree of polarization [see equation (5e)]

$$\mathbf{I}_{(a)}^{(1)(S)} = A(\eta_0, \lambda_0, \eta, \lambda) k_a(\omega, \lambda, \omega_0, \lambda_0) \times \left\{ P_a \begin{bmatrix} 1 \\ \cos 2\Psi \\ \sin 2\Psi \\ 0 \end{bmatrix} + (1 - P_a) \begin{bmatrix} 1 \\ 0 \\ 0 \\ 0 \end{bmatrix} \right\}, \quad (48d)$$

where

$$P_a(\omega, \lambda, \omega', \lambda') = \frac{(\mathbf{I}_{(a)Q}^{(1)2} + \mathbf{I}_{(a)U}^{(1)2} + \mathbf{I}_{(a)V}^{(1)2})}{\mathbf{I}_{(a)I}^{(1)}} = \tfrac{1}{2}(a_{22} - a_{11}). \quad (49)$$

Equation (49) is the explicit expression of the *degree of polarization* for the interaction a. It is the fraction of polarized (scattered) radiation after one single scattering collision

$$(\omega', \lambda') \xrightarrow{a} (\omega, \lambda).$$

The second-order intensity due to the collision chain

$$(\omega_0, \lambda_0) \xrightarrow{a} (\omega', \lambda') \xrightarrow{b} (\omega, \lambda)$$

involving two generic interactions a and b (Fernandez, 1993a) is given by

$$\mathbf{I}_{(a,b)I}^{(2)(S)}(\omega, \lambda) = A(\eta_0, \lambda_0, \eta, \lambda) \int_0^\infty d\lambda' \int_{4\pi} d\omega' \frac{1}{|\eta'|} \times \left\{ \frac{(1 + \operatorname{sgn}\eta')}{2} \frac{k_b(\omega, \lambda, \omega', \lambda') k_a(\omega, \lambda, \omega_0, \lambda_0)(1 + \mathcal{G}_{ab}(\omega, \lambda, \omega', \lambda', \omega_0, \lambda_0))}{\frac{\mu}{|\eta|} + \frac{\mu'}{|\eta'|}} + \frac{(1 - \operatorname{sgn}\eta')}{2} \frac{k_b(\omega, \lambda, \omega', \lambda') k_a(\omega', \lambda', \omega_0, \lambda_0)(1 + \mathcal{G}_{ab}(\omega, \lambda, \omega', \lambda', \omega_0, \lambda_0))}{\frac{\mu_0}{|\eta_0|} + \frac{\mu'}{|\eta'|}} \right\}. \quad (50a)$$

When compared to the expression for the same intensity deduced from the scalar model (with average polarization kernels), there is a difference of a corrective factor $\mathcal{G}_{ab}(\omega, \lambda, \omega', \lambda', \omega_0, \lambda_0)$ which is defined as

$$\mathcal{G}_{ab}(\omega, \lambda, \omega', \lambda', \omega_0, \lambda_0) = P_b(\omega, \lambda, \omega', \lambda') \times P_a(\omega', \lambda', \omega_0, \lambda_0) \cos 2(\Psi_a + \Psi'_b). \quad (50b)$$

$P_a(\omega, \lambda, \omega', \lambda')$ is given by equation (49), and Ψ_a and Ψ'_b are the angles of a spherical triangle (as in Fig. 2, for the interactions a and b, respectively) which are defined by the relationships

$$\cos \Psi_a = \frac{\eta_0 \sqrt{1 - \eta'^2} - \eta' \sqrt{1 - \eta_0^2} \cos(\varphi_0 - \varphi')}{(1 - (\boldsymbol{\omega}' \cdot \boldsymbol{\omega}_0)^2)^{1/2}}, \quad (50c)$$

and

$$\cos \Psi'_b = \frac{\eta \sqrt{1 - \eta'^2} - \eta' \sqrt{1 - \eta^2} \cos(\varphi - \varphi')}{(1 - (\boldsymbol{\omega}' \cdot \boldsymbol{\omega})^2)^{1/2}}. \quad (50d)$$

Subindices a and b denote two valid (probabilistically independent) photon–photon interactions in the low energy γ-ray regime as, for example, the photoelectric, Rayleigh and Compton effects mentioned in Section 4. The expressions for the components Q and U can be also obtained using equation (17), but are substantially more complicated and will not be included in this article. For the second-order we get also

$$\mathbf{I}_{(a,b)V}^{(2)}(\omega, \lambda) = 0, \quad (50e)$$

i.e. the polarized fraction after the second scattering is also linearly polarized. This property was first noted by Spencer (1948) and can be extended to any number of collisions. However, between the first and the second collisions three important properties are changed. The polarized fraction of the beam is the first one, as we shall discuss within the context of Rayleigh and Compton interactions in Section 5.1.3. The second one is the orientation of the line of polarization, which is different for the polarized fractions after one and two collisions. This suggests that by filtering the emitted beam with a polarimeter before detection we are able to separate the contributions from a different number of collisions, in this case, from one and two collisions. This result can be easily extended to higher orders of multiple scattering. The third one is the change in the intensity (component I) which shall be the object of a detailed analysis for the interactions of interest. However, we can make some observations of general character about it. From equations (47a) and (50a) it is easily seen that the scalar model is a first-order

approximation of the I component in the vector model because both descriptions are coincident for the first-order component I. The difference in the second-order intensity is dependent on the extent of the correction $\mathcal{G}$ which does not exist for the scalar model. Conceptually, the difference is that the scalar model uses an averaged polarization state with each interaction, while the vector model updates the correct polarization state after each collision. The validity of the scalar model is supported by the fact that the first-order intensity term is much greater when compared to the higher order intensity terms. However, as we shall see below, second-order contributions involving the Compton effect produce continuous spectra which, although not excessively higher than those predicted with the scalar theory, concentrate the difference in certain portions of the spectrum, making them important for the correct computation.

5.1.1. *Characteristic lines*

The photoionization process contributes to the X-ray spectrum a number of sharp lines that give qualitative and quantitative information about the elements in the target. X-ray fluorescence (XRF), a spectroscopical method of analysis (Bertin, 1975), is based on the existing relation between the line intensities and the composition of the specimen. Certainly, this technique requires the knowledge, as detailed as possible, of all the influences that can modify the intensity of the lines and directly affect the precision of the analysis. On the other hand, the understanding of the changes in the line intensity is necessary for X-ray spectroscopists investigating the atomic parameters involved in the X-ray emission, frequently related to the characteristic lines. The correct prediction of the influence of the experimental conditions on the measurements contributes to appropriate designs of both the experiment and the apparatus, improving the quality of the data.

The study of the multiple scattering of the photoelectric effect in XRF gives a clear example of the theoretical approach used for several decades in X-ray spectrometry: the differential intensity (satisfying the Beer–Lambert attenuation law) is integrated over volume to obtain the intensity contributed by the process. This approach, very intuitive, has two obvious drawbacks. Firstly, with the increase of the multiplicity of scattering, it becomes difficult to write the expression for the differential intensity. Secondly, it is very restrictive in the kind of interactions tractable since it cannot be easily applied to processes with certain complexities, e.g. anisotropy.

The first complete deduction of the primary, secondary and tertiary XRF intensities reported by Sherman (1955, 1959) was performed with that procedure. A decade later Shiraiwa and Fujino (1966), with the same technique, obtained the XRF intensities for polychromatic excitation as a function of the glancing angles of incidence and take-off. These intensities were recently recalculated (Fernández, 1989) applying the solution of the scalar transport equation (10), and the former expressions were corrected. The fourth-order intensity was also found (Fernández and Molinari, 1990), showing the validity of transport theory for the analytical study of higher orders of scattering.

The photons scattered by other processes (i.e. Rayleigh and Compton effects) also contribute to enhance the XRF intensity, modifying the height and the low energy tail of the characteristic lines, and yet the γ-ray lines emitted by radioactive sources (Manninen *et al.*, 1986). Over the past years, there has been a continued interest in revealing this influence. Several authors have attempted calculations of the magnitude of these contributions. The results ranged from a few percent to more than 30% of the first-order characteristic line. They used different approaches, from crude theoretical approximations (Garg *et al.*, 1985; Singh *et al.*, 1987, 1989; Campbell *et al.*, 1989), to Monte Carlo simulations (Rollason *et al.*, 1987; Méray, 1988; Méray and Házi, 1988; He *et al.*, 1990), to a simplified model of photon diffusion with a strong simplification of the anisotropy in the scattering cross-sections (Keith and Loomis, 1978). These results cannot give a satisfactory solution to the problem. In contrast, transport theory has been successfully applied to this problem, giving analytical expressions (Fernández *et al.*, 1990; Fernández, 1992) which describe in detail the four intensity terms corresponding to the possible combinations of one Rayleigh or Compton scattering and one photoelectric collision.

The assumption that the photoelectric interactions are independent of polarization was discussed in Section 4.1. The matrix elements of the polarization kernel verify the condition $\alpha_{11} = \alpha_{12} = \alpha_{22}$. From equation (49) we get $P_P \equiv 0$, and therefore, $\mathcal{G}_{P\alpha} = \mathcal{G}_{\alpha P} \equiv 0$ for any scattering interaction α. Assuming the photoelectric interactions independent of polarization, not only can the first-order intensity (i.e. primary) be calculated with the scalar equation but also the second-order intensities involving any other process, such as Rayleigh or Compton scattering. Following Flügge *et al.* (1972), we should expect to find some difference only in those second order intensities involving transitions from states of vacancy with $j = 3/2$ (L_ℓ, L_α lines) or higher, which we shall not consider in this paper.

The multiple scattering effects on characteristic lines, in the frame of the scalar transport theory, are summarized in the following subsections.

5.1.1.1. Chains involving the pure photoelectric effect. The zeroth-order flux—equation (16)—is independent of the interaction because it is the attenuated source excitation. Therefore, its albedo contribution is zero as may easily be seen.

The first two orders of the XRF intensities can be straightforwardly calculated (Fernández, 1989) from equations (33) and (35)

$$I^{(1)(S)}_{(P)_I}(\omega,\lambda)=\sum_i \delta(\lambda-\lambda_i)\frac{A(\eta_0,\lambda_0,\eta,\lambda_i)}{4\pi} \times Q_{\lambda_i}(\lambda_0)[1-\mathcal{U}(\lambda_0-\lambda_{e_i})], \quad (51)$$

$$I^{(2)(S)}_{(P,P)_I}(\omega,\lambda)=\sum_i \delta(\lambda-\lambda_i)\frac{A(\eta_0,\lambda_0,\eta,\lambda_i)}{4\pi} \times\left\{\sum_j \frac{Q_{\lambda_j}(\lambda_0)Q_{\lambda_i}(\lambda_j)}{2}[1-\mathcal{U}(\lambda_0-\lambda_{e_j})] \times[1-\mathcal{U}(\lambda_j-\lambda_{e_i})]\left\{\frac{|\eta_0|}{\mu_0}\ln\left(1+\frac{\mu_0}{\mu_j|\eta_0|}\right) +\frac{|\eta|}{\mu}\ln\left(1+\frac{\mu}{\mu_j|\eta|}\right)\right\}\right\}, \quad (52)$$

where the auxiliary function A was defined in equation (47b). Both contributions have azimuthal symmetry. Third- and fourth-order intensities have been calculated in a similar way, having recourse to the symbolic algebra program MACSYMA (Fernández and Molinari, 1990).

Since the photoelectric effect is the dominating process in the emission of the characteristic X-rays, the multiple scattering of the pure photoelectric effect has an important weight in the total intensity. However, its importance can fluctuate depending on the absorption properties of the material evaluated at the energies of the participating lines. Besides, a net count of the number of lines contributing to the enhancement is only possible for a given sample and excitation energy. Therefore, the only way to predict the total intensity is by calculating specifically the multiple scattering terms with equations (51) and (52). Third- and fourth-order contributions could be neglected in low-accuracy computations.

It should be noted that the photoelectric enhancement is even possible in pure targets since characteristic photons can produce photoemission in other series of the same species of atom. The L lines, for example, receive enhancement from the excited K lines of the same element. This fact should be kept under consideration for measurements of L series parameters.

5.1.1.2. Chains of mixed interactions involving the photoelectric effect and Rayleigh or Compton scattering. There are four contributions involving one scattering process and one photoelectric effect. Two of them describe the intensity contributed by coherent and incoherent scattered photons that, absorbed by photoelectric effect, result in XRF emission. The other two correspond to Rayleigh and Compton scattering of characteristic radiation to a direction towards the detector. In what follows we shall obtain closed relationships for them, using the results of Section 5.1.

The mathematical complexity in the computation of these intensities depends on whether the scattering is Rayleigh or Compton. The Rayleigh scattering contributions are discrete and have the same energy as the characteristic line that they modify. The intensities contributed by the Compton effect, on the contrary, depend on the coupling between the scattering angle and the energy shift, which introduces some difficulties in the computation.

5.1.1.2.1. Rayleigh–photoelectric: The XRF intensity contributed by the coherently scattered source-beam is obtained by replacing the kernels $\mathcal{K}_a$ and $\mathcal{K}_\ell$ by $\mathcal{K}_R$ and $\mathcal{K}_P$, respectively, and $\mathcal{G}_{RP}\equiv 0$, in equation (50a)

$$I^{(2)(S)}_{(R,P)_I}(\omega,\lambda)=\delta(\lambda-\lambda_i)\frac{A(\eta_0,\lambda_0,\eta,\lambda_i)}{4\pi} \times\frac{\sigma}{Z}Q_{\lambda_i}(\lambda_0)[1-\mathcal{U}(\lambda_0-\lambda_{e_i})] \times\left\{\int_0^{2\pi}d\varphi'\int_0^1\frac{d\eta'}{\eta'}\frac{(1+(\omega'\cdot\omega_0^{(+)})^2)}{\frac{\mu_i}{|\eta|}+\frac{\mu_0}{\eta'}} \times F^2(\lambda_0,\omega'\cdot\omega_0^{(+)},Z)+\int_0^{2\pi}d\varphi' \times\int_0^1\frac{d\eta'}{\eta'}\frac{(1+(\omega'\cdot\omega_0^{(-)})^2)}{\frac{\mu_0}{|\eta_0|}+\frac{\mu_0}{\eta'}} \times F^2(\lambda_0,\omega'\cdot\omega_0^{(-)},Z)\right\}, \quad (53)$$

where

$$\omega_1\cdot\omega_2^{(\pm)}=\pm\eta_1\eta_2+\sqrt{1-\eta_1^2}\sqrt{1-\eta_2^2}\cos(\varphi_1-\varphi_2). \quad (54)$$

The anisotropy of the Rayleigh scattering is given by the square of the dot product of the direction vectors. The anisotropy in this case is along the direction ω_0.

5.1.1.2.2. Photoelectric–Rayleigh: The term due to discrete Rayleigh scattering of XRF characteristic photons towards the detector (i.e. in the ω direction) is given by the substitution of $\mathcal{K}_P$, $\mathcal{K}_R$ and $\mathcal{G}_{PR}\equiv 0$, in equation (50a)

$$I^{(2)(S)}_{(P,R)_I}(\omega,\lambda)=\delta(\lambda-\lambda_i)\frac{A(\eta_0,\lambda_0,\eta,\lambda_i)}{4\pi}\frac{\sigma}{Z}Q_{\lambda_i}(\lambda_0) \times[1-\mathcal{U}(\lambda_0-\lambda_{e_i})] \times\left\{\int_0^{2\pi}d\varphi'\int_0^1\frac{d\eta'}{\eta'}\frac{(1+(\omega'\cdot\omega^{(+)})^2)}{\frac{\mu_i}{|\eta|}+\frac{\mu_i}{\eta'}} \times F^2(\lambda_i,\omega'\cdot\omega^{(+)},Z)+\int_0^{2\pi}d\varphi' \times\int_0^1\frac{d\eta'}{\eta'}\frac{(1+(\omega'\cdot\omega^{(-)})^2)}{\frac{\mu_0}{|\eta_0|}+\frac{\mu_i}{\eta'}}F^2(\lambda_i,\omega'\cdot\omega^{(-)},Z)\right\}. \quad (55)$$

Equation (55) differs from equation (54) in that ω_0 and λ_0 in the integrals have been replaced by ω and λ_i. Therefore, the anisotropy has been shifted from the incidence to the take-off direction. The change of the wavelength has a more subtle effect since it changes the evaluation points of the mass attenuation coefficients which are complicated functions of λ and Z. Clearly, by exchanging the order of the same interactions we obtain different intensity contributions.

5.1.1.2.3. Compton–photoelectric: The intensity contributed by photoelectric absorption of the incoherently scattered photons of the source is given by the substitution of $\mathcal{K}_C$, $\mathcal{K}_P$ and $\mathcal{G}_{CP} \equiv 0$, in equation (50a)

$$
\begin{aligned}
I^{(2)(S)}_{(C,P)_I}(\omega, \lambda) &= \delta(\lambda - \lambda_i)\frac{A(\eta_0, \lambda_0, \eta, \lambda_i)}{2\pi}\frac{\sigma}{\lambda_C} \\
&\times \int_{\lambda_0}^{\lambda_0 + 2\lambda_c} d\lambda' K_{KN}(\lambda', \lambda_0) Q_{\lambda_i}(\lambda') S(\lambda_0, a', Z) \\
&\times [1 - \mathcal{U}(\lambda' - \lambda_{e_i})] \left\{ \int_{\alpha'_1}^{\beta_1} \frac{d\eta'}{\eta'} \frac{\mathcal{U}(\beta'_1 - \alpha'_1)}{\frac{\mu_i}{|\eta|} + \frac{\mu'}{\eta'}} \right. \\
&\times \frac{1}{\sqrt{(1-\eta'^2)(1-\eta_0^2) - (a' - \eta'\eta_0)^2}} \\
&+ \int_{\alpha'_2}^{\beta'_2} \frac{d\eta'}{\eta'} \frac{\mathcal{U}(\beta'_2 - \alpha'_2)}{\frac{\mu_0}{|\eta_0|} + \frac{\mu'}{\eta'}} \\
&\left. \times \frac{1}{\sqrt{(1-\eta'^2)(1-\eta_0^2) - (a' + \eta'\eta_0)^2}} \right\}, \qquad (56)
\end{aligned}
$$

where $a' = 1 + (\lambda_0 - \lambda')/\lambda_C$, $\Delta' = \sqrt{(1-\eta_0^2)(1-a'^2)}$, $\alpha'_1 = \max(0, a'\eta_0 - \Delta')$, $\beta'_1 = \min(1, a'\eta_0 + \Delta')$, $\alpha'_2 = -\min(0, a'\eta_0 + \Delta')$ and $\beta'_2 = -\max(-1, a'\eta_0 - \Delta')$.

5.1.1.2.4. Photoelectric–Compton: The intensity contribution to the XRF photons Compton scattered towards the detector is given by the substitution of $\mathcal{K}_P$, $\mathcal{K}_C$, and $\mathcal{G}_{PC} \equiv 0$, in equation (50a)

$$
\begin{aligned}
I^{(2)(S)}_{(P,C)_I}(\omega, \lambda) &= \frac{A(\eta_0, \lambda_0, \eta, \lambda)}{2\pi}\frac{\sigma}{\lambda_C} K_{KN}(\lambda, \lambda_i) Q_{\lambda_i}(\lambda_0) \\
&\times [1 - \mathcal{U}(\lambda_0 - \lambda_{e_i})] S(\lambda_i, a, Z) \left\{ \int_{\alpha_1}^{\beta_1} \frac{d\eta'}{\eta'} \right. \\
&\times \frac{\mathcal{U}(\beta_1 - \alpha_1)}{\frac{\mu}{|\eta|} + \frac{\mu_i}{\eta'}} \frac{1}{\sqrt{(1-\eta'^2)(1-\eta^2) - (a - \eta'\eta)^2}} \\
&+ \int_{\alpha_2}^{\beta_2} \frac{d\eta'}{\eta'} \frac{\mathcal{U}(\beta_2 - \alpha_2)}{\frac{\mu_0}{|\eta_0|} + \frac{\mu_i}{\eta'}} \\
&\left. \times \frac{1}{\sqrt{(1-\eta'^2)(1-\eta^2) - (a + \eta'\eta)^2}} \right\}, \qquad (57)
\end{aligned}
$$

where $a = 1 + (\lambda_i - \lambda)/\lambda_C$, $\Delta = \sqrt{(1-\eta^2)(1-a^2)}$, $\alpha_1 = \max(0, a\eta - \Delta)$, $\beta_1 = \min(1, a\eta + \Delta)$, $\alpha_2 = -\min(0, a\eta + \Delta)$ and $\beta_2 = -\max(-1, a\eta - \Delta)$.

The integration limits in equation (56) and (57) cannot exceed the extremes -1 and 1. The Heaviside functions indicate the range of validity of the integrals.

The (P, C) intensity is *continuous*, in contrast to the contributions (54), (55) and (56) that are *discrete*. The continuous (P, C) spectrum extends from λ_i to $\lambda_i + 2\lambda_C$ [in energy from $E_i/(1 + 2E_i/(m_0c^2))$ to E_i] and has the effect of modifying the symmetry of the characteristic lines by adding a low energy tail to the peaks (Fernández, 1992).

Equations (54) to (57) describe the chain contribution of one single line of wavelength λ_i. These corrections must be calculated for every characteristic line in the spectrum. The isotropy of the photoelectric effect results in all of the scattering contributions having azimuthal symmetry, i.e. the intensities are constant along the border of a cone of aperture $\vartheta = \arccos(|\eta|)$ and uniform radius.

5.1.1.3. *Some examples for single and composite materials.* The integrals in the above equations were evaluated numerically with a Romberg algorithm (Press *et al.*, 1989) to compute the points in the examples. The outer integrals (when applicable) were calculated with a trapezoidal algorithm over meshes of 20 intervals.

Second- and third-order photoeffect contributions, for the Cr $K\alpha$ line of one infinitely thick alloy specimen, are displayed in Fig. 6 in units of the first-order intensity of the line, showing the relative contribution of some single terms of photoelectric correction. The second-order is the most important correction over all the range of E_0. For this example the second-order contribution is on the order of 30–60% of the primary beam. It can even exceed the primary intensity under certain conditions. The third-order can achieve a few percent as in the example,

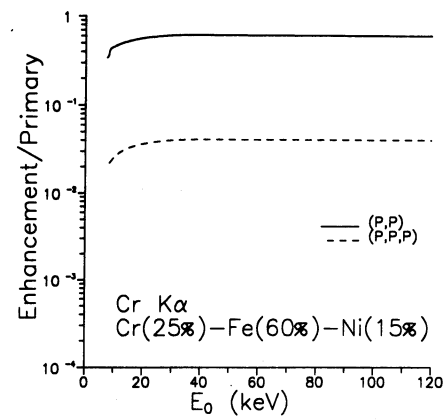

Fig. 6. Second- and third-order photoelectric effect contributions to the characteristic line Cr $K\alpha$ shown for the ternary alloy Cr(25%)–Fe(60%)–Ni(15%). The multiple scattering terms, calculated with transport theory, are plotted in units of first-order intensity [equation (51)].

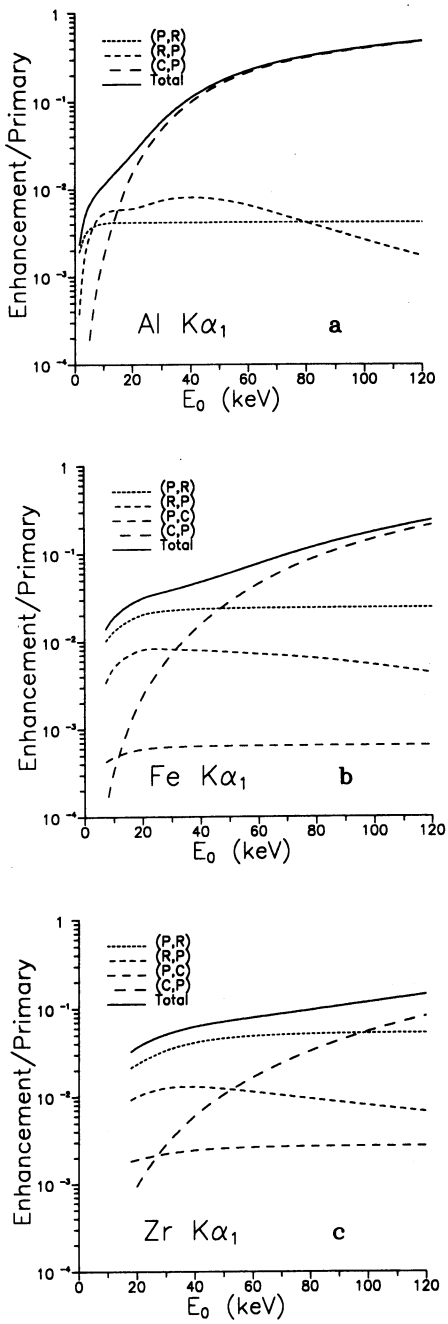

Fig. 7. Components of the scattering interference to the $K\alpha_1$ line (in units of the first-order intensity term for the characteristic line) as a function of the incident beam energy are plotted (a) Al, (b) Fe and (c) Zr. The incidence and take-off directions are defined by $\vartheta_0 = 45°$, $\vartheta = 135°$, $\varphi = \varphi_0 = 0°$ (from Fernández, 1992).

while the fourth-order (not shown in the figure) is normally below 1%.

The intensities contributed by scattering are strongly dependent on E_0. The total contribution to the XRF intensity and the single scattering components (relative to the first-order intensity of the line) are plotted in Fig. 7(a)–(c) for the $K\alpha_1$ lines of

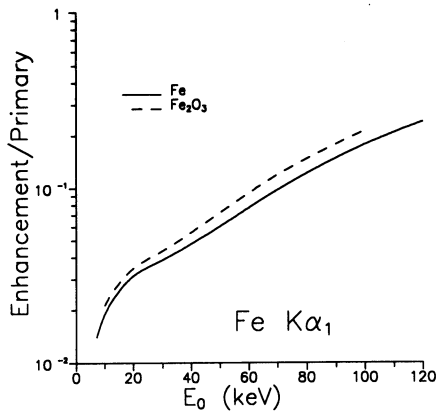

Fig. 8. The enhancement of the Fe $K\alpha_1$ line in the iron and iron oxide due to scattering. This illustrates that the lighter matrix of the oxide favours the scattering (from Fernández, 1992).

Al, Fe and Zr, and for right angle scattering with $\vartheta_0 = 45°$, $\vartheta = 135°$, $\varphi_0 = \varphi = 0$. The energy of the absorption edge marks the start point of the emission in the graphs. The Rayleigh contribution prevails in the low energy region. The Compton contributions grow monotonically and can achieve an important percent of the line. In practice, however, the coherent corrections are important at low excitation energy (higher photoelectric probability).

In respect to Fig. 7, there are no emissions for energies lower than the K-absorption edge. The total intensity contributed by scattering increases monotonically with the excitation energy. The (P, R) intensity dominates for low E_0, except in a light element like Al. The (C, P) intensity prevails for high E_0. In all the cases the total correction becomes greater for increasing E_0, and is more important in light elements. Note that the scattering contribution in

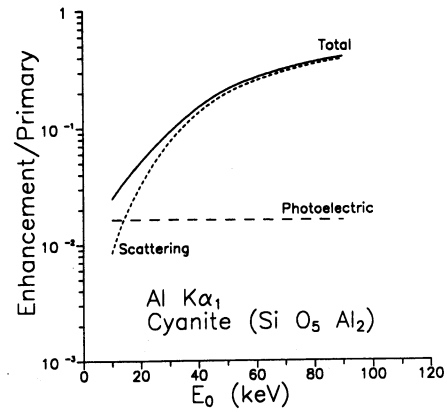

Fig. 9. The secondary XRF (P, P) and the scattering enhancement are the two components of the total second-order intensity modifying the intensity of the characteristic lines. Both components are plotted between 10 and 90 keV for the Al $K\alpha_1$ line of a geological sample (SiO_5Al_2). The scattering contribution, very important in this case, due to the presence of oxygen, is practically the prevailing enhancer (from Fernández, 1992).

those samples is almost always greater than 1%. Similar plots for all the elements between $Z = 11$ and 42 have been recently published (Fernández and Molinari, 1992).

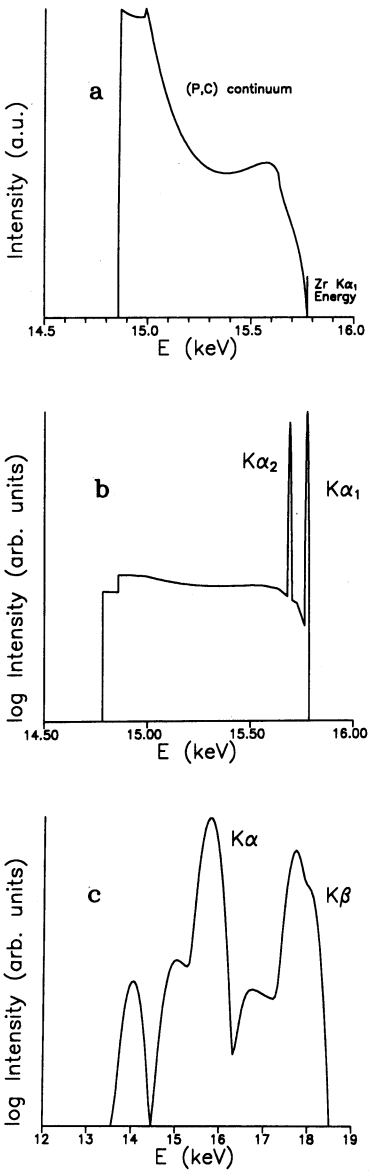

Fig. 10. The (P, C) continuous intensity emitted by a pure Zr sample ($E_0 = 20$ keV, $\vartheta_0 = 45°$, $\vartheta = 135°$, $\varphi = \varphi_0 = 0°$). (a) The theoretical shape of the low energy tail [calculated with equation (57)] is plotted for the Zr $K\alpha_1$ line. The position of the discrete line is marked on the right side of the continuous distribution. The height of the monochromatic line has no meaning. (b) The $K\alpha$ doublet spectrum calculated with the code SHAPE. The lines are represented with gaussians having the natural line width, and are overlapped to the low energy tails of both lines. (c) The K emission spectrum modified by the response of a Si solid-state detector of standard resolution (calculated with SHAPE). From left to right, the escape $K\alpha$, and the unresolved peaks $K\alpha$ and $K\beta$. The shoulders on the left of the peaks are produced by the continuous contributions (P, C). These theoretical data agree with experimental data.

A lighter matrix favours a greater scattering contribution, as is shown in Fig. 8. Figure 9 displays the enhancement to the Al $K\alpha_1$ line for a geological specimen as a function of the energy. For E_0 greater than 13 keV the total scattering intensity exceeds the (P, P) correction. Clearly, any attempt to quantify the matrix effects with only the photoelectric enhancement will fail in this sample.

In EDXRF all of the lines of the spectrum are produced with the same source of excitation. Lines from different edges will suffer different enhancement by scattering. The greater the separation between E_0 and the absorption edge energy, the greater the scattering contribution on the corresponding line. A polychromatic source, an X-ray tube for example, will contribute to the scattering enhancement predominantly in the high energy portion of the spectrum, while the low energy part will contribute through the pure photoeffect.

The (P, C) chain contributes one continuum spectrum which is exemplified in Fig. 10 for a single line $K\alpha_1$, for a doublet $K\alpha$ and for two doublets $K\alpha$ and $K\beta$ modified by the response of the detector. In the two last cases, the height of the correction is compared with that of the characteristic lines. For a given target, the shape of this spectrum varies with E_0, ϑ_0 and ϑ (Fernández, 1992). The (P, C) spectrum overlaps the low energy tail of the peak modifying the symmetry of the line. For low and medium Z characteristic lines of pure elements, the (P, C) spectrum is too weak to be detected experimentally, although this contribution becomes certainly more important in lines from heavier elements, or from elements embedded in light matrices. A good agreement between the transport results [calculated with the computer code SHAPE (Fernández and Sumini, 1991)] and measurements of elements Y to I in a matrix of starch powder with Si(Li) detectors in four different experimental set-ups was recently found (Kis-Varga and Vegh, 1993). This contribution produces the low energy asymmetry of the peaks, well known by experimental spectroscopists studying the response function of the detectors (McNelles and Campbell, 1975; Jorch and Campbell, 1977; Van Espen *et al.*, 1980) but not accepted as produced by multiple Compton scattering until recently (Campbell *et al.*, 1989; He *et al.*, 1990; Fernández, 1992; Kis-Varga and Vegh, 1993). However, it is worth noting that the process of modification of the line shape is intrinsic to the emission spectrum, and not to the detector response.

5.1.2. The continuous background due to Compton and Rayleigh effects

The energy distribution of once incoherently scattered X- and γ-ray photons, the Compton profile, gives valuable information on the momentum distribution of the electrons (Williams, 1977; Cooper, 1985; Schülke, 1989). The technique is particularly sensitive to the behaviour of the binding electrons

and can be used to test their quantum-mechanical description.

In measurements, multiply scattered photons contribute a continuous spectrum which extends from the excitation energy E_0 towards lower energies overlapping the profile. This interference must be stripped off to obtain acceptable data of the profile. Many authors attempted an analytical description of the multiple scattering spectrum using three approaches: the calculation of the scattered electric field (Dumond, 1930; Williams *et al.*, 1974), the integration of a probabilistic differential intensity (as mentioned in Section 5.1) (Tanner and Epstein, 1976a, 1976b; Braun-Keller and Epstein, 1977a, 1977b), and the Boltzmann equation for radiative transfer (Chandrasekhar, 1948; O'Rourke, 1952, 1953; Brockwell, 1965). Most of these studies were performed with the first two methods. The approximations in the calculations—geometry, attenuation and cross-sections—rendered these results qualitative. The few (and old) transport theory applications on this subject were directed to finding general solutions of the Boltzmann equation rather than single terms of multiple scattering. Curiously, some leading authors in this field considered, for this reason, that transport theory is unable to separate the multiple-order contributions (Halonen *et al.*, 1977). Since the mentioned analytical descriptions were insufficient to correct for the Compton profiles (Cooper, 1985; Halonen *et al.*, 1977), the spectral distribution of multiple events was calculated with Monte Carlo simulation (Felsteiner *et al.*, 1974; Felsteiner and Pattison, 1975; Pitkanen *et al.*, 1986).

However, a detailed analytical solution with recourse either to the scalar transport equation (Fernández, 1991; Fernández and Sumini, 1992) or to the vector transport equation (Fernández, 1993a) is possible, as has been recently demonstrated. In what follows we shall summarize these calculations.

In order to calculate the correction factor $\mathcal{G}$ defined in Section 5.1 we shall use the degrees of polarization defined by equations (34) and (40) for Rayleigh and Compton effects, respectively (see Fig. 5). As the degree of polarization can vary between 0 and 1 depending on the excitation energy and the scattering angle, $\mathcal{G}$ varies within the range of the trigonometric function cosine in equation (50b) (i.e. $[-1, 1]$) weighted by the product of the two degrees of polarization at the corresponding phase-space coordinates for the interactions α and δ.

5.1.2.1. The Rayleigh and Compton peaks. The first-order contributions due to one single scattering in a pure element target are given by

$$I^{(1)(S)}_{(R)_I}(\omega, \lambda) = \delta(\lambda - \lambda_0)\frac{\sigma}{Z}A(\eta_0, \lambda_0, \eta, \lambda_0)\,(1 + (\omega \cdot \omega_0)^2)F^2(\lambda_0, \omega \cdot \omega_0, Z), \quad (58)$$

$$I^{(1)(S)}_{(C)_I}(\omega, \lambda) = \delta(\lambda_0 + \lambda_c(1 - \omega \cdot \omega_0) - \lambda)\sigma K_{KN}(\lambda_0 + \lambda_c \times (1 - \omega \cdot \omega_0), \lambda_0)A(\eta_0, \lambda_0, \eta, \lambda_0 + \lambda_c(1 - \omega \cdot \omega_0))S(\lambda_0, \omega \cdot \omega_0, Z). \quad (59)$$

Equations (58) and (59) give, respectively, the intensities of the Rayleigh and Compton peaks. Since we neglected the motion of the electrons, both peaks are monochromatic for the source and geometry assumed in our model.

5.1.2.2. Double scattering involving the Rayleigh and Compton effects. There are four combinations involving a double scattering with the Rayleigh and the Compton effects: Rayleigh–Rayleigh, Rayleigh–Compton, Compton–Rayleigh and Compton–Compton. Details for the computations can be found elsewhere (Fernández, 1991).

5.1.2.2.1. Rayleigh–Rayleigh: This contribution is calculated by substituting the Rayleigh kernel twice into equation (50a), and setting

$$\begin{aligned} I^{(2)(S)}_{(R,R)_I}(\omega, \lambda) = {} & \delta(\lambda - \lambda_0)\left(\frac{\sigma}{Z}\right)^2 A(\eta_0, \lambda_0, \eta, \lambda_0) \\ & \times \left\{ \int_0^{2\pi} d\varphi' \int_0^1 \frac{d\eta'}{\eta'} \frac{(1 + (\omega' \cdot \omega^{(+)})^2)(1 + (\omega' \cdot \omega_0^{(+)})^2)(1 + \mathcal{G}^{(+)}_{RR}(\omega, \lambda, \omega', \lambda', \omega_0, \lambda_0))}{\frac{\mu_0}{|\eta|} + \frac{\mu_0}{\eta'}} \right. \\ & \times F^2(\lambda_0, \omega' \cdot \omega^{(+)}, Z)F^2(\lambda_0, \omega' \cdot \omega_0^{(+)}, Z) \\ & + \int_0^{2\pi} d\varphi' \int_0^1 \frac{d\eta'}{\eta'} \frac{(1 + (\omega' \cdot \omega^{(-)})^2)(1 + (\omega' \cdot \omega_0^{(-)})^2)(1 + \mathcal{G}^{(-)}_{RR}(\omega, \lambda, \omega', \lambda', \omega_0, \lambda_0))}{\frac{\mu_0}{|\eta_0|} + \frac{\mu_0}{\eta'}} \\ & \left. \times F^2(\lambda_0, \omega' \cdot \omega^{(-)}, Z)F^2(\lambda_0, \omega' \cdot \omega_0^{(-)}, Z) \right\}. \end{aligned} \quad (60a)$$

$$\mathcal{G}^{(\pm)}_{RR}(\omega, \lambda, \omega', \lambda', \omega_0, \lambda_0) = \frac{1 - (\omega' \cdot \omega^{(\pm)})^2}{1 + (\omega' \cdot \omega^{(\pm)})^2} \times \frac{1 - (\omega' \cdot \omega_0^{(\pm)})^2}{1 + (\omega' \cdot \omega_0^{(\pm)})^2} \cos 2(\Psi^{(\pm)}_{\alpha} + \Psi'^{(\pm)}_{\delta}). \quad (60b)$$

The dot products in equations (60a) and (60b) were defined in equation (54), and $\Psi_a^{(\pm)}$ and $\Psi_\delta'^{(\pm)}$ are given by

$$\cos\Psi_a^{(\pm)} = \frac{\eta_0\sqrt{1-\eta'^2} \mp \eta'\sqrt{1-\eta_0^2}\cos(\varphi_0-\varphi')}{(1-(\omega'\cdot\omega_0^{(\pm)})^2)^{1/2}}, \tag{60c}$$

and

$$\cos\Psi_\delta'^{(\pm)} = \frac{\eta\sqrt{1-\eta'^2} \mp \eta'\sqrt{1-\eta^2}\cos(\varphi-\varphi')}{(1-(\omega'\cdot\omega^{(\pm)})^2)^{1/2}}. \tag{60d}$$

The (R, R) intensity overlaps the coherent line of equation (58).

5.1.2.2.2. Compton–Compton: The double scattering of the Compton effect is calculated by substituting the Compton kernel twice in equation (50a)

$$\begin{aligned}
I^{(2)(S)}_{(C,C)_I}(\omega,\lambda) &= \frac{\sigma^2}{\omega_R\lambda_C}A(\eta_0,\lambda_0,\eta,\lambda)\\
&\times\left\{\int_{\beta_1}^{\gamma_1}\frac{d\eta'}{\eta'}\frac{\mathcal{U}(\gamma_1-\beta_1)}{\sqrt{(1-\eta'^2)(1-\eta_R^2)}-(\alpha-\eta'\eta_R)^2}\right.\\
&\times\sum_{k=1}^{2}\frac{K_{KN}(\lambda,\tilde\lambda_k^{(+)})K_{KN}(\tilde\lambda_k^{(+)},\lambda_0)}{\frac{\mu}{|\eta|}+\frac{\mu(\tilde\lambda_k^{(+)})}{\eta'}}\\
&\times S(\tilde\lambda_k^{(+)},\omega\cdot\omega_k'^{(+)},Z)S(\lambda_0,\omega_0\cdot\omega_k'^{(+)},Z)\\
&\times(1+\mathcal{G}_{CC_k}^{(+)}(\omega,\lambda,\omega',\lambda',\omega_0,\lambda_0))\\
&+\int_{\beta_2}^{\gamma_2}\frac{d\eta'}{\eta'}\frac{\mathcal{U}(\gamma_2-\beta_2)}{\sqrt{(1-\eta'^2)(1-\eta_R^2)}-(\alpha+\eta'\eta_R)^2}\\
&\times\sum_{k=1}^{2}\frac{K_{KN}(\lambda,\tilde\lambda_k^{(-)})K_{KN}(\tilde\lambda_k^{(-)},\lambda_0)}{\frac{\mu_0}{|\eta_0|}+\frac{\mu(\tilde\lambda_k^{(-)})}{\eta'}}\\
&\times S(\tilde\lambda_k^{(-)},\omega\cdot\omega_k'^{(-)},Z)S(\lambda_0,\omega_0\cdot\omega_k'^{(-)},Z)\\
&\times\left.(1+\mathcal{G}_{CC_k}^{(-)}(\omega,\lambda,\omega',\lambda',\omega_0,\lambda_0))\right\},
\end{aligned} \tag{61a}$$

$$\begin{aligned}
&\mathcal{G}_{CC_k}^{(\pm)}(\omega,\lambda,\omega',\lambda',\omega_0,\lambda_0)\\
&=\frac{\frac{\lambda-\tilde\lambda_k^{(\pm)}}{\lambda_C}\left(2-\frac{\lambda-\tilde\lambda_k^{(\pm)}}{\lambda_C}\right)}{\frac{\lambda}{\tilde\lambda_k^{(\pm)}}+\frac{\tilde\lambda_k^{(\pm)}}{\lambda}+\frac{\lambda-\tilde\lambda_k^{(\pm)}}{\lambda_C}\left(\frac{\lambda-\tilde\lambda_k^{(\pm)}}{\lambda_C}-2\right)}\\
&\times\frac{\frac{\tilde\lambda_k^{(\pm)}-\lambda_0}{\lambda_C}\left(2-\frac{\tilde\lambda_k^{(\pm)}-\lambda_0}{\lambda_C}\right)}{\frac{\lambda_0}{\tilde\lambda_k^{(\pm)}}+\frac{\tilde\lambda_k^{(\pm)}}{\lambda_0}+\frac{\tilde\lambda_k^{(\pm)}-\lambda_0}{\lambda_C}\left(\frac{\tilde\lambda_k^{(\pm)}-\lambda_0}{\lambda_C}-2\right)}\\
&\times\cos 2(\Psi_{a_k}^{(\pm)}+\Psi_{\delta_k}'^{(\pm)})
\end{aligned} \tag{61b}$$

where

$$\cos\Psi_{a_k}^{(\pm)} = \frac{\eta_0\sqrt{1-\eta'^2} \mp \eta'\sqrt{1-\eta_0^2}\cos(\varphi_0-\varphi_k'^{(\pm)})}{(1-(\omega_0\cdot\omega_k'^{(\pm)})^2)^{1/2}}, \tag{61c}$$

and

$$\cos\Psi_{\delta_k}'^{(\pm)} = \frac{\eta\sqrt{1-\eta'^2} \mp \eta'\sqrt{1-\eta^2}\cos(\varphi-\varphi_k'^{(\pm)})}{(1-(\omega\cdot\omega_k'^{(\pm)})^2)^{1/2}}. \tag{61d}$$

For convenience, we have introduced $\beta_1 = \max(0, \alpha\eta_R - D)$, $\gamma_1 = \min(1, \alpha\eta_R + D)$, $\beta_2 = -\min(0, \alpha\eta_R + D)$, $\gamma_2 = -\max(-1, \alpha\eta_R - D)$ and the quantities

$$\tilde\lambda_k^{(\pm)} = \lambda_0 + \lambda_c(1-\omega_0\cdot\omega_k'^{(\pm)}), \tag{61e}$$

$$\omega_0\cdot\omega'^{(\pm)}{}_k = \pm\eta'\eta_0 + \sqrt{1-\eta'^2}\sqrt{1-\eta_0^2}\cos(\varphi_k'^{(\pm)}-\varphi_0), \tag{61f}$$

$$\omega\cdot\omega'^{(\pm)}{}_k = \pm\eta'\eta + \sqrt{1-\eta'^2}\sqrt{1-\eta^2}\cos(\varphi_k'^{(\pm)}-\varphi), \tag{61g}$$

which are defined in terms of the following functions of η_0, φ_0, λ_0, η, φ, λ, and (the scattering angle) Θ

$$\omega_R = |\omega+\omega_0| = \sqrt{2(1+\omega\cdot\omega_0)} = 2\cos\frac{\Theta}{2}, \tag{61h}$$

$$\alpha = \frac{1}{\omega_R}\left(2+\frac{\lambda_0-\lambda}{\lambda_c}\right), \tag{61i}$$

$$\eta_R = \frac{\eta+\eta_0}{\omega_R}, \tag{61j}$$

$$\varphi_R = \arccos\left(\frac{\sqrt{1-\eta_0^2}+\sqrt{1-\eta^2}\cos\varphi}{\sqrt{\omega_R^2-(\eta_0-\eta)^2}}\right), \tag{61k}$$

$$D = \sqrt{(1-\eta_R^2)(1-\alpha^2)}, \tag{61l}$$

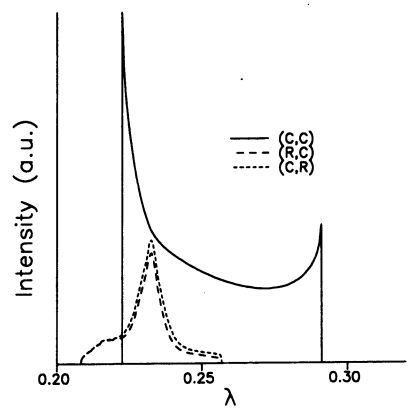

Fig. 11. Characteristic shape of the double scattering contributions due to the combined influence of the Compton and Rayleigh effects. Calculations are for Al excited with 59.54 keV (γ line of ^{241}Am) and for the geometry defined by the incidence and take-off polar angles $\vartheta_0 = 45°$, $\vartheta = 135°$ and azimuthal angles of $\varphi_0 = \varphi = 0$ (from Fernández, 1991).

$$\varphi_1'^{(\pm)} = \varphi_R + \arccos\left(\frac{\alpha \mp \eta'\eta_R}{\sqrt{(1-\eta'^2)(1-\eta_R^2)}}\right), \quad (61m)$$

$$\varphi_2'^{(\pm)} = 2\pi + \varphi_R - (\varphi_1'^{(\pm)} - \varphi_R). \quad (61n)$$

The integration limits β_i and γ_i cannot exceed the values -1 and 1. The Heaviside functions in the integrals are different from zero only when $\gamma_i > \beta_i$ and indicate the validity range of every integral. The (C, C) intensity is continuous, in contrast to the preceding contribution. Its wavelength spectrum extends from $\lambda_0 + \lambda_C(2-\omega_R)$ to $\lambda_0 + \lambda_C(2+\omega_R)$ and has the characteristic shape shown in Fig. 11. Equation (61) is valid for $\omega_R \neq 0$, $\alpha^2 \neq 1$ and $\eta_R^2 \neq 1$. Limit cases for the special values of ω_R, η_R and α can be calculated similarly.

5.1.2.2.3. Rayleigh–Compton: The contribution of Compton scattering of Rayleigh scattered photons is obtained similarly to equation (61)

$$I^{(2)}_{(R,C)_I}(\omega, \lambda) = \frac{\sigma^2}{Z\lambda_C} A(\eta_0, \lambda_0, \eta, \lambda) K_{KN}(\lambda, \lambda_0) S(\lambda_0, a, Z)$$
$$\times \left\{ \int_{\beta_1}^{\gamma_1} \frac{d\eta'}{\eta'} \frac{1}{\frac{\mu}{|\eta|} + \frac{\mu_0}{\eta'}} \frac{\mathcal{U}(\gamma_1 - \beta_1)}{\sqrt{(1-\eta'^2)(1-\eta^2) - (a - \eta'\eta)^2}} \right.$$
$$\times \sum_{k=1}^{2} (1 + (\omega_0 \cdot \omega_k'^{(+)})^2) F^2(\lambda_0, \omega_0 \cdot \omega_k'^{(+)}, Z)$$
$$\times (1 + \mathcal{G}^{(+)}_{RC_k}(\omega, \lambda, \omega', \lambda', \omega_0, \lambda_0))$$
$$+ \int_{\beta_2}^{\gamma_2} \frac{d\eta'}{\eta'} \frac{1}{\frac{\mu_0}{|\eta_0|} + \frac{\mu_0}{\eta'}} \frac{\mathcal{U}(\gamma_2 - \beta_2)}{\sqrt{(1-\eta'^2)(1-\eta^2) - (a + \eta'\eta)^2}}$$
$$\times \sum_{k=1}^{2} (1 + (\omega_0 \cdot \omega_k'^{(-)})^2) F^2(\lambda_0, \omega_0 \cdot \omega_k'^{(-)}, Z)$$
$$\left. \times (1 + \mathcal{G}^{(-)}_{RC_k}(\omega, \lambda, \omega', \lambda', \omega_0, \lambda_0)) \right\}, \quad (62a)$$

$$\mathcal{G}^{(\pm)}_{RC_k}(\omega, \lambda, \omega', \lambda', \omega_0, \lambda_0)$$
$$= \frac{\frac{\lambda - \lambda_0}{\lambda_C}\left(2 - \frac{\lambda - \lambda_0}{\lambda_C}\right)}{\frac{\lambda}{\lambda_0} + \frac{\lambda_0}{\lambda} + \frac{\lambda - \lambda_0}{\lambda_C}\left(\frac{\lambda - \lambda_0}{\lambda_C} - 2\right)}$$
$$\times \frac{1 - (\omega_0 \cdot \omega_k'^{(\pm)})^2}{1 + (\omega_0 \cdot \omega_k'^{(\pm)})^2} \cos 2(\Psi^{(\pm)}_{a_k} + \Psi'^{(\pm)}_{\delta_k}) \quad (62b)$$

where $\Psi^{(\pm)}_{a_k}$ is defined as in equation (61c) and $\Psi'^{(\pm)}_{\delta_k}$ is given by

$$\cos \Psi'^{(\pm)}_{\delta_k} = \frac{\eta\sqrt{1-\eta'^2} \mp \eta'\sqrt{1-\eta^2}\cos(\varphi - \varphi_k'^{(\pm)})}{(1-a^2)^{1/2}}, \quad (62c)$$

$\beta_1 = \max(0, a\eta - D)$, $\gamma_1 = \min(1, a\eta + D)$, $\beta_2 = -\min(0, a\eta + D)$, $\gamma_2 = -\max(-1, a\eta - D)$ and $\omega_0 \cdot \omega_k'^{(\pm)}$—as in equation (61f)—are defined in terms of

$$a = 1 + \frac{\lambda_0 - \lambda}{\lambda_C}, \quad (62d)$$

$$D = \sqrt{(1-\eta^2)(1-a^2)}, \quad (62e)$$

$$\varphi_1'^{(\pm)} = \varphi + \arccos\left(\frac{a \mp \eta'\eta}{\sqrt{(1-\eta'^2)(1-\eta^2)}}\right), \quad (62f)$$

and

$$\varphi_2'^{(\pm)} = 2\pi + \varphi - (\varphi_1'^{(\pm)} - \varphi). \quad (62g)$$

The meaning of the limits β_i and γ_i is as in equation (61a). The (R, C) intensity is continuous and its wavelength spectrum extends from λ_0 to $\lambda_0 + 2\lambda_C$ (in energy from $E_0/(1 + 2E_0/(m_0c^2))$ to E_0); therefore it overlaps partially the (C, C) spectrum. The shape of the (R, C) spectrum is shown in Fig. 11. The characteristic maximum at the energy of the Compton line broadens the profile.

5.1.2.2.4. Compton–Rayleigh: The Rayleigh scattering of Compton scattered photons is obtained similarly

$$I^{(2)}_{(C,R)_I}(\omega, \lambda) = \frac{\sigma^2}{Z\lambda_C} A(\eta_0, \lambda_0, \eta, \lambda) K_{KN}(\lambda, \lambda_0) S(\lambda_0, a, Z)$$
$$\times \left\{ \int_{\beta_1}^{\gamma_1} \frac{d\eta'}{\eta'} \frac{1}{\frac{\mu}{|\eta|} + \frac{\mu}{\eta'}} \frac{\mathcal{U}(\gamma_1 - \beta_1)}{\sqrt{(1-\eta'^2)(1-\eta_0^2) - (a - \eta'\eta_0)^2}} \right.$$
$$\times \sum_{k=1}^{2} (1 + (\omega \cdot \omega_k'^{(+)})^2) F^2(\lambda, \omega \cdot \omega_k'^{(+)}, Z)$$
$$\times (1 + \mathcal{G}^{(+)}_{CR_k}(\omega, \lambda, \omega', \lambda', \omega_0, \lambda_0))$$
$$+ \int_{\beta_2}^{\gamma_2} \frac{d\eta'}{\eta'} \frac{1}{\frac{\mu_0}{|\eta_0|} + \frac{\mu}{\eta'}} \frac{\mathcal{U}(\gamma_2 - \beta_2)}{\sqrt{(1-\eta'^2)(1-\eta_0^2) - (a + \eta'\eta_0)^2}}$$
$$\times \sum_{k=1}^{2} (1 + (\omega \cdot \omega_k'^{(-)})^2) F^2(\lambda, \omega \cdot \omega_k'^{(-)}, Z)$$
$$\left. \times (1 + \mathcal{G}^{(-)}_{CR_k}(\omega, \lambda, \omega', \lambda', \omega_0, \lambda_0)) \right\}, \quad (63a)$$

$$\mathcal{G}^{(\pm)}_{CR_k}(\omega, \lambda, \omega', \lambda', \omega_0, \lambda_0)$$
$$= \frac{\frac{\lambda - \lambda_0}{\lambda_C}\left(2 - \frac{\lambda - \lambda_0}{\lambda_C}\right)}{\frac{\lambda}{\lambda_0} + \frac{\lambda_0}{\lambda} + \frac{\lambda - \lambda_0}{\lambda_C}\left(\frac{\lambda - \lambda_0}{\lambda_C} - 2\right)}$$
$$\times \frac{1 - (\omega \cdot \omega_k'^{(\pm)})^2}{1 + (\omega \cdot \omega_k'^{(\pm)})^2} \cos 2(\Psi^{(\pm)}_{a_k} + \Psi'^{(\pm)}_{\delta_k}) \quad (63b)$$

where $\Psi'^{(\pm)}_{\delta_k}$ is defined as in equation (61d) and $\Psi^{(\pm)}_{a_k}$ is given by

$$\cos \Psi^{(\pm)}_{a_k} = \frac{\eta_0\sqrt{1-\eta'^2} \mp \eta'\sqrt{1-\eta_0^2}\cos(\varphi_0 - \varphi_k'^{(\pm)})}{(1-a^2)^{1/2}}, \quad (63c)$$

$\beta_1 = \max(0, a\eta_0 - D)$, $\gamma_1 = \min(1, a\eta_0 + D)$, $\beta_2 = -\min(0, a\eta_0 + D)$, $\gamma_2 = -\max(-1, a\eta_0 - D)$, and $\omega \cdot \omega_k'^{(\pm)}$—as in equation (61g)—are defined in terms of

$$a = 1 + \frac{\lambda_0 - \lambda}{\lambda_C}, \quad (63d)$$

$$D = \sqrt{(1-\eta_0^2)(1-a^2)}, \quad (63e)$$

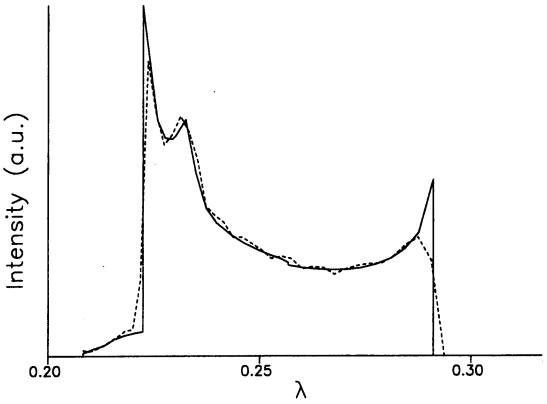

Fig. 12. Analytical prediction (——) of a second-order spectrum [(C, C) + (C, R) + (R, C))] compared to a 50,000 histories MC simulation (- - -) under the same conditions assumed in Sections 2 and 3. The target is Al excited with 59.54 keV at $\vartheta_0 = 45°$, $\vartheta = 135°$, $\varphi_0 = \varphi = 0$ (from Sartori and Fernández, 1992).

$$\varphi_1'^{(\pm)} = \varphi_0 + \arccos\left(\frac{a \mp \eta'\eta_0}{\sqrt{(1-\eta'^2)(1-\eta_0^2)}}\right), \quad (63f)$$

and

$$\varphi_2'^{(\pm)} = 2\pi + \varphi_0 - (\varphi_1'^{(\pm)} - \varphi_0). \quad (63g)$$

The meaning of the limits β_i and γ_i is as in the preceding equation. The (C, R) intensity is continuous and its wavelength spectrum extends from λ_0 to $\lambda_0 + 2\lambda_C$ (as in the preceding case). Therefore, it overlaps partially the (C, C) and fully the (R, C) spectra. The shape of the (C, R) spectrum is similar but not equal to that of (R, C) as shown in Fig. 11.

5.1.2.3. Higher orders of scattering. The analytical results of the scalar equation were checked with a Monte Carlo computer simulation (Sartori and Fernández, 1992) reproducing the same physical problem described in Section 3. The predicted MC spectrum matches closely the analytical one, as is shown in Fig. 12. There are three "peaks" well differentiated, two of which belong to the extremes of the (C, C) distribution, and the central one being the peaked distribution due to the sum of the (C, R) plus the (R, C) intensities whose maximum coincides with the Compton peak energy. Depending on the target, the excitation wavelength, and the geometry, the three peaks can look like two, or like only one.

Since analytical expressions are still not available for the third- and fourth-order components, they were simulated with the mentioned Monte Carlo program. Figure 13 displays the spectra for O, Al and Cu. With regard to the figure, higher order scattering becomes more important for light elements. These spectra were normalized to unit intensity. Between them their ratios are 1 : 20 : 40 for the Cu : Al : O. Another aspect of quantification is the height of the coherent line (near the right side in the plots) that becomes more important for increasing Z. Third- and fourth-order contributions cannot be neglected in low Z targets. The results show that multiple Compton scattering gives the most important contribution in every case. These contributions are very important in light elements, but can be safely neglected in the medium Z range.

5.1.2.4. Some examples for pure targets. Under the assumptions of this work, the first-order Compton term gives a "broad" monochromatic line, whereas the multiple-order terms with the Compton effect contribute continuous spectra. Therefore, the terms of the Neumann series of equation (15) can be associated with different shapes in the spectrum, having an almost identical experimental manifestation. This fact supports the validity of the iterative approach applied in Section 4.

In what follows, we shall summarize some properties characterizing the continuous spectra due to double scattering of γ-rays in pure element targets.

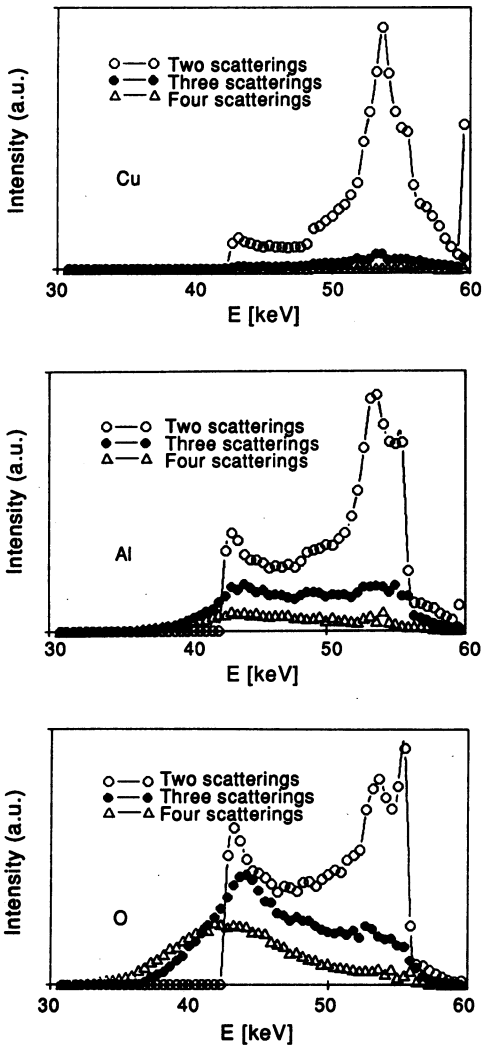

Fig. 13. Two-, three- and four-collision total intensities simulated with MC for three elements excited with the same energy $E_0 = 59.54$ keV (from Sartori and Fernández, 1992).

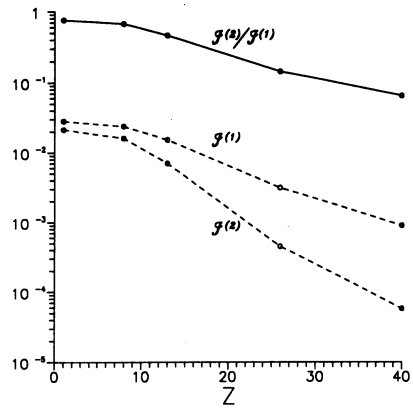

Fig. 14. The single and double scattering integrated intensities describe the overall contribution of the corresponding order of scattering. These are plotted as a function of the atomic number Z of the target for some representative elements (H, O, Al, Fe, Zr), angles $\vartheta_0 = 45°$, $\vartheta = 135°$, $\varphi_0 = \varphi = 0°$, and an excitation of 59.54 keV. The double-to-single-intensity ratio $\mathcal{J}^{(2)}/\mathcal{J}^{(1)}$, measuring the importance of the continuous second order area $[(C, C) + (C, R) + (R, C)]$ relative to the intensity of the Compton peak, is plotted as a solid line in the same graph.

Figure 14 shows the behaviour of the Compton peak intensity, the total double scattering intensity under the Compton peak, and its ratio as a function of Z. The ratio vanishes for increasing Z, rendering cleaner the Compton profile. For low Z, double scattering can be high (>70% of the Compton peak for H) and, therefore, higher orders of multiple scattering should be calculated.

Figure 15 displays the single intensity terms due to double scattering as a function of Z to show its relative importance. The (C, C) term decreases monotonically, whereas the mixed scattering terms, (R, C) and (C, R), reach a maximum near Al and decrease with lower slope than the chain (C, C). Near Fe the three components contribute similar fractions of the total. For elements lighter than Fe the (C, C) intensity dominates. For heavier elements the other components become higher than the (C, C), and their peaked shape produce a greater distortion of the Compton profile. Note that the sum of the mixed components reach first the (C, C) level near Ca.

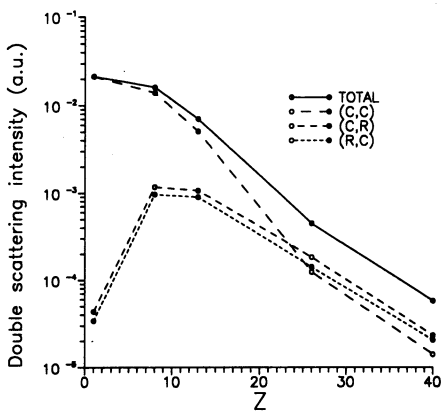

Fig. 15. Partial double scattering intensities as a function of the atomic number Z. The (C, C), (C, R) and (R, C) continuous contributions are plotted as dashed line. The total double scattering is plotted with a solid line. Angles are $\vartheta_0 = 45°$, $\vartheta = 135°$, $\varphi_0 = \varphi = 0°$, and energy is 59.54 keV.

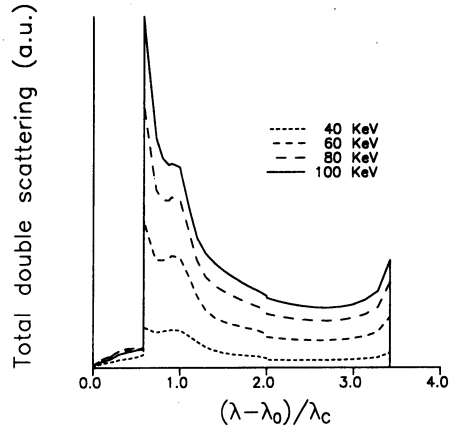

Fig. 16. Total double scattering spectrum in Al as a function of the ratio $(\lambda - \lambda)/\lambda_c$ for several incidence energies E_0. The angles are $\vartheta_0 = 45°$, $\vartheta = 135°$, $\varphi_0 = \varphi = 0°$.

The excitation wavelength λ_0 (energy E_0) determines the position of the intervals for both the attenuation of the beam into the target and the next scattering. Figure 16 shows how the integral intensity increases with energy (E_0) without modifying the dispersion (but shifting the wavelength origin) of the spectrum.

Although the shape of the spectrum is dependent on angular coordinates ϑ, ϑ_0 and $\varphi - \varphi_0$ (or the scattering angle Θ), it is difficult to establish a general behaviour beyond the following properties (Fernández, 1991). The angle Θ defines the width of the continuous wavelength spectrum in the (C, C)

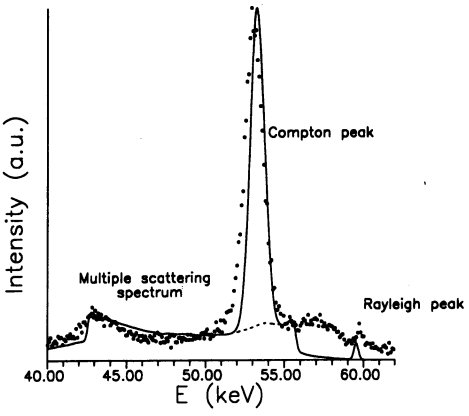

Fig. 17. X-ray spectrum of H_2O excited with the 59.54 keV line. Geometry is $\vartheta_0 = 45°$, $\vartheta = 135°$, $\varphi_0 = \varphi = 0°$. The solid line represents the theoretical estimation computed with the code SHAPE (Fernández and Sumini, 1991) and corrected with the third and fourth order contributions calculated with MC (Sartori and Fernández, 1992). Circles denote experimental data (courtesy of R. Sartori, FaMAF, University of Córdoba).

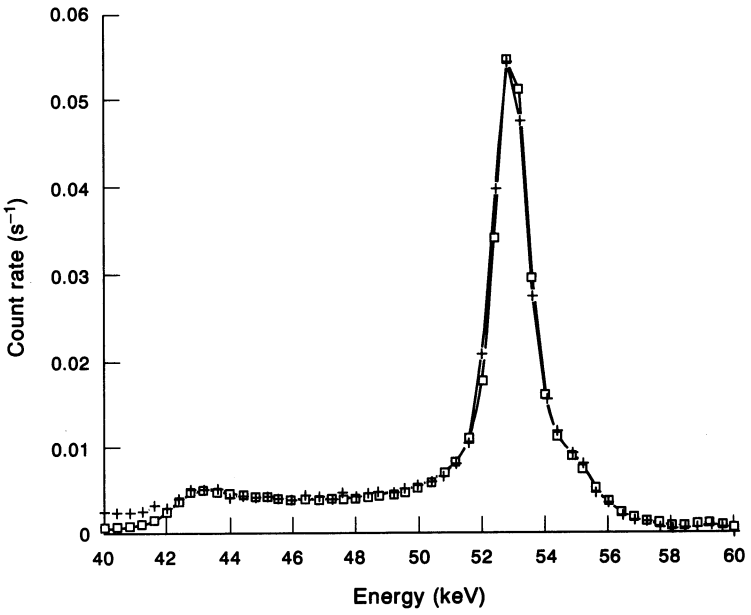

Fig. 18. Experimental scattered photon spectrum of water excited with the 59.54 keV line of an ^{241}Am source, and with a scattering angle of 90°. (+) Experimental; (□) theory: SHAPE data convoluted with water Compton profile and detector response (from Tartari *et al.*, 1993).

case. A change in ϑ_0 and ϑ maintaining Θ fixed varies the relative contribution of the partial second-order intensities to the double scattering spectrum, and modifies the shape of the (C, C) intensity. Since Θ is constant, the wavelength limits of the spectra remain unchanged. The spectrum becomes narrower for increasing ϑ. The increase of Θ produces the concentration of the spectrum at the energy of the Compton peak.

5.1.2.5. Comparison with experimental data. In order to compare the theoretical results with experimental data, a full spectrum of water was built by joining both the monochromatic and the multiple scattering continuous parts. The first- and second-order contributions were calculated with the computer program SHAPE (Fernández and Sumini, 1991) using the analytical expressions described in this work. The third- and fourth-order components were determined with MC simulation. The monochromatic peaks were artificially broadened with a Gaussian shape to improve the fit of the whole spectrum. The multiple scattering orders are not retouched. The spectrum so obtained matches well the experimental points as is shown in Fig. 17. The dashed line identifies the multiple scattering contribution. As can be appreciated, multiple scattering introduces low deformation for this geometry. The experimental set-up was a plastic tank filled with water with a thin mylar window on one side. The water was irradiated through the window using collimated ^{241}Am γ-rays. Right angle scattered radiation was collimated before reaching a Ge detector with resolution 130 eV@Mn $K\alpha$. The thickness of the target was approximately 10 mean free paths.

Another test for water was performed by Tartari *et al.* (1993) with a similar set-up. In this case the Compton peak† was broadened using Compton profiles calculated in the frame of the Impulse Approximation Theory (Biggs *et al.*, 1975). The continuous second-order spectrum was doubly convoluted with the same profile used for the Compton peak to simulate the effect of the profile on double scattering. Figure 18 shows the agreement between this theoretical spectrum and the experimental spectrum.

5.1.2.6. Influence of polarization. We have already seen that the scalar and the vector models predict the same first-order component I, and that second-order intensities differ in a corrective term weighted by the factor $\mathcal{G}$. Although $\mathcal{G}$ admits a quite simple description [see equation (50b)], it affects the integrand of one (or two) angular integral(s) and its effects cannot be described straightforwardly. The influence of polarization is better appreciated if one is shown calculations of the same γ-ray spectrum with the scalar and the vector theories (Fernández and Molinari, 1993; Fernández, 1993a). Figure 19 shows several spectra from water built with the code SHAPE by adding the contributions of the first two orders of scattering. The spectra were calculated assuming: a detector response without escape peak;

†The Compton "peak" is really a sum of several distributions, each of which results from its own interaction (Hanson *et al.*, 1988; Hanson and Gigante, 1989). The effect of divergency indeed increases the FWHM of the peak. However, for the scattering geometry of these experiments and the collimators used, the broadening due to this correction was much lower than the added widths of the Compton profile plus the detector resolution.

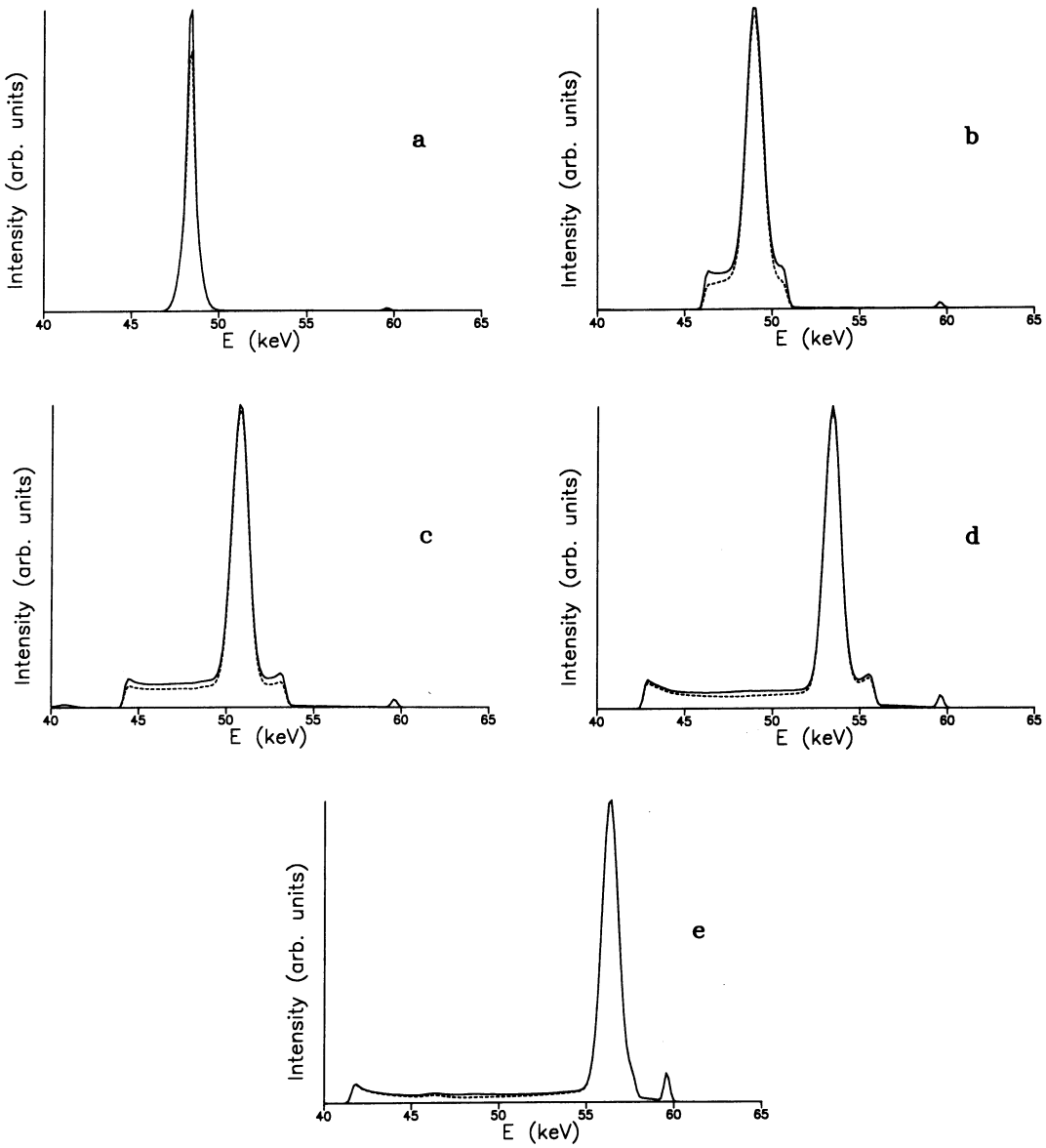

Fig. 19. Total double-scattering spectra for water excited with $E_0 = 60$ keV as calculated with SHAPE. The polar incidence and take-off angles are changed on the plane of scattering to obtain scattering angles of (a) 178°, (b) 150°, (c) 120°, (d) 90° and (e) 60°. The plots show the spectra calculated with both the vector (——) and scalar (- - -) equations. The extent of the correction increases with the scattering angle.

an excitation with the 59.54 keV line of ^{241}Am; and five different scattering angles Θ. All of the spectra were obtained by modifying the incidence and take-off polar angles on the normal plane of scattering ($\varphi_0 = 0$ and $\varphi = 0$). The extent of the correction is illustrated in Fig. 20, plots of the differences between the spectra calculated with the scalar and the vector solution after normalization to the scalar spectrum. On the spectra of Fig. 19 the correction seems to be quite small for all the scattering angles investigated. However, Fig. 20 gives us more insight. The importance of the correction increases and concentrates within a narrow interval of energy as the scattering angle increases. Therefore, the greater difference will occur for scattering angles near 180°, precisely the angles used for measuring Compton profiles. The importance will be concentrated under the maximum of the profile, modifying it asymmetrically. The correction shown in Fig. 20 for $\Theta = 178°$ exceeds 10% of the prediction with the scalar equation and is placed under the center of the Compton peak.

The extent of the correction on two chains with only the Rayleigh effect, i.e. for discrete peak and second-order contributions, is shown in Fig. 21(a) and (b). The correction exceeds the 10% of the second-order intensity calculated with the scalar equation, but since the second-order intensity term is a small fraction of the first-order one [as can be seen

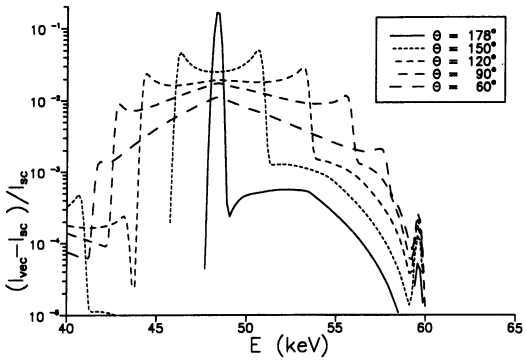

Fig. 20. The difference between the spectra calculated with the scalar and vector equations (in units of the spectra calculated with the scalar equation) renders the extent of the correction in the energy range spanned by each spectrum. For increasing scattering angles the correction becomes more important and concentrates under the Compton peak.

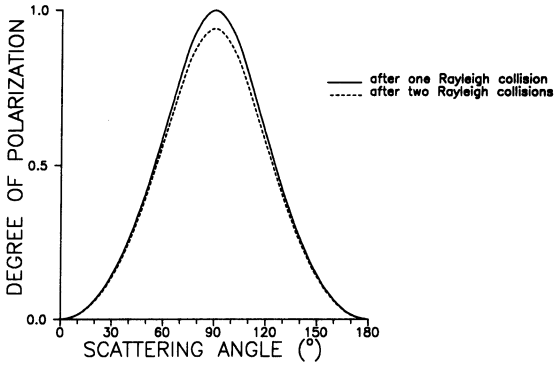

Fig. 22. Fraction of polarized (scattered) radiation (in units of the component I of the intensity) obtained after one and two collisions of the Rayleigh effect, as a function of the scattering angle. The change in the degree of polarization is due to the change of both the state of polarization and the angular distribution of the photons undergoing the first and the second scattering.

in Fig. 21(a)], the correction is not important in this case. However, the example is useful to analyse how the state of polarization changes when unpolarized source radiation undergoes first- and second-order

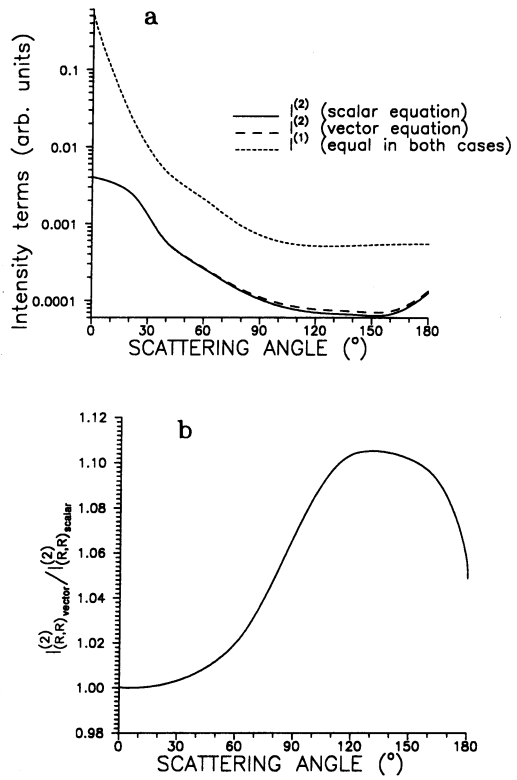

Fig. 21. First and second-order intensities of the pure Rayleigh effect are shown for Al excited with 60 keV photons calculated with both transport equations, scalar and vector. Polar incidence and take-off angles are changed in the same plane of scattering to give different scattering angles ($\vartheta_0 = \pi - \vartheta$, $\varphi_0 = \varphi = 0°$). (a) Comparison between the results of both equations. The once scattered intensity (equal in both cases) is plotted for reference. All the intensities are computed in units of the incoming intensity. (b) Ratio of the second-order intensities calculated with both equations as a function of the scattering angle.

collisions. Figure 22 shows the degrees of polarization calculated with equation (5e) using only the first-order Rayleigh intensity (first-order approximation), and first- plus second-order Rayleigh intensities (second-order approximation). The fraction of polarized radiation, after the first collision, coincides with the degree of polarization of the interaction as it is expected. It is worth noting that after two collisions the beam is no more entirely polarized at 90°. This fact allows us to hypothesize that successive collisions will degrade the degree of polarization, making the high-order intensity terms more and more close to the ones calculated with the scalar model. The maximum degree of polarization occurs after one scattering and is maximized into 90°. The reason for this is that the "perpendicular" component has zero probability for scattering into 90°. After this there can only be an increase in the perpendicular component. This increase come from multiple scattering into 90° and into the "perpendicular" plane.

From these results, we conclude first that the correction to the intensity component I is more important for the continuous second-order spectrum than for the Rayleigh peak. Second, the omission of the corrective term derived with the vector transport equation (with rigorous account of polarization) provides an underestimation of the spectrum principally in the region under the Compton profile. In addition, the vector equation is a useful tool to compute the other Stokes components of the intensity, providing information about the state of polarization of the beam after each set of collisions. This is not possible with the scalar equation.

6. EFFECT OF POLARIZATION ON THE MULTIPLE SCATTERING INTENSITIES FROM POLARIZED SOURCES

Two advantageous characteristics of the synchrotron X-ray beam, high intensity and good monochromaticity, have rendered the synchrotron light a very

important source nowadays for a large number of applications in radiation physics (Koch, 1983), requiring a deeper knowledge of the multiple scattering spectra produced by this source. As long as the synchrotron X-ray photons are observed within the orbit plane of the electrons, they are completely *linearly polarized* having their polarization line coincident with the plane of the orbit. However, observation at a small angle out of this plane will detect *elliptically polarized* radiation, which makes necessary the use of the full solutions in equations (19) and (20). As we have already seen in the preceding section, an unpolarized beam scattered at right angles is also a source of linearly polarized radiation. For simplicity, we shall study the effects of linear and circular polarization on the scattering of polarized X- and γ-rays. We prefer *circularly polarized* radiation because it is well differentiated from the linear polariz ation and reduces the number of Stokes parameters necessary to describe the state of polarization of elliptical polarization. This choice is sufficient to analyse the transport of photons produced with natural sources of polarized radiation (Fagg and Hanna, 1959; McMaster, 1961) as much as with the mentioned artificial sources.

this system, by the source function (see Table 2).

$$\mathscr{S}^{(S)}(\omega, \lambda) = I_0\, \delta(\omega - \omega_0)\, \delta(\lambda - \lambda_0) \begin{bmatrix} 1 \\ \cos 2\chi \\ \sin 2\chi \\ 0 \end{bmatrix} . \quad (64)$$

Furthermore, the interaction processes considered in Section 4 (symbolized as a generic process a) have matrix kernels which can be written (in the Stokes system) as:

$$\mathbb{K}_a^{(S)}(\omega, \lambda, \omega', \lambda') = k_a(\omega, \lambda, \omega', \lambda') \times \begin{bmatrix} 1 & a'_{12} & 0 & 0 \\ a'_{21} & a'_{22} & 0 & 0 \\ 0 & 0 & a'_{33} & 0 \\ 0 & 0 & 0 & a'_{44} \end{bmatrix} . \quad (65a)$$

The scalar kernel $k_a(\omega, \lambda, \omega', \lambda')$ has the same meaning as in equation (46), i.e. it depends on the average polarization state. Primed symbols in equation (65a) identify the coefficients in the Stokes system, which must be distinguished from the unprimed (system L) coefficients found in equation (46) and in section 4.

A straightforward kernel transformation from the system L (unprimed) to the system S (primed) is performed according to the relationship

$$\begin{bmatrix} 1 & a'_{12} & 0 & 0 \\ a'_{21} & a'_{22} & 0 & 0 \\ 0 & 0 & a'_{33} & 0 \\ 0 & 0 & 0 & a'_{44} \end{bmatrix} = \begin{bmatrix} \frac{1}{2}(a_{11} + a_{12} + a_{21} + a_{22}) & \frac{1}{2}(a_{11} - a_{12} + a_{21} - a_{22}) & 0 & 0 \\ \frac{1}{2}(a_{11} + a_{12} - a_{21} - a_{22}) & \frac{1}{2}(a_{11} - a_{12} - a_{21} + a_{22}) & 0 & 0 \\ 0 & 0 & a_{33} & 0 \\ 0 & 0 & 0 & a_{44} \end{bmatrix} \quad (65b)$$

6.1. *Multiple Scattering Intensities for Linearly Polarized Sources*

The polarization states corresponding to the several multiple-scattering contributions to the backscattered intensity were described, in Section 3, for arbitrary source polarization and interactions. In this section we shall compute the intensity terms for the special case of a linearly polarized source. For simplicity, we shall describe the transport in the system S of Stokes. An arbitrarily linearly polarized source of monochromatic and collimated γ-rays of I_0 photons $\mathrm{cm}^{-2}\,\mathrm{s}^{-1}$ is represented mathematically, in

Substitution of equations (64) and (65a) in the solution of the transport equation gives the following relationship for the first-order intensity vector corresponding to the single collision chain

$$(\omega_0, \lambda_0) \xrightarrow{a} (\omega, \lambda)$$

involving the generic interaction a

$$\mathbf{I}_{(a)}^{(1)(S)}(\omega, \lambda) = A(\eta_0, \lambda_0, \eta, \lambda)\, k_a(\omega, \lambda, \omega_0, \lambda_0) \times \begin{bmatrix} 1 + a'_{12} \cos 2(\Psi' + \chi) \\ \cos 2\Psi [a'_{21} + a'_{22} \cos 2(\Psi' + \chi)] - \sin 2\Psi\, a'_{33} \sin 2(\Psi' + \chi) \\ \sin 2\Psi [a'_{21} + a'_{22} \cos 2(\Psi' + \chi)] + \cos 2\Psi\, a'_{33} \sin 2(\Psi' + \chi) \\ 0 \end{bmatrix} , \quad (66)$$

where Ψ and Ψ' are defined as in equations (11c) and (11d), with ω_0 in place of ω'. As in equation (48) we can represent the first-order intensity vector $\mathbf{I}_{(a)}^{(1)(S)}$ decomposed into two fractional beams, the

unpolarized and the polarized fractions

$$\mathbf{I}^{(1)(S)}_{(a)} = \mathbf{I}^{(1)(S)u}_{(a)} + \mathbf{I}^{(1)(S)p}_{(a)}, \tag{67a}$$

with the fractions given by the relationships

$$\mathbf{I}^{(1)(S)u}_{(a)} = A(\eta_0, \lambda_0, \eta, \lambda) k_a(\omega, \lambda, \omega_0, \lambda_0) \times (1 + a'_{12} \cos 2(\Psi' + \chi))(1 - P_a) \begin{bmatrix} 1 \\ 0 \\ 0 \\ 0 \end{bmatrix}, \tag{67b}$$

and

$$\mathbf{I}^{(1)(S)p}_{(a)} = A(\eta_0, \lambda_0, \eta, \lambda) k_a(\omega, \lambda, \omega_0, \lambda_0) \times (1 + a'_{12} \cos 2(\Psi' + \chi)) P_a \begin{bmatrix} 1 \\ \cos 2\xi \\ \sin 2\xi \\ 0 \end{bmatrix}. \tag{67c}$$

P_a represents the degree of polarization of the interaction a for a linearly polarized source. By equation (5e), it is given as

$$P_a(\omega, \lambda, \omega_0, l_0) = \frac{(\mathbf{I}^{(1)(S)2}_{(a)Q} + \mathbf{I}^{(1)(S)2}_{(a)U} + \mathbf{I}^{(1)(S)2}_{(a)V})^{1/2}}{\mathbf{I}^{(1)(S)}_{(a)I}} = \frac{([a'_{21} + a'_{22} \cos 2(\Psi' + \chi)]^2 + [a'_{33} \sin 2(\Psi' + \chi)]^2)^{1/2}}{1 + a'_{12} \cos 2(\Psi' + \chi)}. \tag{67d}$$

The polarized fraction (67c) represents a linearly polarized scattered beam whose polarization line forms an angle ξ with the scattering plane. The angle ξ is defined analogously to χ in equation (3b).

The component I of the first-order intensity, representing the intensity collected by a polarization insensitive detector, is the first component of the intensity vector (66),

$$\mathbf{I}^{(1)(S)}_{(a)I}(\omega, \lambda) = A(\eta_0, \lambda_0, \eta, \lambda) k_a(\omega, \lambda, \omega_0, \lambda_0) \times (1 + a'_{12} \cos 2(\Psi' + \chi)). \tag{68}$$

Analogously the second-order intensity due to the collision chain

$$(\omega_0, \lambda_0) \xrightarrow{a} (\omega', \lambda') \xrightarrow{\delta} (\omega, \lambda)$$

involving two generic interactions a and δ is given by

$$\mathbf{I}^{(2)(S)}_{(a,\delta)I}(\omega, \lambda) = A(\eta_0, \lambda_0, \eta, \lambda) \int_0^\infty d\lambda' \int_{4\pi} d\omega' \frac{1}{|\eta'|} \times \left\{ \frac{(1 + \operatorname{sgn} \eta')}{2} \frac{k_\delta(\omega, \lambda, \omega', \lambda') k_a(\omega', \lambda', \omega_0, \lambda_0)(1 + \mathscr{G}'_{a\delta}(\omega, \lambda, \omega', \lambda', \omega_0, \lambda_0, \chi))}{\frac{\mu}{|\eta|} + \frac{\mu'}{|\eta'|}} + \frac{(1 - \operatorname{sgn} \eta')}{2} \frac{k_\delta(\omega, \lambda, \omega', \lambda') k_a(\omega', \lambda', \omega_0, \lambda_0)(1 + \mathscr{G}'_{a\delta}(\omega, \lambda, \omega', \lambda', \omega_0, \lambda_0, \chi))}{\frac{\mu_0}{|\eta_0|} + \frac{\mu'}{|\eta'|}} \right\} \tag{69a}$$

which compared with the expression for the same intensity term deduced with the unpolarized source (see Section 5.1), differs only in the expression of the corrective factor $\mathscr{G}'_{a\delta}(\omega, \lambda, \omega', \lambda', \omega_0, \lambda_0, \chi)$, which depend explicitly on the angle χ, and is defined in terms of the primed matrix coefficients as

$$\mathscr{G}'_{a\delta}(\omega, \lambda, \omega', \lambda', \omega_0, \lambda_0, \chi) = a'_{12} \cos 2(\Psi'_a + \chi) + a'_{21} \delta'_{12} \cos 2(\Psi_a + \Psi'_\delta) + \tfrac{1}{2} \delta'_{12} [(a'_{22} + a'_{33}) \cos 2(\Psi'_a + \Psi_a + \Psi'_\delta + \chi) + (a'_{22} - a'_{33}) \cos 2(\Psi'_a - \Psi_a - \Psi'_\delta + \chi)], \tag{69b}$$

where Ψ_a, Ψ'_a and Ψ'_δ are angles of spherical triangles for the interactions a and δ, respectively, similar as those shown in Figure 2 for one single interaction. These angles are defined, respectively, by equations (50c), (50d) and by the relationship

$$\cos \Psi'_a = \frac{\eta' \sqrt{1 - \eta_0^2} - \eta_0 \sqrt{1 - \eta'^2} \cos(\varphi' - \varphi_0)}{(1 - (\omega_0 \cdot \omega')^2)^{1/2}}. \tag{69c}$$

The expressions for the components Q and U are substantially more complicated and will not be included in this article. We get also the component V of the intensity

$$\mathbf{I}^{(2)(S)}_{(a,\delta)V}(\omega, \lambda) = 0, \tag{69d}$$

meaning that the polarized fraction remains linearly polarized after the second scattering, i.e. no elliptical component is created as a sequence of the scattering process when it is not initially present in the source.

Some properties of the one- and two-collisions intensities, equations (68) and (69a), are similar to the ones already mentioned in Section 5 for the unpolarized source. Firstly, it remains, as before, a polarized fraction of the beam after the first collision. This fraction is dominant (see Section 6.1.3), i.e. the beam remains almost completely polarized after the scattering, in contrast with what occurs with the unpolarized source, where a full polarization state corresponds only to right angle scattering. Secondly, the angle defining the position of the polarization line is different after one and two collisions. This confirms what we already suggested in Section 5.1, i.e. that it is possible to separate the contribitions from a different number of collisions by filtering the beam with a polarizer before the detector.

The detected intensity (sum of components I for different numbers of collisions) will be object of a more detailed analysis for the interactions of interest. However, we can make some general observations about it. Comparing equations (68) and (69a) with equations (47a) and (50a) it is easily seen that a linearly polarized source brings the effects of polarization to the most intense first-order intensity terms, i.e. to the peaks. Therefore, a scalar model with the average polarization kernel is not more valid as a first-order approximation of the I component. It is apparent from equation (68) that, for any process, the first-order intensity is different from the scalar intensity (47a) (unless all the matrix coefficients are null) because of the additional term that depends on the scattering geometry and the orientation of the source polarization line. As we shall see below, the first-order intensity could also be obtained by replacing the averaged kernel with an appropriated scalar (polarization dependent) kernel. On the other hand, the second-order intensity depends on the extent of the correction $\mathscr{G}'$ [different from the factor $\mathscr{G}$ in equation (50a)], which depends on the matrix coefficients α' and δ', the scattering geometries of both interactions, and the angle χ, as was described in equation (69b).

6.1.1. *Characteristic lines*

Assuming the photoelectric effect is not a polarization dependent process we obtain, from equation (67d), the polarization degree

$$P_P(\omega, \lambda, \omega_0, \lambda_0) = 0. \tag{70a}$$

Thus, the corresponding first-order intensity term can be written as

$$\mathbf{I}_{(P)}^{(1)(S)}(\omega, \lambda) = A(\eta_0, \lambda_0, \eta, \lambda) k_P(\omega, \lambda, \omega_0, \lambda_0) \begin{bmatrix} 1 \\ 0 \\ 0 \\ 0 \end{bmatrix}, \tag{70b}$$

which is analogous to the expression obtained with the unpolarized source, i.e. the photoelectric effect completely depolarizes the beam, producing completely unpolarized radiation after the first collision.

The photoelectric effect has this behaviour because the coefficients of the polarization matrix in the Stokes system are null, i.e. $\alpha'_{12} = \alpha'_{21} = \alpha'_{22} = \alpha'_{33} = \alpha'_{44} = 0$ in equation (65a), as can be easily shown from equations (30) and (65b). This implies that all the intensity terms containing pure photoelectric effect interactions will maintain the expressions obtained in Section 5.1.1.1 for the unpolarized source. This property can be extended to some of the second-order intensity terms containing other scattering processes besides the photoelectric effect, as long as the photoelectric effect remains the first interaction in the chain. As can be verified by inspecting the coefficients in equation (69b), we get $\mathscr{G}'_{P\delta} \equiv 0$ for any scattering interaction δ. However, this condition is not fulfilled if the photon undergoes a Compton or Rayleigh scattering *before* the photoelectric effect. For these cases we must consider the corresponding factor $\mathscr{G}'_{CP}$ or $\mathscr{G}'_{RP}$ ($\mathscr{G}'_{CP} \neq \mathscr{G}'_{RP} \neq 0$) in equation (69a), modifying the intensity terms given earlier by equations (53) and (56). It is worth remembering that the scattering contributions are always present in an important proportion in intensity measurements of characteristic lines, mainly when a light element is a major component of the target. They amount (all added), at working energies, to typical values of 5–10% of the unmodified line for pure element targets or 10–50% for trace elements in light matrices, that makes important a correct estimate of this enhancement. As we mentioned, only two of the four corrective terms are modified by using a linearly polarized source, and therefore, it is not possible to reduce all the multiple scattering contributions by making recourse to polarization. We should note that the continuous (P, C) term responsible for the modification of the shape of the line is not changed by this source, as well as the (P, R) term, which is the dominant term of the correction for high and medium Z pure targets (see Section 5.1.1 for a discussion on these contributions).

The multiple scattering effects on the characteristic lines modifying the results already reported in Section 5, in particular the intensity terms (R, P) and (C, P) are summarized in the following subsections.

6.1.1.1. Chains involving the pure photoelectric effect. As we have seen, there are no changes for the intensity terms containing only photoelectric effect interactions. Therefore, the first- and second-order intensities are described by equations (51) and (52), as well as the third- and fourth-order ones which are coincident with those reported by Fernández (Fernández, 1989; Fernández and Molinari, 1990).

6.1.1.2. Chains of mixed interactions involving the photoelectric effect and Rayleigh or Compton scattering. The four contributions involving the possible combinations of one scattering process (Rayleigh or Compton) and one photoelectric effect were already described in Section 5.1.1.2. Two of them describe the intensity contributed by coherently and incoherently scattered photons that, absorbed by photoelectric effect, result in XRF emission. The other two correspond to XRF radiation Rayleigh and Compton scattered towards the detector.

Due to the vanishing of the photoelectric effect matrix coefficients, two scattering contributions to the second-order intensity remain unmodified. They are the (P, R) and (P, C) terms which continue to be described, respectively, by equations (55) and (57). The remaining two intensity terms, (R, P) and (C, P), change because the polarized source modifies the angular distribution of the radiation scattered in the first collision, which successively undergoes absorption by the photoelectric effect. The expressions for

the intensities of these terms, are given in the following sections.

6.1.1.2.1. Rayleigh–photoelectric: The XRF intensity contributed by Rayleigh photons produced in the first collision of the beam is obtained by replacing the kernels $\mathcal{K}_a$ and $\mathcal{K}_\ell$ by $\mathcal{K}_R$ and $\mathcal{K}_P$, respectively, and $\mathcal{G}'_{RP}$ in equation (69a)

$$I^{(2)(S)}_{(R,P)_I}(\omega,\lambda)=\delta(\lambda-\lambda_i)\frac{A(\eta_0,\lambda_0,\eta,\lambda_i)}{2\pi}\frac{\sigma}{Z}\times Q_{\lambda_i}(\lambda_0)[1-\mathcal{U}(\lambda_0-\lambda_{e_i})]\times\left\{\int_0^{2\pi}d\varphi'\int_0^1\frac{d\eta'}{\eta'}\frac{F^2(\lambda_0,\omega'\cdot\omega_0^{(+)},Z)}{\frac{\mu_i}{|\eta|}+\frac{\mu_0}{\eta'}}\times[1-(1-(\omega'\cdot\omega_0^{(+)})^2)\cos^2(\Psi'^{(+)}_a+\chi)]\right.$$
$$\left.+\int_0^{2\pi}d\varphi'\int_0^1\frac{d\eta'}{\eta'}\frac{F^2(\lambda_0,\omega'\cdot\omega_0^{(-)},Z)}{\frac{\mu_0}{|\eta_0|}+\frac{\mu_0}{\eta'}}\times[1-(1-(\omega'\cdot\omega_0^{(-)})^2)\cos^2(\Psi'^{(-)}_a+\chi)]\right\}, \quad (71a)$$

where $\Psi'^{(\pm)}_a$ is given by

$$\cos\Psi'^{(\pm)}_a=\frac{\pm\eta'\sqrt{1-\eta_0^2}-\eta_0\sqrt{1-\eta'^2}\cos\varphi'}{(1-(\omega'\cdot\omega_0^{(\pm)})^2)^{1/2}}, \quad (71b)$$

and $\omega_1\cdot\omega_2^{(\pm)}$ was defined in equation (54).

Note that the factor 4π in the denominator of the right hand side of equation (53) has changed to 2π in equation (71a). Furthermore, the angular factor between brackets, depending explicitly on χ, now replaces the factor $1+(\omega'\cdot\omega_0^{(\pm)})^2$ in the average polarization kernel. Note also that the new factor is the same that we find in the first-order Rayleigh intensity calculated from equation (68) (see Section 6.1.2.1). It means that the angular distribution of the Rayleigh scattered intensity undergoing the photoelectric effect was modified by the source polarization.

6.1.1.2.2. Compton–photoelectric: The intensity term contributes by XRF due to photoelectric absorption of incoherently scattered source photons is given by the substitution of $\mathcal{K}_C$, $\mathcal{K}_P$, and $\mathcal{G}'_{CP}$, in equation (69a)

$$I^{(2)(S)}_{(C,P)_I}(\omega,\lambda)=\delta(\lambda-\lambda_i)\frac{A(\eta_0,\lambda_0,\eta,\lambda_i)}{2\pi}\frac{\sigma}{\lambda_C}\times\int_{\lambda_0}^{\lambda_0+2\lambda_c}d\lambda' Q_{\lambda_i}(\lambda')S(\lambda_0,a',Z)[1-\mathcal{U}(\lambda'-\lambda_{e_i})]$$
$$+\left\{\int_{\alpha'_1}^{\beta'_1}\frac{d\eta'}{\eta'}\frac{\mathcal{U}(\beta'_1-\alpha'_1)}{\frac{\mu_i}{|\eta|}+\frac{\mu'}{\eta'}}\times\frac{K(\lambda',\lambda_0,\Psi'^{(+)}_a,\chi)}{\sqrt{(1-\eta'^2)(1-\eta_0^2)-(a'-\eta'\eta_0)^2}}\right.$$
$$\left.+\int_{\alpha'_2}^{\beta'_2}\frac{d\eta'}{\eta'}\frac{\mathcal{U}(\beta'_2-\alpha'_2)}{\frac{\mu_0}{|\eta_0|}+\frac{\mu'}{\eta'}}\times\frac{K(\lambda',\lambda_0,\Psi'^{(-)}_a,\chi)}{\sqrt{(1-\eta'^2)(1-\eta_0^2)-(a'+\eta'\eta_0)^2}}\right\}, \quad (72a)$$

where

$$K(\lambda',\lambda_0,\Psi'^{(\pm)}_a,\chi)=\frac{\lambda_0}{\lambda'}+\frac{\lambda'}{\lambda_0}-2\frac{\lambda'-\lambda_0}{\lambda_C}\times\left(2-\frac{\lambda'}{\lambda_C}\frac{\lambda_0}{\lambda_C}\right)\cos^2(\Psi'^{(\pm)}_a+\chi), \quad (72b)$$

$\Psi'^{(\pm)}_a$ is defined by the relationship

$$\cos\Psi'^{(\pm)}_a=\frac{\pm\eta'-\eta_0 a'}{((1-a'^2)(1-\eta_0^2))^{1/2}}, \quad (72c)$$

and the remaining symbols are $a'=1+(\lambda_0-\lambda')/\lambda_C$, $\Delta'=\sqrt{(1-\eta_0^2)(1-a'^2)}$, $\alpha'_1=\max(0,a'\eta_0-\Delta')$, $\beta'_1=\min(1,a'\eta_0+\Delta')$, $\alpha'_2=-\min(0,a'\eta_0+\Delta')$, and $\beta'_2=-\max(-1,a'\eta_0-\Delta')$.

The factor $K(\lambda',\lambda_0,\Psi'^{(\pm)}_a,\chi)$, which depends explicitly on χ now replaces the factor $K(\lambda',\lambda_0)$ of the average polarization kernel. The factor K is the same as that we find for the first-order Compton intensity deduced from equation (68) (see Section 6.1.2.1). The difference between K and K_{KN} is due to the source polarization which modifies the angular distribution of the Compton scattered photons undergoing a collision of the photoelectric effect.

6.1.2. The continuous background due to Compton and Rayleigh effects

Many attempts have been performed in the past to evaluate the influence of the multiple scattering due to Compton and Rayleigh effects upon excitation with a polarized source, as it is apparent in the exhaustive annotated bibliography by Hubbell (1992). A review of the literature cited shows the greater effort concentrated between the middle 40's and the middle 50's to state the mathematical basis of polarized photons transport and the correct angular dependence in the polarization matrices. The equations of transfer allowing properly for the polarization of the scattered radiation were first formulated by Chandrasekhar (1946a, 1946b, 1947, 1950) for Rayleigh scattering (without including form factors), and constitute the foundations for the approach used in this article. After these seminal works, the study on polarization effects in multiple scattering of X- and γ-ray photons with the Compton effect was continued by Spencer and Wolff (1953). The vector transport approach and the use of polarization matrices were reviewed, respectively, by Fano *et al.*

(1959) and McMaster (1961) with special regard to the Stokes formulation. Other review articles, regarding theoretical or experimental aspects of photon polarization, were due to Fagg and Hanna (1959), Cole (1963) and Olsen (1968). During the next decade, from the middle 50s to the middle 60s, the efforts were concentrated on making experimental checks of the theory, and theoretical adjustments of the polarization matrices. After the middle 60s the interest waned, except for some applications on X-ray diffraction, until a recent revival induced by the availability of the synchrotron light as a source.

In these works, Compton and Rayleigh effects received a separated treatment, i.e. either Rayleigh or Compton collisions were considered. There are no known references to chains of mixed interactions of both effects, Compton *and* Rayleigh. Form factors and scattering functions have been ignored in the scarce theoretical estimations, offering low accuracy for absolute estimations. Most of the theoretical work has been devoted to determining the components of the Rayleigh and Compton polarization matrices, used in turn to estimate crudely the importance of up to two scattering collisions in infinite media and the parallel-to-perpendicular component ratio of the scattered beam intensity. No transport calculations, other than the foundational references for this article, were performed. Therefore, the mentioned estimations of intensity have never included the attenuation in the volume of the target.

In what follows, we shall use the analytical solution of the vector transport equation to obtain expressions of the scattered intensities using accurate Rayleigh and Compton cross sections and including attenuation effects.

6.1.2.1. The Rayleigh and Compton peaks.

6.1.2.1.1. Rayleigh peak: From equation (67d) we get the degree of polarization for the Rayleigh effect

$$P_R(\omega, \lambda, \omega_0, \lambda_0) = 1. \tag{73a}$$

Equation (73a) shows that Rayleigh scattering of linearly polarized source photons produce *only* linearly polarized photons. No unpolarized photons are emitted, and therefore, the first-order intensity vector for the Rayleigh peak contains exclusively the polarized fraction

$$\mathbf{I}^{(1)(S)}_{(R)} = 2A(\eta_0, \lambda_0, \eta, \lambda)\frac{k_R(\omega, \lambda, \omega_0, \lambda_0)}{1+\cos^2\Theta} \times (1-\sin^2\Theta\cos^2(\Psi'+\chi))\begin{bmatrix}1\\ \cos 2\xi\\ \sin 2\xi\\ 0\end{bmatrix}. \tag{73b}$$

Θ represents the scattering angle, and the polarization angle ξ of the scattered beam is defined by any one of the relationships

$$\cos\xi = \frac{\cos\Theta\cos(\Psi'+\chi)\cos\Psi - \sin(\Psi'+\chi)\sin\Psi}{1-\sin^2\Theta\cos^2(\Psi'+\chi)}, \tag{73c}$$

$$\sin\xi = \frac{\cos\Theta\cos(\Psi'+\chi)\sin\Psi + \sin(\Psi'+\chi)\cos\Psi}{1-\sin^2\Theta\cos^2(\Psi'+\chi)}. \tag{73d}$$

The I component of equation (73b) predicts the detected first-order intensity for the Rayleigh peak

$$\mathbf{I}^{(1)(S)}_{(R)I}(\omega, \lambda) = 2\frac{\sigma}{Z}\delta(\lambda-\lambda_0)A(\eta_0, \lambda_0, \eta, \lambda_0) \times F^2(\lambda_0, \omega\cdot\omega_0, Z) \times (1-\sin^2\Theta\cos^2(\Psi'+\chi)). \tag{73e}$$

Note that Ψ' in equation (73e) is defined by

$$\cos\Psi' = \frac{\eta\sqrt{1-\eta_0^2} - \eta_0\sqrt{1-\eta^2}\cos\varphi}{\sin\Theta}. \tag{73f}$$

The angular part of equation (73e) agrees with the well known result (Heitler, 1936) relating the intensity with the scattering angle and with the angle between the polarization line of the incident beam and the propagation direction of the scattered beam.

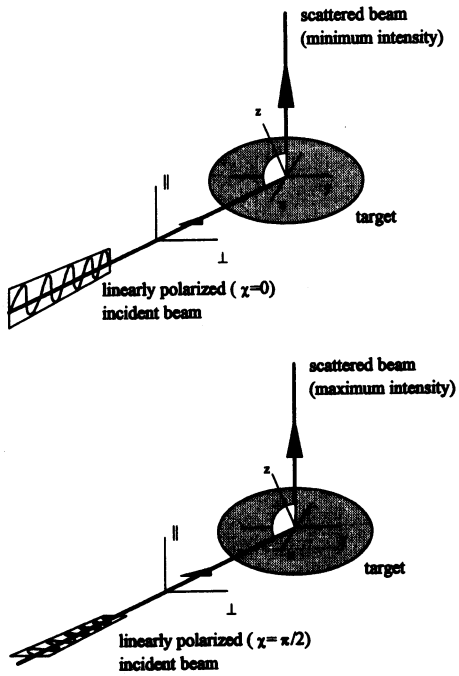

Fig. 23. A linearly polarized incident beam with the electric field lying on the plane parallel (perpendicular) to the scattering plane gives minimum (maximum) first-order intensities for 90° Rayleigh and Compton scattering. In the figure we assume that both directions, incidence and take-off, lie in the x–z plane normal to the target.

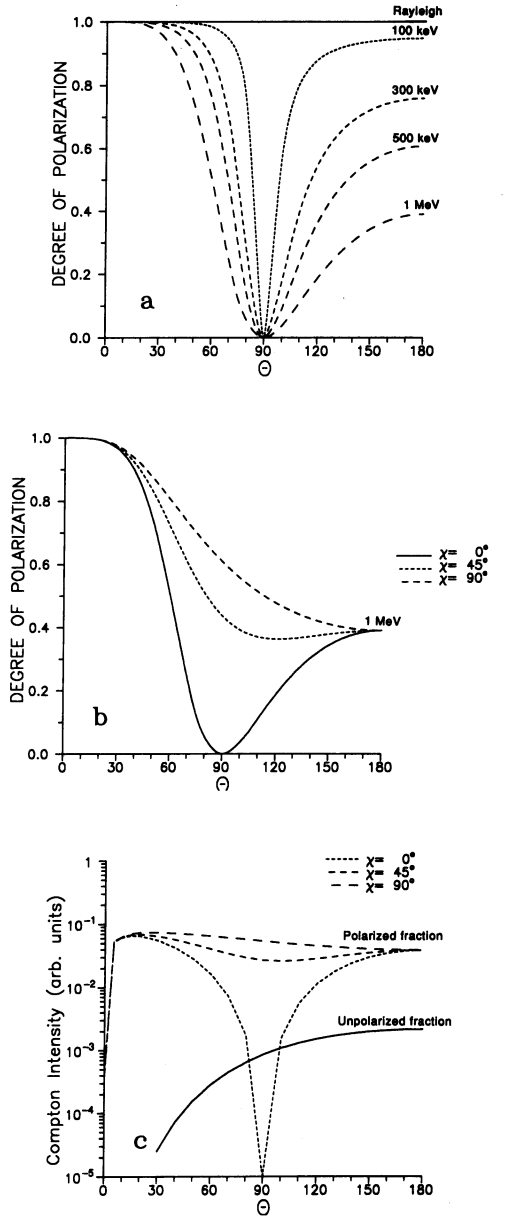

Fig. 24. The degrees of polarization and the first-order intensity for the Compton and Rayleigh effects, for a linearly polarized incident beam, are shown as functions of the incident energy, the scattering angle and the orientation of the polarization line. The Rayleigh degree is constant. In contrast, the Compton degree depends on the above three variables and is responsible for the gradual depolarization of the beam. (a) The Rayleigh and Compton degrees as a function of the scattering angle for several energies of the incident beam. The depolarization of the beam is minimum (null) for forward scattering, and maximum for right angle scattering. The polarization line of the incident beam is assumed parallel to the scattering plane. (b) The Compton degree as a function of the scattering angle for some orientations of the polarization line. The depolarization is minimum for parallel orientation ($\chi = 0$) and maximum for perpendicular orientation ($\chi = \pi/2$). The energy of the incident beam is 1 MeV. (c) The unpolarized and polarized fractions of the first-order Compton intensity as a function of the scattering angle Θ and the polarization of the incident beam, for carbon excited with 100 keV X-rays.

For the special case of right angle scattering in the x–z plane we get $\sin^2\Theta = 1$, $\varphi = 0$, $\Psi' = \pi$, and the Rayleigh peak intensity becomes

$$I^{(I)(S)}_{(R)I}|_{\Theta=\pi/2} = 2\frac{\sigma}{Z}\delta(\lambda - \lambda_0)A(\eta_0, \lambda_0, \eta, \lambda_0) \times F^2(\lambda_0\, 0, Z)\sin^2\chi, \quad (73g)$$

with η satisfying the relationship

$$\eta = -(1 - \eta_0^2)^{1/2}. \quad (73h)$$

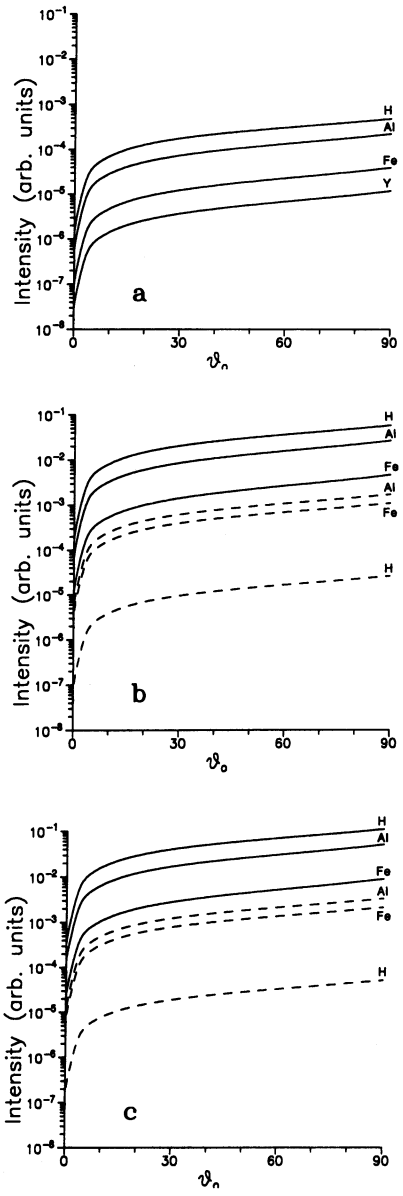

Fig. 25. Rayleigh (- - -) and Compton (——) peak intensities as a function of the polar angle of incidence for right angle scattering in the x–z plane of 50 keV photons, and for three orientations of the incident polarization line. (a) Parallel to the scattering plane ($\chi = 0$). The first-order Rayleigh intensity is null. (b) At 45° to the scattering plane ($\chi = \pi/4$). (c) Normal to the scattering plane ($\chi = \pi/2$).

The intensity (73g) is minimum (null) for an incident beam with its polarization line parallel to the scattering plane ($\chi = 0$), and maximum for a polarization line perpendicular to the sattering plane ($\chi = \pi/2$), as it is shown in Fig. 23. Figure 25 displays the first-order intensity (73g) for some pure elements and orientations of the incident polarization line at fixed 50 keV excitation energy and 90° scattering angle, as a function of the polar angle ϑ_0 of incidence. The Rayleigh peak intensity increases with ϑ_0 due to the variation of the paths corresponding to the incidence and take-off beams which modify the attenuation into the target. Complementary properties for the parallel and perpendicular components of the Rayleigh polarized cross-sections (i.e. without attenuation) for 90° scattering were discussed by Hanson (1986a, 1986b, 1986c).

6.1.2.1.2. Compton peak: From equation (67d) we obtain the degree of polarization for the Compton effect as

$$P_C(\omega, \lambda, \omega_0, \lambda_0) = \frac{1 - b(2-b)\cos^2(\Psi' + \chi)}{a/2 - b(2-b)\cos^2(\Psi' + \chi)}, \quad (74a)$$

where $a(\lambda, \lambda_0) = \lambda/\lambda_0 + \lambda_0/\lambda$, $b(\lambda, \lambda_0) = (\lambda - \lambda_0)/\lambda_C$ and $\Psi'(\omega, \omega_0)$ is defined as in equation (73f). Equation (74a) shows that Compton scattering of linearly polarized source photons produces both linearly polarized and unpolarized photons. This depolarization effect was first predicted by Klein and Nishina (1929) using the Dirac's relativistic electron theory. For $\lambda \to \lambda_0$ and for $\lambda_0 \to \infty$, the degree of polarization (74a) approximates the degree for the Rayleigh effect as it is shown in Fig. 24(a). It is apparent that the Compton degree becomes more and more different from the Rayleigh degree for increasing incident energy and increasing scattering angle. The greater the departure from 1, the higher the depolarization due to the Compton scattering. The unpolarized component is zero in the forward direction ($\Theta = 0$) and maximum in the perpendicular direction ($\Theta = \pi/2$), from which it goes to an intermediate value in the backward direction ($\Theta = \pi$). Figure 24(b) shows the effect of changing the orientation of the polarization line on the Compton degree. For a given incident energy, the parallel orientation gives the minimum depolarization in the perpendicular direction ($\Theta = \pi/2$), while orientations closer to the perpendicular position favours the depolarization. In the forward ($\Theta = 0$) and backward ($\Theta = \pi$) directions, the degree of polarization is totally independent of the polarization of the incident X-rays. Figure 24(c) shows the unpolarized and polarized fractions of the first-order Compton intensity as a function of the scattering angle Θ. The unpolarized fraction is independent of the orientation of the incident polarization. The polarized fraction changes from the upper curve ($\chi = \pi/2$) to the lower curve ($\chi = 0$) having a zero for $\Theta = \pi/2$. Some of these characteristics were already noted by Hanson [see for instance Figs 15, 17 and 19 in Hanson (1988a)] with a different approach based on the study of the depolarization terms appearing in angularly integrated cross-sections for narrow detectors.

Therefore, the first-order intensity vector for the Compton peak contains the polarized and unpolarized fractions

$$\mathbf{I}_{(C)}^{(1)(S)u} = 2A(\eta_0, \lambda_0, \eta, \lambda)\frac{k_C(\omega, \lambda, \omega_0, \lambda_0)}{K_{KN}(\lambda, \lambda_0)} \times \left(\frac{\lambda_0}{\lambda}\right)^2 (a/2 - 1) \begin{bmatrix} 1 \\ 0 \\ 0 \\ 0 \end{bmatrix}, \quad (74b)$$

and

$$\mathbf{I}_{(C)}^{(1)(S)p} = 2A(\eta_0, \lambda_0, \eta, \lambda)\frac{k_C(\omega, \lambda, \omega_0, \lambda_0)}{K_{KN}(\lambda, \lambda_0)} \times \left(\frac{\lambda_0}{\lambda}\right)^2 (1 - b(2-b)\cos^2(\Psi' + \chi)) \begin{bmatrix} 1 \\ \cos 2\xi \\ \sin 2\xi \\ 0 \end{bmatrix}, \quad (74c)$$

where $b(2-b) \equiv \sin^2\Theta$, with Θ representing the scattering angle, and the polarization angle ξ of the polarized beam is defined by any of the following relationships

$$\cos\xi = \frac{(1-b)\cos(\Psi' + \chi)\cos\Psi - \sin(\Psi' + \chi)\sin\Psi}{1 - b(2-b)\cos^2(\Psi' + \chi)}, \quad (74d)$$

$$\sin\xi = \frac{(1-b)\cos(\Psi' + \chi)\sin\Psi + \sin(\Psi' + \chi)\cos\Psi}{1 - b(2-b)\cos^2(\Psi' + \chi)}, \quad (74e)$$

The I component of the intensity vector [given by the addition of equations (73b) and (73c)] predicts the detected first-order intensity for the Compton peak

$$\mathbf{I}_{(C)I}^{(1)(S)}(\omega, \lambda) = 2\sigma\left(\frac{\lambda_0}{\lambda}\right)^2 S(\lambda_0, \omega \cdot \omega_0, Z) \times \delta(\lambda_C(1 - \omega \cdot \omega_0) + \lambda_0 - \lambda)A(\eta_0, \lambda_0, \eta, \lambda) \times (a/2 - b(2-b)\cos^2(\Psi' + \chi)). \quad (74f)$$

For the special case of right angle scattering in the $x - z$ plane we get $b(2-b) = \sin^2\Theta \equiv 1$ (i.e. $b = 1$

and $\lambda = \lambda_0 + \lambda_C$), $\varphi = 0$, $\Psi' = \pi$, and the Compton peak intensity becomes

$$I^{(1)(S)}_{(C)I}|_{\vartheta=\pi/2} = 2\sigma\,\delta(\lambda_C + \lambda_0 - \lambda) \times A(\eta_0, \lambda_0, \eta, \lambda_0 + \lambda_C) S(\lambda_0, 0, Z) \times \left(\frac{\lambda_0}{\lambda_0 + \lambda_C}\right)^2 \left\{\frac{1}{2}\left(\frac{\lambda_0 + \lambda_C}{\lambda_0} + \frac{\lambda_0}{\lambda_0 + \lambda_C}\right) - \cos^2\chi\right\}, \tag{74g}$$

with η given by equation (73h). The intensity is minimum if the incident beam has its polarization line parallel to the scattering plane ($\chi = 0$), and maximum if the polarization line is perpendicular to the scattering plane ($\chi = \pi/2$), as is shown in Fig. 23. In contrast with the Rayleigh peak, the Compton peak intensity does not vanish for $\chi = 0$ [see Fig. 25(a)]. Figure 25 displays the first-order intensity (74g) for some pure elements and orientations of the incident polarization line at a fixed 50 keV excitation energy and 90° scattering angle, as a function of the polar angle ϑ_0 of incidence. At this energy, the Compton peak intensity is always greater than the Rayleigh one. Both intensities increase if the angle ϑ_0 increases, because of the variation of the attenuation paths into the target corresponding to the incidence and take-off beams. The Rayleigh/Compton intensity ratio for each element [sometimes used as a measure of the average density of multi component targets (see e.g. Cesareo *et al.*, 1992)] is modified by the orientation of the polarization line of the incident beam.

Complementary properties regarding the parallel and perpendicular components of the Compton polarized cross-sections (i.e. without including attenuation effects) for 90° scattering were discussed by Hanson (1986a, 1986b, 1986c).

6.1.2.2. Chains of double scattering involving the Rayleigh and Compton effects. In order to calculate the correction factor $\mathscr{G}'$ defined in Section 6.1 for the second-order terms we use the Rayleigh and Compton matrices which result from applying the transformation (65b) to equations (34) and (40), respectively. $\mathscr{G}'$ varies according to the range of the cosine trigonometric functions in equation (69b) (i.e. $[-1, 1]$) weighted by some simple factors involving the matrix coefficients a'_{ij} and b'_{ij}, corresponding to the interactions a and b. The expressions for the four combinations involving a double scattering with the Rayleigh and the Compton effects: Rayleigh–Rayleigh, Rayleigh–Compton, Compton–Rayleigh and Compton–Compton are given below. Details for the computations can be found elsewhere (Fernández, 1993c).

6.1.2.2.1. Rayleigh–Rayleigh: This contribution is calculated by substituting the Rayleigh kernel twice into equation (69a), and setting

$$I^{(2)(S)}_{(R,R)I}(\omega, \lambda, \chi) = \delta(\lambda - \lambda_0)\left(\frac{\sigma}{Z}\right)^2 A(\eta_0, \lambda_0, \eta, \lambda_0) \times \left\{\int_0^{2\pi} d\varphi' \int_0^1 \frac{d\eta'}{\eta'} \frac{(1 + (\omega' \cdot \omega^{(+)})^2)(1 + (\omega' \cdot \omega_0^{(+)})^2)(1 + \mathscr{G}'^{(+)}_{RR}(\omega, \lambda, \omega', \lambda', \omega_0, \lambda_0, \chi))}{\frac{\mu_0}{|\eta|} + \frac{\mu_0}{\eta'}} \times F^2(\lambda_0, \omega' \cdot \omega^{(+)}, Z) F^2(\lambda_0, \omega' \cdot \omega_0^{(+)}, Z) + \int_0^{2\pi} d\varphi' \int_0^1 \frac{d\eta'}{\eta'} \frac{(1 + (\omega' \cdot \omega^{(-)})^2)(1 + (\omega' \cdot \omega_0^{(-)})^2)(1 + \mathscr{G}'^{(-)}_{RR}(\omega, \lambda, \omega', \lambda', \omega_0, \lambda_0, \chi))}{\frac{\mu_0}{|\eta_0|} + \frac{\mu_0}{\eta'}} \times F^2(\lambda_0, \omega' \cdot \omega^{(-)}, Z) F^2(\lambda_0, \omega' \cdot \omega_0^{(-)}, Z)\right\}, \tag{75a}$$

where

$$\mathscr{G}'^{(\pm)}_{RR}(\omega, \lambda, \omega', \lambda', \omega_0, \lambda_0, \chi) = \frac{(\omega' \cdot \omega_0^{(\pm)})^2 - 1}{(\omega' \cdot \omega_0^{(\pm)})^2 + 1}\left(\cos 2(\Psi'^{(\pm)}_a + \chi) + \frac{(\omega' \cdot \omega^{(\pm)})^2 - 1}{(\omega' \cdot \omega^{(\pm)})^2 + 1} \cos 2(\Psi'^{(\pm)}_a + \Psi'^{(\pm)}_b)\right) + \frac{1}{2}\frac{(\omega' \cdot \omega^{(\pm)})^2 - 1}{(\omega' \cdot \omega^{(\pm)})^2 + 1}\left\{\frac{(\omega' \cdot \omega_0^{(\pm)} + 1)^2}{(\omega' \cdot \omega_0^{(\pm)})^2 + 1} \cos 2(\Psi'^{(\pm)}_a + \Psi^{(\pm)}_a + \Psi'^{(\pm)}_b + \chi) + \frac{(\omega' \cdot \omega_0^{(\pm)} - 1)^2}{(\omega' \cdot \omega_0^{(\pm)})^2 + 1} \cos 2(\Psi'^{(\pm)}_a - \Psi^{(\pm)}_a - \Psi'^{(\pm)}_b + \chi)\right\} \tag{75b}$$

$\Psi_a^{(\pm)}$, $\Psi_\ell'^{(\pm)}$ and $\Psi_a'^{(\pm)}$ are given by equations (60c), (60d) and (71b). The dot products are defined as in equation (54). The (R, R) intensity overlaps the coherent line (73e).

6.1.2.2.2. Compton–Compton: The double scattering of the Compton effect is calculated by substituting the Compton kernel twice in equation (50a):

$$
\begin{aligned}
I^{(2)(S)}_{(C,C)_I}(\omega,\lambda,\chi) &= \frac{\sigma^2}{\omega_R \lambda_C} A(\eta_0,\lambda_0,\eta,\lambda) \\
&\times \left\{ \int_{\beta_1}^{\gamma_1} \frac{d\eta'}{\eta'} \frac{\mathcal{U}(\gamma_1-\beta_1)}{\sqrt{(1-\eta'^2)(1-\eta_R^2)-(\alpha-\eta'\eta_R)^2}} \right. \\
&\times \sum_{k=1}^{2} \frac{K_{KN}(\lambda,\tilde\lambda_k^{(+)}) K_{KN}(\tilde\lambda_k^{(+)},\lambda_0)}{\dfrac{\mu}{|\eta|}+\dfrac{\mu(\tilde\lambda_k^{(+)})}{\eta'}} \\
&\times S(\tilde\lambda_k^{(+)}, \omega\cdot\omega_k'^{(+)}, Z) S(\lambda_0, \omega_0\cdot\omega_k'^{(+)}, Z) \\
&\times (1+\mathcal{G}'^{(+)}_{CC_k}(\omega,\lambda,\omega',\lambda',\omega_0,\lambda_0,\chi)) \\
&+ \int_{\beta_2}^{\gamma_2} \frac{d\eta'}{\eta'} \frac{\mathcal{U}(\gamma_2-\beta_2)}{\sqrt{(1-\eta'^2)(1-\eta_R^2)-(\alpha+\eta'\eta_R)^2}} \\
&\times \sum_{k=1}^{2} \frac{K_{KN}(\lambda,\tilde\lambda_k^{(-)}) K_{KN}(\tilde\lambda_k^{(-)},\lambda_0)}{\dfrac{\mu_0}{|\eta_0|}+\dfrac{\mu(\tilde\lambda_k^{(-)})}{\eta'}} \\
&\times S(\tilde\lambda_k^{(-)}, \omega\cdot\omega_k'^{(-)}, Z) S(\lambda_0, \omega_0\cdot\omega_k'^{(-)}, Z) \\
&\left. \times (1+\mathcal{G}'^{(-)}_{CC_k}(\omega,\lambda,\omega',\lambda',\omega_0,\lambda_0,\chi)) \right\}, \qquad (76a)
\end{aligned}
$$

where

$$
\begin{aligned}
&\mathcal{G}'^{(\pm)}_{CC_k}(\omega,\lambda,\omega',\lambda',\omega_0,\lambda_0,\chi) \\
&= \frac{\dfrac{\tilde\lambda_k^{(\pm)}-\lambda_0}{\lambda_C}\left(\dfrac{\tilde\lambda_k^{(\pm)}-\lambda_0}{\lambda_C}-2\right)}{\dfrac{\lambda_0}{\tilde\lambda_k^{(\pm)}}+\dfrac{\tilde\lambda_k^{(\pm)}}{\lambda_0}+\dfrac{\tilde\lambda_k^{(\pm)}-\lambda_0}{\lambda_C}\left(\dfrac{\tilde\lambda_k^{(\pm)}-\lambda_0}{\lambda_C}-2\right)} \\
&\times \left[\cos 2(\Psi_{a_k}^{(\pm)}+\chi) \right. \\
&+ \frac{\dfrac{\lambda-\tilde\lambda_k^{(\pm)}}{\lambda_C}\left(\dfrac{\lambda-\tilde\lambda_k^{(\pm)}}{\lambda_C}-2\right)}{\dfrac{\lambda}{\tilde\lambda_k^{(\pm)}}+\dfrac{\tilde\lambda_k^{(\pm)}}{\lambda}+\dfrac{\lambda-\tilde\lambda_k^{(\pm)}}{\lambda_C}\left(\dfrac{\lambda-\tilde\lambda_k^{(\pm)}}{\lambda_C}-2\right)} \\
&\left. \times \cos 2(\Psi_{a_k}^{(\pm)}+\Psi_{\delta_k}'^{(\pm)}) \right]
\end{aligned}
$$

$$
\begin{aligned}
&+\frac{1}{2}\frac{\dfrac{\lambda-\tilde\lambda_k^{(\pm)}}{\lambda_C}\left(\dfrac{\lambda-\tilde\lambda_k^{(\pm)}}{\lambda_C}-2\right)}{\dfrac{\lambda}{\tilde\lambda_k^{(\pm)}}+\dfrac{\tilde\lambda_k^{(\pm)}}{\lambda}+\dfrac{\lambda-\tilde\lambda_k^{(\pm)}}{\lambda_C}\left(\dfrac{\lambda-\tilde\lambda_k^{(\pm)}}{\lambda_C}-2\right)} \\
&\times \left[\frac{\left(2-\dfrac{\tilde\lambda_k^{(\pm)}-\lambda_0}{\lambda_C}\right)^2}{\dfrac{\lambda_0}{\tilde\lambda_k^{(\pm)}}+\dfrac{\tilde\lambda_k^{(\pm)}}{\lambda_0}+\dfrac{\tilde\lambda_k^{(\pm)}-\lambda_0}{\lambda_C}\left(\dfrac{\tilde\lambda_k^{(\pm)}-\lambda_0}{\lambda_C}-2\right)} \right. \\
&\times \cos 2(\Psi_{a_k}'^{(\pm)}+\Psi_{a_k}^{(\pm)}+\Psi_{\delta_k}'^{(\pm)}+\chi) \\
&+ \frac{\left(\dfrac{\tilde\lambda_k^{(\pm)}-\lambda_0}{\lambda_C}\right)^2}{\dfrac{\lambda_0}{\tilde\lambda_k^{(\pm)}}+\dfrac{\tilde\lambda_k^{(\pm)}}{\lambda_0}+\dfrac{\tilde\lambda_k^{(\pm)}-\lambda_0}{\lambda_C}\left(\dfrac{\tilde\lambda_k^{(\pm)}-\lambda_0}{\lambda_C}-2\right)} \\
&\left. \left. \times \cos 2(\Psi_{a_k}'^{(\pm)}-\Psi_{a_k}^{(\pm)}-\Psi_{\delta_k}'^{(\pm)}+\chi) \right] \right. . \qquad (76b)
\end{aligned}
$$

$\Psi_{a_k}^{(\pm)}$ and $\Psi_{\delta_k}'^{(\pm)}$ are given by equations (61c) and (61d), $\Psi_{a_k}'^{(\pm)}$ by

$$
\begin{aligned}
&\cos \Psi_{a_k}'^{(\pm)} \\
&= \frac{\pm\eta'\sqrt{1-\eta_0^2}-\eta_0\sqrt{1-\eta'^2}\cos(\varphi_0-\varphi_k'^{(\pm)})}{(1-(\omega_0\cdot\omega_k'^{(\pm)})^2)^{1/2}}, \qquad (76c)
\end{aligned}
$$

the dot products by equations (61f) and (61g), and $\tilde\lambda_k^{(\pm)}$ by equation (61e). For convenience, we have introduced $\beta_1 = \max(0, \alpha\eta_R - D)$, $\gamma_1 = \min(1, \alpha\eta_R + D)$, $\beta_2 = -\min(0, \alpha\eta_R + D)$, $\gamma_2 = -\max(-1, \alpha\eta_R - D)$. The quantities ω_R, α, η_R, D, $\varphi_1'^{(\pm)}$ and $\varphi_2'^{(\pm)}$ were already defined by equations (61h–n). The integration limits β_i and γ_i cannot exceed the values -1 and 1. The Heaviside functions in the integrals are different from zero only when $\gamma_i > \beta_i$ and indicate the validity range of every integral. The wavelength spectrum of the (C, C) intensity term extends from $\lambda_0 + \lambda_c(2-\omega_R)$ to $\lambda_0 + \lambda_C(2+\omega_R)$. Equation (76a) is valid for $\omega_R \neq 0$, $\alpha^2 \neq 1$ and $\eta_R^2 \neq 1$. Limiting cases for the special values of ω_R, η_R and α can be calculated similarly.

6.1.2.2.3. Rayleigh–Compton: The contribution of Compton scattering of Rayleigh scattered photons is obtained similarly to equation (76)

$$
\begin{aligned}
I^{(2)(S)}_{(R,C)_I}(\omega,\lambda,\chi) &= \frac{\sigma^2}{Z\lambda_C} A(\eta_0,\lambda_0,\eta,\lambda) \\
&\times K_{KN}(\lambda,\lambda_0) S(\lambda_0, a, Z) \left\{ \int_{\beta_1}^{\gamma_1} \frac{d\eta'}{\eta'} \frac{1}{\dfrac{\mu}{|\eta|}+\dfrac{\mu_0}{\eta'}} \right. \\
&\times \frac{\mathcal{U}(\gamma_1-\beta_1)}{\sqrt{(1-\eta'^2)(1-\eta^2)-(a-\eta'\eta)^2}} \\
&\times \sum_{k=1}^{2} (1+(\omega_0\cdot\omega_k'^{(+)})^2) F^2(\lambda_0, \omega_0\cdot\omega_k'^{(+)}, Z)
\end{aligned}
$$

$$\times(1+\mathscr{G}'^{(+)}_{RC_k}(\omega,\lambda,\omega',\lambda',\omega_0,\lambda_0,\chi))$$

$$+\int_{\beta_2}^{\gamma_2}\frac{d\eta'}{\eta}\frac{1}{\frac{\mu_0}{|\eta_0|}+\frac{\mu_0}{\eta'}}\frac{\mathscr{U}(\gamma_2-\beta_2)}{\sqrt{(1-\eta'^2)(1-\eta^2)-(a+\eta'\eta)^2}}$$

$$\times\sum_{k=1}^{2}(1+(\omega_0\cdot\omega'^{(-)}_k)^2)F^2(\lambda_0,\omega_0\cdot\omega'^{(-)}_k,Z)$$

$$\times(1+\mathscr{G}'^{(-)}_{RC_k}(\omega,\lambda,\omega',\lambda',\omega_0,\lambda_0,\chi))\Bigg\}, \qquad (77a)$$

where

$$\mathscr{G}'^{(\pm)}_{RC_k}(\omega,\lambda,\omega',\lambda',\omega_0,\lambda_0,\chi)=\frac{(\omega_0\cdot\omega'^{(\pm)}_k)^2-1}{(\omega_0\cdot\omega'^{(\pm)}_k)^2+1}$$

$$\times\Bigg[\cos 2(\Psi^{(\pm)}_{a_k}+\chi)$$

$$+\frac{\frac{\lambda-\lambda_0}{\lambda_C}\left(\frac{\lambda-\lambda_0}{\lambda_C}-2\right)}{\frac{\lambda}{\lambda_0}+\frac{\lambda_0}{\lambda}+\frac{\lambda-\lambda_0}{\lambda_C}\left(\frac{\lambda-\lambda_0}{\lambda_C}-2\right)}$$

$$\times\cos 2(\Psi^{(\pm)}_{a_k}+\Psi'^{(\pm)}_{\delta_k})\Bigg]$$

$$+\frac{1}{2}\frac{\frac{\lambda-\lambda_0}{\lambda_C}\left(\frac{\lambda-\lambda_0}{\lambda_C}-2\right)}{\frac{\lambda}{\lambda_0}+\frac{\lambda_0}{\lambda}+\frac{\lambda-\lambda_0}{\lambda_C}\left(\frac{\lambda-\lambda_0}{\lambda_C}-2\right)}$$

$$\times\Bigg\{\frac{(\omega_0\cdot\omega'^{(\pm)}_k+1)^2}{(\omega_0\cdot\omega'^{(\pm)}_k)^2+1}$$

$$\times\cos 2(\Psi'^{(\pm)}_{a_k}+\Psi^{(\pm)}_{a_k}+\Psi'^{(\pm)}_{\delta_k}+\chi)$$

$$+\frac{(\omega_0\cdot\omega'^{(\pm)}_k-1)^2}{(\omega_0\cdot\omega'^{(\pm)}_k)^2+1}$$

$$\times\cos 2(\Psi'^{(\pm)}_{a_k}-\Psi^{(\pm)}_{a_k}-\Psi'^{(\pm)}_{\delta_k}+\chi)\Bigg\}, \qquad (77b)$$

$\Psi^{(\pm)}_{a_k}$, $\Psi'^{(\pm)}_{a_k}$ and $\Psi'^{(\pm)}_{\delta_k}$ are defined by equations (61c), (76c) and (62c), $\beta_1=\max(0,a\eta-D)$, $\gamma_1=\min(1,a\eta+D)$, $\beta_2=-\min(0,a\eta+D)$, $\gamma_2=-\max(-1,a\eta-D)$ and $\omega_0\cdot\omega'^{(\pm)}_k$—as in equation (61f)—are defined in terms of a, D, $\varphi'^{(\pm)}_1$ and $\varphi'^{(\pm)}_2$, defined by equations (62d–g). The meaning of the limits β_i and γ_i is as in equation (76a). The (R, C) intensity is continuous and its wavelength spectrum extends from λ_0 to $\lambda_0+2\lambda_C$ (in energy from $E_0/(1+2E_0/(m_0c^2))$ to E_0).

6.1.2.2.4. Compton–Rayleigh: The Rayleigh scattering of Compton scattered photons is obtained similarly

$$I^{(2)(S)}_{(R,C)_I}(\omega,\lambda,\chi)=\frac{\sigma^2}{Z\lambda_C}A(\eta_0,\lambda_0,\eta,\lambda)$$

$$\times K_{KN}(\lambda,\lambda_0)S(\lambda_0,a,Z)$$

$$\times\Bigg\{\int_{\beta_1}^{\gamma_1}\frac{d\eta'}{\eta'}\frac{1}{\frac{\mu}{|\eta|}+\frac{\mu}{\eta'}}$$

$$\times\frac{\mathscr{U}(\gamma_1-\beta_1)}{\sqrt{(1-\eta'^2)(1-\eta_0^2)-(a-\eta'\eta_0)^2}}$$

$$\times\sum_{k=1}^{2}(1+(\omega\cdot\omega'^{(+)}_k)^2)F^2(\lambda,\omega_0\cdot\omega'^{(+)}_k,Z)$$

$$\times(1+\mathscr{G}'^{(+)}_{CR_k}(\omega,\lambda,\omega',\lambda',\omega_0,\lambda_0,\chi))$$

$$+\int_{\beta_2}^{\gamma_2}\frac{d\eta'}{\eta'}\frac{1}{\frac{\mu_0}{|\eta_0|}+\frac{\mu}{\eta'}}$$

$$\times\frac{\mathscr{U}(\gamma_2-\beta_2)}{\sqrt{(1-\eta'^2)(1-\eta_0^2)-(a+\eta'\eta_0)^2}}$$

$$\times\sum_{k=1}^{2}(1+(\omega_0\cdot\omega'^{(-)}_k)^2)F^2(\lambda,\omega_0\cdot\omega'^{(-)}_k,Z)$$

$$\times(1+\mathscr{G}'^{(-)}_{CR_k}(\omega,\lambda,\omega',\lambda',\omega_0,\lambda_0,\chi))\Bigg\}, \qquad (78a)$$

where

$$\mathscr{G}'^{(\pm)}_{CR_K}(\omega,\lambda,\omega',\lambda',\omega_0,\lambda_0,\chi)$$

$$=\frac{\frac{\lambda-\lambda_0}{\lambda_C}\left(\frac{\lambda-\lambda_0}{\lambda_C}-2\right)}{\frac{\lambda}{\lambda_0}+\frac{\lambda_0}{\lambda}+\frac{\lambda-\lambda_0}{\lambda_C}\left(\frac{\lambda-\lambda_0}{\lambda_C}-2\right)}$$

$$\times\left(\cos 2(\Psi^{(\pm)}_{a_k}+\chi)+\frac{(\omega_0\cdot\omega'^{(\pm)}_k)^2-1}{(\omega_0\cdot\omega'^{(\pm)}_k)^2+1}\right.$$

$$\left.\times\cos 2(\Psi^{(\pm)}_{a_k}+\Psi'^{(\pm)}_{\delta_k})\right)$$

$$+\frac{1}{2}\frac{(\omega\cdot\omega'^{(\pm)}_k)^2-1}{(\omega\cdot\omega'^{(\pm)}_k)^2+1}$$

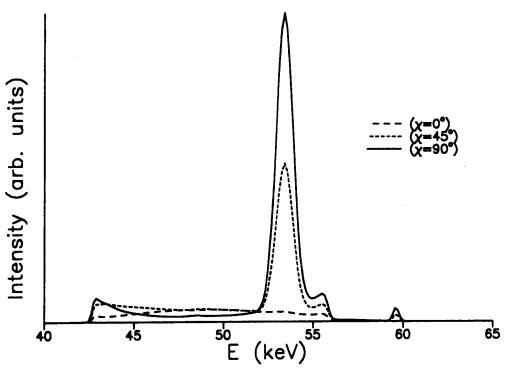

Fig. 26. Total double-scattering spectra for water excited with $E_0=60$ keV and calculated with the code SHAPE modified for linearly polarized incidence (Fernandez, 1993b). The geometry is $\vartheta_0=45°$, $\vartheta=135°$, $\varphi_0=\varphi=0$, i.e. the scattering angle Θ is 90°. The plot shows the spectra calculated with three orientations of the polarization line of the incident beam: $\chi=0°$ (parallel), $\chi=45°$ and $\chi=90°$ (perpendicular).

$$\times\left\{\frac{\left(2-\frac{\lambda-\lambda_0}{\lambda_C}\right)^2}{\frac{\lambda}{\lambda_0}+\frac{\lambda_0}{\lambda}+\frac{\lambda-\lambda_0}{\lambda_C}\left(\frac{\lambda-\lambda_0}{\lambda_C}-2\right)}\right.$$

$$\times\cos 2(\Psi'^{(\pm)}_{a_k}+\Psi^{(\pm)}_{a_k}+\Psi'^{(\pm)}_{\delta_k}+\chi)$$

$$+\frac{\left(\frac{\lambda-\lambda_0}{\lambda_C}\right)^2}{\frac{\lambda}{\lambda_0}+\frac{\lambda_0}{\lambda}+\frac{\lambda-\lambda_0}{\lambda_C}\left(\frac{\lambda-\lambda_0}{\lambda_C}-2\right)}$$

$$\left.\times\cos 2(\Psi'^{(\pm)}_{a_k}-\Psi^{(\pm)}_{a_k}-\Psi'^{(\pm)}_{\delta_k}+\chi)\right\}, \quad (78b)$$

$\Psi'^{(\pm)}_{\delta_k}$ and $\Psi^{(\pm)}_{a_k}$ are given by equations (61d) and (63c), $\Psi'^{(\pm)}_{a_k}$ by

$$\cos \Psi'^{(\pm)}_{a_k} = \frac{\pm\eta'\sqrt{1-\eta_0^2}-\eta_0\sqrt{1-\eta'^2}\cos(\varphi_0-\varphi'^{(\pm)}_k)}{(1-a^2)^{1/2}}. \quad (78c)$$

$\beta_1=\max(0, a\eta_0-D)$, $\gamma_1=\min(1, a\eta_0+D)$, $\beta_2=-\min(0, a\eta_0+D)$, $\gamma_2=-\max(-1, a\eta_0-D)$, and $\omega\cdot\omega'^{(\pm)}_k$—as in equation (61g)—are defined in terms of a, D, $\varphi'^{(\pm)}_1$ and $\varphi'^{(\pm)}_2$, given by equations (63d–g). The meaning of the limits β_i and γ_i is as in the preceding equation. The (C, R) intensity is continuous and its wavelength spectrum extends from λ_0 to $\lambda_0+2\lambda_C$ (as in the preceding case).

6.1.2.3. Influence of the polarization plane orientation. The vector model predicts first- and second-order (component I) intensities which depend on the angle χ measuring the tilt of the polarization line with respect to the scattering plane. The degrees of polarization and the intensities of these scattering effects present a quite different sensitivity to the incident polarization. The Rayleigh effect gives totally polarized radiation after the first collision for any angle χ not null. The first-collision Rayleigh intensity is straightforwardly related to χ vanishing for parallel polarization ($\chi=0$). On the other hand, the Compton effect gives mixed unpolarized and polarized fractions at almost all scattering angles. It is fully polarized in the backward direction, and introduces a strong depolarization at right and higher angles scattering whose strength is very dependent on the angle χ. The first-collision Compton intensity is also strongly influenced by χ, but does not vanish for $\chi=0$ as for the Rayleigh effect. These different behaviours play an important role in multiple scattering terms where participate scattering contributions from atoms located in all directions. The influence of χ in second-order intensities is contained in the factor $\mathscr{G}'$. Although $\mathscr{G}'$ admits a closed description [see equation (69b)], it belong to the integrand of one (or two) angular integral(s) and its effects cannot be described straightforwardly.

The influence of the incident polarization is better appreciated if one is shown calculations of the same γ-ray spectrum with different orientations of the polarization line. Figure 26 shows several spectra of water built with the code SHAPE by adding the contributions of the first two orders of scattering and filtering with a Ge detector response including escape peak. These spectra correspond to an excitation with the 59.54 keV line of ^{241}Am and a right scattering angle ($\Theta=90°$), obtained with incidence and take-off polar angles on the normal plane of scattering ($\vartheta_0=45°$, $\vartheta=135°$, $\varphi=\varphi_0=0$). The monochromatic peaks are broadened with a Gaussian shape as in Fig. 19. The multiple scattering orders are not retouched. On the spectra of Fig. 26 the effect of χ is important to determine the signal/noise (or peak/background) ratio, a figure of merit frequently used in spectroscopic measurements. The best signal/noise ratio is obtained for $\chi=90°$, i.e. for polarization normal to the scattering plane, which is also the condition for maximum scattered intensity. This signal/noise ratio improves that of the similar spectrum simulated with unpolarized radiation [shown in Fig. 19(d)], which agrees with the experimental practice of using polarized sources for background reduction (Christoffersson and Mattson, 1983).

6.2. Multiple Scattering Intensities for Circularly Polarized Sources

In this section we shall compute the intensity terms for the special case of a circularly polarized source. For simplicity, we shall describe the transport in the system S of Stokes. An arbitrarily linearly polarized source of monochromatic and collimated γ-rays of I_0 photons cm^{-2} s^{-2} is represented mathematically, in the Stokes system, by a source function (see Table 2).

$$\mathscr{S}^{(S)}(\omega,\lambda)=I_0\,\delta(\omega-\omega_0)\,\delta(\lambda-\lambda_0)\begin{bmatrix}1\\0\\0\\1\end{bmatrix}. \quad (79a)$$

which corresponds to ellipticity 1, i.e. $\beta=\pi/4$. Alternatively, circular polarization with the opposite sense of polarization, corresponding to $\beta=-\pi/4$, is obtained with the source

$$\mathscr{S}^{(S)}(\omega,\lambda)=I_0\,\delta(\omega-\omega_0)\,\delta(\lambda-\lambda_0)\begin{bmatrix}1\\0\\0\\-1\end{bmatrix}. \quad (79b)$$

In this section we shall use equation (79a).

Substitution of equations (64) and (65a) in the solution of the transport equation gives, for the first-order intensity vector corresponding to the one-collision chain

$$(\omega,\lambda_0)\xrightarrow{a}(\omega,\lambda)$$

involving the generic interaction a, the relationship

$$\mathbf{I}^{(1)(S)}_{(a)}(\omega,\lambda) = A(\eta_0,\lambda_0,\eta,\lambda) \times k_a(\omega,\lambda,\omega_0,\lambda_0)\begin{bmatrix} 1 \\ a'_{21}\cos 2\Psi \\ a'_{21}\sin 2\Psi \\ a'_{44} \end{bmatrix}, \quad (80)$$

where Ψ is defined as in equation (11c), with ω_0 in place of ω'. As in equation (67a), we can represent the first-order intensity vector $\mathbf{I}^{(1)(S)}_{(a)}$ decomposed in two fraction beams, the unpolarized and the polarized fractions, with the two fractions given by the relationships

$$\mathbf{I}^{(1)(S)u}_{(a)} = A(\eta_0,\lambda_0,\eta,\lambda) \times k_a(\omega,\lambda,\omega_0,\lambda_0)(1-P_a)\begin{bmatrix} 1 \\ 0 \\ 0 \\ 0 \end{bmatrix}, \quad (81a)$$

and

$$\mathbf{I}^{(1)(S)p}_{(a)} = A(\eta_0,\lambda_0,\eta,\lambda) \times k_a(\omega,\lambda,\omega_0,\lambda_0)P_a\begin{bmatrix} 1 \\ \cos 2\xi\cos 2\zeta \\ \sin 2\xi\cos 2\zeta \\ \sin 2\zeta \end{bmatrix} \quad (81b)$$

where P_a represents the degree of polarization [see equation (5e)] of the interaction a for the circularly polarized source

$$P_a(\omega,\lambda,\omega_0,\lambda_0) = \frac{(\mathbf{I}^{(1)(S)2}_{(a)Q} + \mathbf{I}^{(1)(S)2}_{(a)U} + \mathbf{I}^{(1)(S)2}_{(a)V})^{1/2}}{\mathbf{I}^{(1)(S)2}_{(a)I}} = (a'^2_{21} + a'^2_{44})^{1/2}. \quad (81c)$$

The polarized fraction (81b) represents an elliptically polarized scattered beam whose major axis of polarization forms an angle $\xi = \Psi$ (as in equation (11c) with ω_0 in place of ω') with the scattering plane, and whose ellipticity is given by any one of the relationships

$$\cos\zeta = \frac{a'_{21}}{(a'^2_{21} + a'^2_{44})^{1/2}}, \quad (81d)$$

$$\sin\zeta = \frac{a'_{44}}{(a'^2_{21} + a'^2_{44})^{1/2}}. \quad (81e)$$

The angles ζ and ξ are defined analogously to the angles β and χ of equations (3a) and (3b).

The component I of the first-order intensity, representing the intensity collected by a polarization insensitive detector, is given by the first component of the intensity vector (80),

$$\mathbf{I}^{(1)(S)}_{(a)I}(\omega,\lambda) = A(\eta_0,\lambda_0,\eta,\lambda)k_a(\omega,\lambda,\omega_0,\lambda_0), \quad (82)$$

which is coincident with the first-order intensity obtained with the unpolarized source [compare equation (82) with equation (47a)]. Analogously, the second-order intensity due to the collision chain

$$(\omega_0,\lambda_0) \xrightarrow{a} (\omega',\lambda') \xrightarrow{b} (\omega,\lambda)$$

involving two generic interactions a and b is given by

$$\mathbf{I}^{(2)(S)}_{(a,b)I}(\omega,\lambda) = A(\eta_0,\lambda_0,\eta,\lambda)\int_0^\infty d\lambda' \int_{4\pi} d\omega' \frac{1}{|\eta'|} \times \frac{(1+\operatorname{sgn}\eta')}{2}\frac{k_b(\omega,\lambda,\omega',\lambda')k_a(\omega',\lambda',\omega_0,\lambda_0)(1+\mathscr{G}''_{ab}(\omega,\lambda,\omega',\lambda',\omega_0,\lambda_0))}{\frac{\mu}{|\eta|}+\frac{\mu'}{|\eta'|}} + \frac{(1-\operatorname{sgn}\eta')}{2}\frac{k_b(\omega,\lambda,\omega',\lambda')k_a(\omega',\lambda',\omega_0,\lambda_0)(1+\mathscr{G}''_{ab}(\omega,\lambda,\omega',\lambda',\omega_0,\lambda_0))}{\frac{\mu_0}{|\eta_0|}+\frac{\mu'}{|\eta'|}} \quad (83a)$$

which compared with the expression for the same intensity term deduced with the unpolarized source (Section 5.1), differs only in the symbol for the corrective factor $\mathscr{G}''_{ab}(\omega,\lambda,\omega',\lambda',\omega_0,\lambda_0)$, defined in terms of the primed matrix coefficients as

$$\mathscr{G}''_{ab}(\omega,\lambda,\omega',\lambda',\omega_0,\lambda_0) = a'_{21}b'_{12}\cos 2(\Psi_a + \Psi'_b) = \mathscr{G}_{ab}(\omega,\lambda,\omega',\lambda',\omega_0,\lambda_0), \quad (83b)$$

where Ψ_a and Ψ'_b are angles of spherical triangles for the interactions a and b, respectively, similar as those shown in Fig. 2 for one single interaction. These angles are defined, respectively, by equations (50c) and (50d). The expression (83b) is identical to equation (50b), when that is expressed in terms of the primed coefficients. Obviously, the coefficients in equation (83b) cannot assume the previous meaning of degree of polarization as in equation (50b). Furthermore, the expressions for the components Q and U, substantially more complicated and not included in this article, also coincide with the corresponding expressions calculated for the unpolarized source. Therefore, the first three Stokes components of the second-order intensity are identical to the corresponding components for the unpolarized source. In contrast, the component V of the intensity is given by

$$\mathbf{I}^{(2)(S)}_{(a,b)V}(\omega,\lambda) = a'_{44}b'_{44}, \quad (83c)$$

meaning that the polarized fraction is also elliptically polarized after the second scattering.

The mentioned properties are sufficient to make a comparison between the multiple scattering intensity terms for the circularly polarized source with the

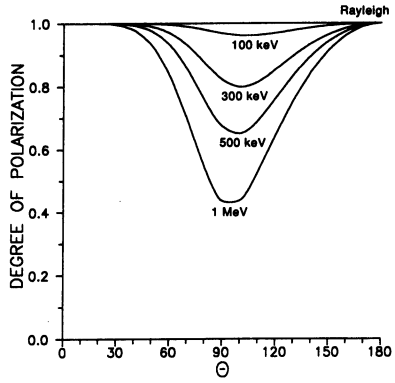

Fig. 27. The degrees of polarization for the Compton and Rayleigh effects, for a circularly polarized incident beam, are shown as functions of the scattering angle for several values of the incident energy. The degree of polarization by Rayleigh scattering is constant. In contrast, the Compton degree depends on the above two variables and is responsible for the gradual depolarization of the beam. The depolarization of the beam is minimum (null) for forward and backward scattering, and maximum for right angle scattering.

corresponding intensity terms for the unpolarized source. The only difference betwen the first- and second-order intensities for both sources is precisely the component V of the intensity, which is null for the unpolarized source, and not null for the circularly polarized one. Since the other components are identical (component to component) for the first two terms, the V component is the only responsible for the change in the degree of polarization which regulates the intensity of the polarized and unpolarized fractions of the beam after the collision. The degrees of polarization for the Rayleigh and Compton effects are, respectively,

$$P_R(\omega, \lambda, \omega_0, \lambda_0) = 1, \tag{84a}$$

and

$$P_C(\omega, \lambda, \omega_0, \lambda_0) = \frac{(b^2(2-b)^2 + a^2(1-b)^2)^{1/2}}{a - b(2-b)}, \tag{84b}$$

where $a(\lambda, \lambda_0) = \lambda/\lambda_0 + \lambda_0/\lambda$, $b(\lambda, \lambda_0) = (\lambda - \lambda_0)/\lambda_C$. It is easily seen that the unitary degree of polarization for Rayleigh scattering means that only fully polarized radiation is produced in the first collision for any scattering angle. Figure 27 shows the degree of polarization for Compton scattering for several energies of the incident beam. The depolarization increases with the energy, and is concentrated around the scattering at right angle ($\Theta = 90°$). For forward and backward scattering, the depolarization is almost non existent.

Due to the mentioned similarities, the expressions for the intensity terms involving the photoelectric, Rayleigh and Compton effects are equal to those already given in Section 5, and will not be repeated here.

6.3. *Complementary References on Polarization Effects*

Linear polarization has been intensively studies by other authors who investigated aspects and applications not covered in this article. The following complementary references are specific to linear polarization: Miller and Wilcox (1961), Maximon (1989), Maximom and Olsen (1962), Ewan *et al.* (1969), Honzatko and Kajfosz (1969), Kel'ner (1969), Kel'ner *et al.* (1975), Olekhnovich (1969), Litherland *et al.* (1970), Logan (1971), Evans *et al.* (1977), Hart (1978, 1991, 1992), Hart *et al.* (1991b), Le Page *et al.* (1979), Flack and Vincent (1980), Vincent and Flack (1980a, 1980b), Vincent (1982), Lawrence (1982, 1983), Dwiggins (1983), Brummer *et al.* (1984), Ohkawa and Hashimoto (1984), Materlik and Suortti (1984), Alexandrov *et al.* (1989), Siddons *et al.* (1989), Wielopolski *et al.* (1989), Scofield (1990), Ribberfors and Matscheko (1992).

Circularly polarized photons have been recently used to probe the magnetic properties of some materials (Gibbs *et al.*, 1989; Sakai *et al.*, 1989), with recourse to the explicit dependence of some terms in the polarization matrix on the spin of the electrons. These terms were not discussed in this article, because we assumed randomly distributed spins (see Section 4.3). Complementary theoretical and experimental articles on circular polarization are Schopper (1958), Huber *et al.* (1963), Schultz *et al.* (1989), Ishikawa (1989).

Elliptically polarized photons were specifically studied by Brummer *et al.* (1982) and Koide *et al.* (1991).

7. EFFECTS OF THE POLARIZATION IN THE MONTE CARLO CODES FOR PHOTON TRANSPORT

The Boltzmann transport equation for inhomogeneous targets with complex boundaries, or complex source distributions, or involving several kinds of particles, cannot be attacked with analytical techniques of the kind shown in this article and must be solved numerically. Numerical calculations of the X-ray flux can be obtained by constructing model trajectories of photons according to the Monte Carlo sampling method (Fano *et al.*, 1959; Cashwell and Everett, 1959; Carter and Cashwell, 1975; Kalos and Whitlock, 1986).

The Monte Carlo method was probably invented, but not so named, by Fermi in the early 30's to give accurate predictions of experimental results (Metropolis, 1985). It was developed until reaching its modern form by Metropolis, Richtmyer, Ulam, von Neumann, Everett and Cashwell in the post-war Los Alamos Scientific Laboratory with the first paper of this group submitted for publication in the spring of 1949. Other groups contributing to the first steps of Monte Carlo were at National Bureau of Standards, Rand Corporation and IBM. The unpublished paper from Spencer (1948) that we mentioned

above is a very early documented application of Monte Carlo performed at NBS.

The code MCNP (Monte Carlo Neutron Photon) developed by the group X-6 is the workhorse at LANL for neutron, photon, and coupled neutron–photon calculations using the Monte Carlo method (Foster and Godfrey, 1985; Briesmeister, 1986). MCNP appeared in 1976 as a combination of the codes MCN [Monte Carlo Neutron, (Cashwell *et al.*, 1972)], MCG and MCP [Monte Carlo Gamma and Monte Carlo Photon, (Cashwell, *et al.*, 1973; Everett and Cashwell, 1973)]. MCNP uses detailed neutron and photon physics models that contain the most up-to-date cross-sections and reaction information from the ENDF/B and other evaluations. MCNP transports particles in generalized three-dimensional geometries are built up using different surfaces. State-of-the-art Monte Carlo methods are used in all phases of the particle transport including the source, geometry-tracking, variance-reduction and tally-estimation processes. Version 4 of MCNP, presently under test, integrates the code ITS (i.e. electrons) to MCNP (Mack *et al.*, 1985). In its actual state MCNP includes Rayleigh and Compton scattering, but neglects polarization effects.

Current transport calculations using the Monte Carlo technique, including the now widely-used ETRAN codes of Seltzer and Berger (Seltzer, 1988a, 1988b, 1991), generally ignore coherent (Rayleigh) scattering. The reasons for ignoring coherent scattering are that the scattered-photon energy is unchanged from that of the primary photon, the angular distribution at high photon energies is strongly forward-peaked, and its contribution to the total photon interaction cross section is small, reaching its maximum contribution of only 10% just below the photoelectric effect K absorption edge, for high-Z elements.

In certain situations, such as in medical diagnostic and industrial flaw-detection X-ray imaging, coherent scattering can have a significant effect on the image sharpness, as their single-scatter calculations show that coherently scattered photons diverge sufficiently from the primary ray to degrade image contrast, and that they account for a significant fraction of the total scattered energy fluence at the image receptor.

ITS (Integrated TIGER System) is a code derived from ETRAN for coupled electron and photon transport with and without the presence of macroscopic electric and magnetic fields of arbitrary dependence, developed at Sandia National Laboratories by Halbleib and Mehlhorn (1984). ITS can treat 3-D geometries and include a P-code supplement with detailed ionization/relaxation physics devoted to low energy photon studies, but it does not include Rayleigh scattering and binding corrections to incoherent scattering. It does not consider polarization effects.

In addition to the NBS/NIST ETRAN codes of Seltzer and Berger, another system of radiation transport codes, EGS, has been developed at SLAC by Ford and Nelson (1978), of which the EGS4 version has been described by Nelson, Hirayama and Rogers (1985) and more recently by Nelson and Namito (1990). EGS4 does include coherent scattering as an option. This option of EGS4 was used by Rogers and Bielajew (1990) to calculate narrow-beam and broad-beam central-axis depth dose for 30-keV photons incident on water, for penetration depths up to 27 mean free paths. Their results indicated that the narrow-beam geometry is much more sensitive to the inclusion of coherent scattering than is the broad-beam geometry. In either case, the with and without coherent scattering differences were found to be substantial. At 4 mean free paths, inclusion of coherent scattering decreases the broad-beam result by only 0.7%, but decreases the narrow-beam result by 20%, and at 18 mean free paths these decreases are 19 and 105%, respectively. Recently, EGS4 has been extended to include linear polarization effects in coherent and incoherent scattering (Namito *et al.*, 1993).

A detailed comparison between the biggest codes for Monte Carlo simulation together with an exhaustive list of applications can be found in the review article by Andreo (1991). However, it is apparent that almost all of these codes neglect polarization effects. This fact precludes not only their use with polarized sources where a correct approach is essential, but also for the case of unpolarized sources introduces the error in the photon transport that we pointed out in Section 5. As the secondary electrons from these interactions are polarized (which changes the angular distribution of charged particles into the target), the codes for electron transport are also very sensitive to this approximation. A more subtle error is possible for those codes regarding coupled photon–electron transport under external fields. The Compton polarization matrix that we give in Section 4 (and with which we compute the vector intensities), corresponds to randomly oriented spins of the electrons in the atoms of the target. A material exposed to an external magnetic field presents a polarization matrix with non-zero coefficients in the last row and column, giving a changed response (not considered in this article) to the unpolarized source.

Some effort has been made in developing polarization dependent Monte Carlo simulation codes. Actually, just a few computer codes that compute intensities including polarization can be used with unpolarized and linearly polarized sources. Unfortunately, these codes either are devoted to a specific problem such as the simulation of Compton profiles (Felsteiner *et al.*, 1974; Felsteiner and Pattison, 1975; Tanner and Epstein, 1976c; Chomilier *et al.*, 1985; Pitkanen *et al.*, 1986), or are still under development and have been not sufficiently tested (Janssens *et al.*, 1993; Vincze *et al.*, 1993). None of them includes electron transport. These codes do not use a general beam of a partically elliptically polarized source, and do not estimate the other parameters (other than the intensity) that completely define the polarization state.

8. SUMMARY AND CONCLUSIONS

The effects of polarization on the multiple scattering of X-ray and low energy γ-ray photons have been considered within the framework of the Boltzmann transport theory. We have used an iterative analytical solution to the integro-differential transport equation to build up the intensity contributions to the scattering spectrum of thick targets for a generic elliptically (partially) polarized source beam. The vector solution gives the Stokes components for the partial intensity terms of first- and second-order (corresponding to one and two collisions). These terms were calculated for all the combinations of the prevailing interactions in the low energy γ-ray regime: photoelectric effect, and Rayleigh and Compton scattering. The polarization matrix for all of the interactions was given. Rayleigh and Compton cross-sections included respectively the form factor and the scattering function. The calculated intensities have accounted for the attenuation in the target. The overlapping of the calculated terms allowed the build-up of detailed backscattering spectra for three types of sources: unpolarized, linearly polarized and circularly polarized.

The scattering of unpolarized photons gives a partially polarized beam with a fraction of linearly polarized photons. The intensity of the spectrum is higher when compared with results from the equivalent scalar transport equation and averaged polarization cross-sections. This is due to the greater penetration of polarized X-rays. The degrees of polarization for Compton and Rayleigh scattering are similar and have their maxima at or near 90° scattering, for which the scattered beam is almost completely polarized. The multiple scattering reduces this degree of polarization, increasing the unpolarized component. Not all the intensity terms are modified by the effect of polarization. Only the terms with Rayleigh or Compton scattering present differences. The terms with at least one photoelectric scattering remain unchanged (assuming photoelectric effect independent of polarization). This fact ensures us the complete validity of previous calculations with the scalar equation in this case.

Linearly polarized photons scatter into linearly polarized photons, with maximum degree of polarization of Compton photons for backward scattering, and minimum for right angle scattering, i.e. Compton scattering depolarizes the beam. Rayleigh scattering gives a fully polarized scattered beam for any scattering angle. Multiple scattering reduces the depolarization. The intensity is dependent on the orientation of the polarization line of the incident beam. The maximum intensity corresponds to a polarization line perpendicular to the scattering plane. A linearly polarized source "perpendicular" serves to improve the peak-to-background ratio with respect to an identical Compton scattering experiment performed with unpolarized radiation.

Circularly polarized photons produce elliptically polarized photons. Compton scattering partially depolarizes the beam, having the maximum depolarization for 90° scattering. In contrast, Rayleigh scattering gives only a polarized scattering beam. Multiple scattering reduces the depolarization. The first- and second-order intensities have the same expressions as for the unpolarized source.

A survey on the bigger Monte Carlo codes for photon transport shows that only EGS4 includes linear polarization. This omission makes that the codes underestimate Compton–Rayleigh background for the case of unpolarized sources. A few new Monte Carlo codes can handle linear polarization, and therefore, are practicable for synchrotron light sources. However these codes cannot handle a general elliptically polarized source and they are not sufficiently tested.

The expressions for the intensity terms have been integrated to improve the preexisting code SHAPE, which offers the possibility of investigating the extent of the several interferences building scattered X-ray spectra for different geometries of excitation–detection, excitation energies, composition of the target, and polarization of the source. This code can substitute advantageously Monte Carlo simulations in those cases where the simple geometry considered is sufficient. The expressions shown in the article, as the code SHAPE, can be straightforwardly adapted to the more general case of a multi-layer composed of many multielement layers. An additional modification to the polarization matrix to include the missing terms which depend on the spin of the electrons can render this code a useful tool to study magnetic properties of multi-layers by using polarized γ-rays.

REFERENCES

Agarwal B. K. (1991) *X-Ray Spectroscopy*, 2nd edn. Springer, Berlin.

Alexandropoulos N. G., Parks S. H. and Kuriyama M. (1971) Polarization of the X-ray Compton–Raman radiation. *Phys. Lett.* **A35,** 369.

Alexandropoulos N. G., Chatzigeogiou T., Evangelakis G., Cooper M. J. and Manninen S. (1988) Bremsstrahlung and its contributions to the gamma ray spectra of solids. *Nucl. Intrum. Meth.* **A271,** 543.

Alexandrov Yu. M., Vinogradov A. V., Zorev N. N., Kozhevnikov I. V., Kondratenko V. V., Koshevoi M. O., Murashova V. A., Rupasov A. A., Fedorenko A. I., Shikanov A. S. and Yakimenko M. N. (1989) Study of polarization properties of multilayer X-ray mirrors. *Nucl. Instrum. Meth.* **A282,** 551.

Amusia M. Ya. (1990) *Atomic Photoeffect*. Plenum Press, New York.

Anand S., Singh M. and Sood B. S. (1965) Effects of L-shell electrons on the polarization of elastic scattering of gamma rays. *Curr. Sci.* **34,** 45.

Andreo P. (1991) Monte Carlo techniques in medical radiation physics. *Phys. Med. Biol.* **36,** 861.

Bambynek W., Crasemann B., Fink R. W., Freund H. U. and Mark M. (1972) X-ray fluorescence yields, Auger, and Koster–Kronig transition probabilities. *Rev. Mod. Phys.* **44,** 716.

Barkla C. G. (1905) Polarized Rontgen radiation. *Phil. Trans. Roy. Soc. Lond.* **A204,** 467.

Barkla C. G. (1906) Polarization in secondary Rontgen radiation. *Proc. Roy. Soc. Lond.* **A77,** 247.

Bearden J. A. (1967) X-ray wavelengths. *Rev. Mod. Phys.* **39,** 78.

Bearden J. A. and Burr A. F. (1967) Reevaluation of X-ray atomic energy levels. *Rev. Mod. Phys.* **39,** 125.

Bertin E. P. (1975) *Principles and Practice of X-Ray Spectrometric Analysis.* Plenum Press, New York.

Biggs F., Mendelsohn L. B. and Mann J. B. (1975) Hartree-Fock Compton profiles for the elements. *Atom. Data Nucl. Data Tables* **16,** 201.

Bishop H. E. and Riviere J. C. (1969) Estimates of the efficiencies of production and detection of electron-excited Auger emission. *J. App. Phys.* **40,** 1740.

Bobel G. and Passatore G. (1960) On the polarization of photons elastically scattered by mercury atoms. *N. Cimento* **15,** 979.

Bock P. (1971) Theory of polarization phenomena in Compton scattering by electrons. *Nucl. Phys.* **A177,** 289.

Braun-Keller E. and Epstein I. R. (1977a) Multiple scattering in the Compton effect. IV. Operator formalism for nonstationary electrons. *Phys. Rev.* **A16,** 1146.

Braun-Keller E. and Epstein I. R. (1977b) Multiple scattering in the Compton effect. V. Bounds on errors associated with multiple-scattering corrections. *Phys. Rev.* **A16,** 1154.

Brenner S., Brown G. E. and Wodward J. B. (1954) The coherent scattering of gamma-rays by K electrons in heavy atoms. II. The scattering of $0.32\,mc^2$ gamma-rays in mercury. *Proc. Roy. Soc. Lond.* **A227,** 59.

Briesmeister J. (Ed.) (1986) MCNP—A General Monte Carlo Code for Neutron and Photon Transport. Version 3A. Los Alamos National Laboratory Report LA-7396-M, Rev. 2.

Brini D., Fuschini E., Peli L. and Veronesi P. (1958) Elastic scattering of polarized photons. *N. Cimento* **7,** 877.

Brini D., Fuschini E., Murty D. S. R. and Veronesi P. (1959) Rayleigh scattering of polarized photons. *N. Cimento* **11,** 533.

Brockwell P. J. (1965) The multiple Compton scattering of low energy-gamma radiation. *Phil. Mag.* **12,** 515.

Brown G. E. and Mayers D. F. (1956) The coherent scattering of gamma-rays by *K* electrons in heavy atoms. III. The scattering of $0.64\,mc^2$ gamma-rays in mercury. *Proc. Roy. Soc. Lond.* **A234,** 387.

Brown G. E. and Mayers D. F. (1957) The coherent scattering of gamma-rays by *K* electrons in heavy atoms. IV. The scattering of 1.28 and $2.56\,mc^2$ gamma-rays in mercury. *Proc. Roy. Soc. Lond.* **A242,** 89.

Brummer O., Eisenschmidt Ch. and Hoche H. R. (1982) Generation and proof of elliptically polarized X-rays. *Z. Naturf.* **A37,** 524.

Brummer O., Eisenschmidt Ch. and Hoche H. R. (1984) Polarization phenomena of X-rays in the Bragg case. *Acta Cryst.* **A40,** 394.

Bui C. and Milazzo M. (1989) Measurements of anomalous dispersion in Rayleigh scattering of characteristic X-ray fluorescence. *N. Cimento* **D11,** 655.

Campbell J. L., Wang J.-X. and Teesdale W. J. (1989) Compton-scattering contribution to response function of Si(Li) X-ray detectors. *Nucl. Instrum. Meth.* **B43,** 490.

Carter L. L. and Cashwell E. D. (1975) Particle transport simulation with the Monte Carlo method. ERDA Critical Review Series, TID-26607.

Cashwell E. D. and Everett C. J. (1959) *A Practical Manual on the Monte Carlo Method.* Pergamon Press. London.

Cashwell E. D., Neergaard J. R., Taylor W. M. and Turner G. D. (1972) MCN: A Neutron Monte Carlo Code. Los Alamos National Laboratory Report LA-4751.

Cashwell E. D. Neergaard J. R., Everett C. J., Schrandt R. G., Taylor W. M. and Turner G. D. (1973) Monte Carlo Photon Codes: MCG and MCP. Los Alamos National Laboratory Report LA-5157-MS.

Cesareo R., Hanson A. L., Gigante G. E., Pedraza L. J. and Mahtaboally S. Q. G. (1992) Interaction of keV photons with matter and new applications. *Phys. Rep.* **213,** 117.

Chandrasekhar S. (1946a) On the radiative equilibrium of a stellar atmosphere. X. *Astrophys. J.* **103,** 351.

Chandrasekhar S. (1946b) On the radiative equilibrium of a stellar atmosphere. XI. *Astrophys. J.* **104,** 110.

Chandrasekhar S. (1947) On the radiative equilibrium of a stellar atmosphere. XV. *Astrophys. J.* **105,** 424.

Chandrasekhar S. (1948) The softening of radiation by multiple Compton scattering. *Proc. Roy. Soc.* **A192,** 508.

Chandrasekhar S. (1950) The equations of transfer. *Radiative Transfer*, Chap. 1. Clarendon Press. Oxford [(1960) Reprinted with corrections by Dover, New York]. Particularly Section 15 (The representation of polarized light).

Chomilier J., Loupias G. and Felsteiner J. (1985) Correction for multiple scattering in Compton profile experiments: Application for synchrotron source photons. *Nucl. Instrum. Meth.* **A235,** 603.

Christoffersson J.-O. and Mattson S. (1983) Polarized X-rays in XRF-analysis for improved *in vivo* detectability of cadmium in man. *Phys. Med. Biol.* **28,** 1135.

Cohen D. D. (1987) Average L shell fluorescence yields. *Nucl. Intrum. Meth.* **B22,** 55.

Cole H. (1963) Polarization of X-rays. In *The Encyclopedia of X-Rays and Gamma Rays*, p. 774. Reinhold, New York.

Compton A. H. (1923) A quantum theory of the scattering of X-rays by light elements. *Phys. Rev.* **21,** 483.

Compton A. H. and Allison S. K. (1935) *X-Rays in Theory and Experiment*, 2nd edn. Van Nostrand, New York.

Compton A. H. and Hagenow C. F. (1924) A measurement of the polarization of secondary X-rays. *J. Opt. Soc. Am. Rev. Sci. Instr.* **8,** 487.

Cooper M. J. (1985) Compton scattering and electron momentum determination. *Rep. Prog. Phys.* **48,** 415.

Creagh D. C. (1987) The resolution of discrepancies in tables of photon attenuation coefficients. *Nucl. Instrum. Meth.* **A255,** 1.

Cromer D. T. and Waber J. T. (1974) Atomic scattering factors for X-rays. In *International Tables for X-Ray Crystallography*, Vol. 4, p. 71. Kynoch Press, Birmingham.

Cullen D. E., Chen M. H., Hubbell J. H., Perkins S. T., Plechaty E. F., Rathkopf J. A. and Scofield J. H. (1989) Tables and graphs of photon-interaction cross-sections from 10 eV to 100 GeV derived from the LLNL evaluated photon data library (EPDL), Lawrence Livermore National Laboratory Report UCRL-50400, Vol. 6, Parts A and B, Rev. 4.

Davisson C. M. and Evans R. D. (1952) Gamma-ray absorption coefficients. *Rev. Mod. Phys.* **24,** 79.

Dumond J. W. M. (1930) Multiple scattering in the Compton effect. *Phys. Rev.* **36,** 1685.

Dwiggins C. W. (1983) General calculation of the polarization factor for multiple coherent scattering of unpolarized and plane-polarized X-rays. *Acta Cryst.* **A39,** 773.

Ebel H., Landler F. and Dirchmid H. (1971) Zur Anregung charakteristischer Röntgen-Strahlung durch Photoelektronen. *Z. Naturf.* **26a,** 927.

Evans K. D., Leigh B. and Lewis M. (1977) The absolute determination of the reflection integral of Bragg X-ray analyser crystals. Two-reflection methods. *X-Ray Spectrom.* **6,** 132.

Evans R. D. (1955) *The Atomic Nucleus.* McGraw-Hill, New York.

Evans R. D. (1958) Compton effect. In *Handbuch der Physik*, Vol. XXXIV, p. 218. Springer, Berlin.

Everett C. J. and Cashwell E. D. (1973) MCP Code Fluorescence-Routine Revision. Los Alamos National Laboratory Report LA-5240-MS.

Ewald H. and Franz W. (1976) Scattering of a polarized photon by a polarized electron. *Z. Naturf.* **A31,** 808.

Ewan G. T., Andersson G. I., Bartholomew G. A. and Litherland A. E. (1969) Gamma-ray polarization measurements with a single Ge(Li) detector. *Phys. Lett.* **B29,** 352.

Fagg L. W. and Hanna S. S. (1959) Polarization measurements on nuclear gamma-rays. *Rev. Mod. Phys.* **31,** 711.

Fano U. (1949a) Remarks on the classical and quantum-mechanical treatment of partial polarization. *J. Opt. Soc. Am.* **39,** 859.

Fano U. (1949b) Penetration and diffusion of X-rays through thick barriers. II. The asymptotic behavior when pair production is important. *Phys. Rev.* **76,** 739.

Fano U. and Cooper J. W. (1968) Spectral distribution of atomic oscillator strengths. *Rev. Mod. Phys.* **40,** 441.

Fano U., Spencer L. V. and Berger M. J. (1959) Penetration and diffusion of X-rays. In *Encyclopedia of Physics*, Vol. 38/2, p. 660. Springer, Berlin.

Felsteiner J. and Pattison P. (1975) Monte Carlo study of multiple scattering of photons in Compton profile measurements. *Nucl. Instrum. Meth.* **124,** 449.

Felsteiner J., Pattison P. and Cooper M. (1974) Effect of multiple scattering on experimental Compton profiles. *Phil. Mag.* **30,** 537.

Fernández J. E. (1989) XRF intensity in the frame of the transport theory. *X-Ray Spectrom.* **18,** 271.

Fernández J. E. (1991) Rayleigh and Compton double scattering of unpolarised X-rays. *Phys. Rev.* **A44,** 4232.

Fernández J. E. (1992) Rayleigh and Compton scattering contributions to the XRF intensity. *X-Ray Spectrom.* **21,** 57.

Fernández J. E. (1993a) Polarization effects in X-ray photon diffusion. *X-Ray Spectrom.* In press.

Fernández J. E. (1993b) SHAPELP: an upgrade of the code SHAPE for the computer simulation of energy dispersive X-ray spectra from linearly polarized sources. Unpublished.

Fernández J. E. (1993c) Polarization effects in the diffusion of X-ray photons from linearly and circularly polarized sources. Unpublished.

Fernández J. E. and Molinari V. G. (1990) Theoretical estimation of the fourth-order XRF intensity. In *Advances in X-Ray Analysis*, Vol. 33, p. 573. Plenum Press, New York.

Fernández J. E. and Molinari V. G. (1991) X-Ray Photon Spectroscopy Calculations. In *Advances in Nuclear Science and Technology*, Vol. 22, p. 45. Plenum Press, New York.

Fernández J. E. and Molinari V. G. (1992) Systematic computation of scattering corrections with the code SHAPE. In *Advances in X-Ray Analysis*, Vol. 35, p. 757. Plenum Press, New York.

Fernández J. E. and Molinari V. G. (1993) Diffusion of polarized photons in the frame of transport theory. *Nucl. Instrum. Meth.* **B73,** 341.

Fernández J. E. and Sumini M. (1991) SHAPE: a computer simulation of energy dispersive X-ray spectra. *X-Ray Spectrom.* **20,** 315.

Fernández J. E. and Sumini M. (1992) Adjoint calculations for multiple scattering of Compton and Rayleigh effects. *Nucl. Instrum. Meth.* **B71,** 111.

Fernández J. E. Molinari V. G. and Sumini M. (1989) Effect of the X-ray scattering anisotropy on the diffusion of photons in the frame of the transport theory. *Nucl. Instrum. Meth.* **A280,** 212.

Fernández J. E., Molinari V. G. and Sumini M. (1990) Corrections for the effect of scattering on XRF intensity. In *Advances in X-Ray Analysis*, Vol. 33, p. 553. Plenum Press, New York.

Fink R. W., Jopson R. C., Mark H. and Swift C. D. (1966) Atomic fluorescence yields. *Rev. Mod. Phys.* **38,** 513.

Flack H. D. and Vincent M. G. (1980) On the polarization factor for crystal-monochromated X-radiation. III. A weighting scheme for products. *Acta Cryst.* **A36,** 620.

Flügge S., Melhorn W. and Schmidt V. (1972) Angular distribution of Auger electorns following photoionization. *Phys. Rev. Lett.* **29,** 7.

Ford R. L. and Nelson W. R. (1978) The EGS Code System, SLAC Report No. 210.

Foster R. A. and Godfrey T. N. K. (1985) MCNP—A General Monte Carlo Code for Neutrons and Photon Transport. In *Monte Carlo Methods and Applications in Neutronics, Photonics and Statistical Physics. Lecture Notes in Physics*, Vol. 240, p. 33. Springer, Berlin.

Franz W. (1936) Rayleighsche Streuung harter Strahlung an schweren Atomen. *Z. Physik* **98,** 314.

Franz W. (1938) Die Streuung von Strahlung am magnetischen Elektron. *Ann. Physik* **33,** 47.

Frolov G. V. (1960) Polarization phenomena in the Compton effect. *Zh. Eksp. Teor. Fiz.* **39,** 1829 (1960); English translation in *Sov. Phys. JETP* **12,** 1277 (1961).

Fuschini E., Murty D. S. R. and Veronesi P. (1960) Polarization effects in the elastic scattering of photons. *N. Cimento* **15,** 847.

Garg M. L., Kumar S., Metha D., Verma H. R., Mangal P. C. and Trehan P. N. (1985) Measurement of photon-induced *L* X-ray fluorescence cross-sections for Ta, W, Au, Tl and Bi in the 15–60 keV energy range. *J. Phys.* **B18,** 4529.

Gibbs D., Blume M., Harshman D. R. and McWhan D. B. (1989) Polarization analysis of magnetic X-ray scattering. *Rev. Sci. Instrum.* **60,** 1655.

Haga H. (1907) Uber die Polarisation der Rontgenstrahlen und der Sekundarstrahlen. *Annln der Physik* **23,** 439.

Halbleib J. A. and Mehlhorn T. A. (1984) ITS: the Integrated TIGER Series of Coupled Electron/Photon Monte Carlo Transport Codes. Sandia National Laboratories Report SAND 84–0573.

Halonen V., Epstein I. R., Tanner A. C. and Williams B. G. (1977) Multiple scattering. In *Compton Scattering: The Investigation of Electron Momentum Distributions*, pp. 79. McGraw-Hill, London.

Hamilton M. C. and McIntyre J. A. (1967) Measurement of the polarization of the gamma rays inelastically scattered in lead. M.S. Thesis (Hamilton), Texas A&M University.

Hansen J. S., Freund H. U. and Fink R. W. (1970) Radiative X-ray transition probabilities to the *K*-shell. *Nucl. Phys.* **A142,** 604.

Hanson A. L. (1985) An analytical solution to the Rayleigh scattering cross section integral. *Nucl. Instrum. Meth.* **A234,** 552.

Hanson A. L. (1986a) The polarization of X-rays scattered into 90°. *Nucl. Instrum. Meth.* **A249,** 515.

Hanson A. L. (1986b) Further comments on the integrated incoherent scattering cross sections for polarized X-rays. *Nucl. Instrum. Meth.* **A249,** 522.

Hanson A. L. (1986c) The calculation of scattering cross sections for polarized X-rays. *Nucl. Instrum. Meth.* **A243,** 583.

Hanson A. L. (1988a) The calculation of coherent and incoherent scattering cross sections for polarized X-rays into an arbitrarily placed circular aperture. *Nucl. Instrum. Meth.* **A264,** 471.

Hanson A. L. (1988b) An easy and accurate approximation to the integrated Compton cross section for the scattering of polarized X-rays into an arbitrarily circular aperature. *Nucl. Instrum. Meth.* **A264,** 484.

Hanson A. L. (1990) Coherent and incoherent scattering cross sections for polarized X-rays integrated over a small distributed source. *Nucl. Instrum. Meth.* **A290,** 167.

Hanson A. L. and Gigante G. E. (1989) Evaluation of geometrical contributions to the spread of the Compton-scatter energy distribution. *Phys. Rev.* **A40,** 171.

Hanson A. L. and Meron M. (1988) Errors associated with the measurement of scattered polarized X-rays. *Nucl. Instrum. Meth.* **A264,** 488.

Hanson A. L., Gigante, G. E. and Meron, M. (1988) Contours of constant scattering angle. *Phys. Rev. Lett.* **61,** 135.

Hanson A. L., Jones K. W., Gordon B. M., Pounds J. G., Kwiatek W. M., Long G. J., Rivers M. L. and Sutton S. R. (1987) Trace elements measurements using white synchrotron radiation. *Nucl. Instrum. Meth.* **B24,** 400.

Hanson A. L., Kraner H. W., Jones K. W., Gordon B. M., Mills R. E. and Chen J. R. (1983) Trace elements measurements with synchrotron radiation. *IEEE Trans. Nucl. Sci.* **NS-30,** 1339.

Hart M. (1978) X-Ray polarization phenomena. *Phil. Mag.* **B38,** 41.

Hart M. (1991) Polarizing X-ray optics for synchrotron radiation. *SPIE* **1548,** 46.

Hart M. (1992) A novel astronomical X-ray polarimeter. *Nucl. Instrum. Meth.* **A316,** 416.

Hart M., Siddons D. P., Amemiya Y. and Stojanoff V. (1991) Tunable X-ray polarimeters for synchrotron radiation sources. *Rev. Sci. Instrum.* **62,** 2540.

He T., Gardner R. P. and Verghese K. (1990) An improved Si(Li) detector response function. *Nucl. Instrum. Meth.* **A299,** 354.

Heitler W. (1936) *The Quantum Theory of Radiation.* Clarendon, Oxford.

Honzatko J. and Kajfosz J. (1969) Linear polarization measurements by Ge(Li) detector. *Czech. J. Phys.* **B19,** 1281.

Hoover J. I., Faust W. R. and Dohne C. F. (1952) Polarization of scattered quanta. *Phys. Rev.* **85,** 58.

Huber H., Galster S. and Schopper H. (1963) The influence of multiple scattering on the measurement of the circular polarization of gamma-rays. *Nucl. Instrum. Meth.* **21,** 338.

Hubbell J. H. (1982) Photon mass attenuation and energy absorption coefficients from 1 keV to 20 MeV. *Int. J. Appl. Rad. Isot.* **33,** 1269.

Hubbell J. H. (1989) Bibliography and current status of *K, L,* and higher shell fluorescence yields for computation of photon energy-absorption coefficients, National Institute of Standards and Technology Report NISTIR 89–4144.

Hubbell J. H. (1992) Polarization Effects in Coherent and Incoherent Photon Scattering: Survey of Measurements and Theory Relevant to Radiation Transport Calculations. National Institute of Standards and Technology Report NISTIR 4881.

Hubbell J. H. and Øverbø I. (1979) Relativistic atomic form factors and photon coherent scattering cross-sections. *J. Phys. Chem. Ref. Data* **8,** 69.

Hubbell J. H., Gerstenberg H. M. and Saloman E. B. (1986) Bibliography of photon total cross-section (attenuation coefficient) measurements 10 eV to 13.5 GeV, National Bureau of Standards Report NBSIR 86-3461.

Hubbell J. H., Gimm H. A. and Øverbø I. (1980) Pair, triplet, and total atomic cross-sections (and mass attenuation coefficients for 1 MeV–100 GeV photons for elements $Z = 1$ to 100. *J. Phys. Chem. Ref. Data* **9,** 1023.

Hubbell J. H., McMaster W. H., Kerr del Grande N. and Mallett J. H. (1974) X-ray cross-sections and attenuation coefficients. In *International Tables for X-Ray Crystallography,* Vol. 4, p. 47. Kynoch Press, Birmingham.

Hubbell J. H., Veigele W. J., Briggs E. A., Brown R. T., Cromer D. T. and Howerton R. J. (1975) Atomic form factors, incoherent scattering functions, and photon scattering cross-sections. *J. Phys. Chem. Ref. Data* **4,** 471; (1977) Erratum, *J. Phys. Chem. Ref. Data* **6,** 615.

Iida A., Matsushita T. and Goshi Y. (1985) Energy dispersive XRF analysis with synchrotron radiation. *Nucl. Instrum. Meth.* **228,** 556.

Ishikawa T. (1989) X-ray monochromators for circularly polarized incident radiation. *Rev. Sci. Instrum.* **60,** 2058.

Jacklevic J. M., Giauque R. D. and Thompson A. C. (1985) Quantitative XRF analysis using monochromatic synchrotron radiation. *Nucl. Instrum. Meth.* **B10,** 303.

Janssens K., Vincze L., Van Espen P. and Adams F. (1993) Monte Carlo simulation of conventional and synchrotron energy-dispersive X-ray spectrometers. *X-Ray Spectrom.* In press.

Jauch J. M. and Rohrlich F. (1976) *The Theory of Photons and Electrons.* Springer, Berlin.

Jorch H. H. and Campbell J. L. (1977) On the analytic fitting of full energy peaks for Ge(Li) and Si(Li) photon detectors. *Nucl. Intrum. Meth.* **143,** 551.

Kahlon K. S., Aulakh H. S., Singh N., Mittal R., Allawadhi K. L. and Sood B. S. (1991) Measurement of angular distribution and polarization of photon-induced fluorescent X-rays in thorium and uranium. *Phys. Rev.* **A43,** 1455.

Kalos M. H. and Whitlock P. A. (1986) *Monte Carlo Methods. Volume I: Basics.* John Wiley, New York.

Kane P. P., Kissel L., Pratt R. H. and Roy S. C. (1986) Elastic scattering of γ-rays and X-rays by atoms. *Phys. Rep.* **140,** 75.

Keith H. D. and Loomis T. C. (1978) Correction for scattering in X-ray fluorescence experiments. *X-Ray Spectrom.* **7,** 225.

Kel'ner S. R. (1969) Dependence of the azimuthal asymmetry of pair production plane on the photon polarization. *Yad. Fiz.* **10,** 605; English translation in *Sov. J. Nucl. Phys.* **10,** 349 (1970).

Kel'ner S. R. Kotov Yu. D. and Logunov V. M. (1975) Methods of measuring linear polarization of gamma quanta. *Yad. Fiz.* **21,** 604; English translation in *Sov. J. Nucl. Phys.* **21,** 313 (1975).

Khan Md. R. and Karimi M. (1980) $K\beta/K\alpha$ ratios in energy dispersive X-ray emission analysis. *X-Ray Spectrom.* **9,** 32.

Kis-Varga M. and Vegh J. (1993) Influence of in-sample scattering of fluorescent radiation on line shapes of Si(Li) detectors in XRF studies. *X-Ray Spectrom.* In press.

Kissel L. and Pratt R. H. (1987) Status of cross-section data for photon scattering of atoms. *Trans. Am. Nucl. Soc.* **55,** 199.

Klein O. and Nishina Y. (1929) Über die streuung von strahlung durch freie elektronen nach der neuen relativistischen quantendynamik von Dirac. *Z. Phys.* **52,** 853.

Knöchel A., Petersen W. and Tolkiehn G. (1985) XRF Spectrometry with synchrotron radiation. *Analyt. Chim. Acta* **173,** 105.

Koch E. E. (Ed.) (1983) *Handbook on Synchrotron Radiation.* Vol. 1a. North-Holland, Amsterdam.

Koide T., Shidara T., Yuri M., Kandaka N., Yamaguchi K. and Fukutani H. (1991) Elliptical-polarization analyses of synchrotron radiation in the 5–80-eV Region with a reflection polarimeter. *Nucl. Instrum. Meth.* **A308,** 635.

Krause M. O. (1979) Atomic radiative and radiationless yields for *K* and *L* shells. *J. Phys. Chem. Data* **8,** 307.

Krause M. O. and Oliver J. H. (1979) Natural widths of atomic *K* and *L* levels, $K\alpha$ X-ray lines and several *KLL* Auger lines. *J. Phys. Chem. Ref. Data* **8,** 329.

Langenberg A. and Van Eck J. (1979) An evaluation of *K*-shell fluorescence yields; observation of outer-shell effects. *J. Phys.* **B12,** 1331.

Lawrence J. L. (1982) The reflectivity of a pyrolytic graphite monochromator. *Acta Cryst.* **A38,** 859.

Lawrence J. L. (1983) Polarization ratios for repeatedly reflected X-ray beams. *Acta Cryst.* **A39,** 753.

Le Page Y., Gabe E. J. and Calvert L. D. (1979) X-ray beam polarization measurements. *J. Appl. Cryst.* **12,** 25.

Leubner C. and Metzler H. P. (1984) Frequency distribution and total-cross section of synchro-Compton radiation in a linearly polarized plane vacuum wave of arbitrary intensity. *Astron. Astrophys.* **131,** 329.

Lipps F. W. and Tolhoek H. A. (1954a) Polarization phenomena of electrons and photons. I. General method and applications to Compton scattering. *Physica* **20,** 85.

Lipps F. W. and Tolhoek H. A. (1954b) Polarization phenomena of electrons and photons. II. Results for Compton scattering. *Physica* **20,** 395.

Litherland A. E., Ewan G. T. and Lam S. T. (1970) Use of single planar Ge(Li) detectors as gamma-ray polarimeters. *Can. J. Phys.* **48,** 2320.

Logan B. A. (1971) Detection of the plane of polarization of 121 keV linearly polarized photons. *Can J. Phys.* **49,** 2612.

Mack J. M., Morel J. E. and Hughes H. G. (1985) Monte Carlo electron/photon transport. In *Monte Carlo Methods and Applications in Neutronics, Photonics and Statistical Physics. Lecture Notes in Physics*, Vol. 240, p. 272. Springer, Berlin.

Manninen S. O., Cooper M. J. and Cardwell D. A. (1986) Gamma ray source line broadening and Compton line profile analysis. *Nucl. Instrum. Meth.* **A245,** 485.

Manuzio G. and Vitale S. (1961) Elastic scattering of 1.25 MeV gamma rays by lead. *N. Cimento* **20,** 638.

Materlik G. and Suortti P. (1984) Measurement of the polarization of X-rays from a synchrotron source. *J. Appl. Cryst.* **17,** 7.

Maximon L. C. (1989) Scattering of polarized photons by protons. *Phys. Rev.* **C39,** 347.

Maximon L. C. and Olsen H. (1962) Measurement of linear photon polarization by pair production. *Phys. Rev.* **126,** 310.

May M. and Wick G. C. (1951) On the production of polarized high energy X-rays. *Phys. Rev.* **81,** 628.

McMaster W. H. (1954) Polarization and the Stokes parameters. *Am. J. Phys.* **22,** 351.

McMaster W. H. (1960). Polarization phenomena for positron annihilation-in-flight. *N. Cimento* **17,** 395.

McMaster W. H. (1961) Matrix representation of polarization. *Rev. Mod. Phys.* **33,** 8.

McMaster W. H., Kerr del Grande N., Mallett J. H. and Hubbell J. H. (1969) Compilation of X-ray cross-sections, Lawrence Livermore National Laboratory Report UCRL-50174, Section 2, Rev. 1.

McNelles L. A. and Campbell J. L. (1975) Analytic approximations to peak shapes produced by Ge(Li) and Si(Li) spectrometers. *Nucl. Instrum. Meth.* **127,** 73.

Méray L. (1988) Simulation of X-ray and gamma-ray scatterings in light matrices. *J. Radionalyt. Nucl. Chem. Lett.* **126,** 323.

Méray L. and Házi E. (1988) Effect of scattered photons on the intensity of X-ray characteristic lines. *Acta Phys. Hung.* **63,** 171.

Metropolis N. (1985) Monte Carlo: In the beginning and some great expectations. In *Monte Carlo Methods and Applications in Neutronics, Photonics and Statistical Physics. Lecture Notes in Physics*, Vol. 240, p. 62. Springer, Berlin.

Metzger F. and Deutsch M. (1950) A study of the polarization-direction correlation of successive gamma-Ray quanta. *Phys. Rev.* **78,** 551.

Miller S. C. and Wilcox R. M. (1961) Left–right asymmetry in Compton scattering by transversely polarized electrons. *Phys. Rev.* **124,** 637.

Milton K. A., Tsai W.-y. and DeRaad L. L. (1972) Compton scattering. I. Spectral forms for the invariant amplitudes to order e4, *Phys. Rev.* **D6,** 1411.

Molak B., Ilakovac K, and Ljubicic A. (1971) *Z* Dependence of linear polarization in elastic scattering. *Fizika* **3,** 239.

Namito Y., Ban S. and Hirayama H. (1993) Implementation of linearly-polarized photon scattering into the EGS4 code. *Nucl. Instrum. Methods.* In press.

Nelson W. R. and Namito Y. (1990) The EGS4 Code System: Solution of Gamma-Ray and Electron Transport Problems, SLAC Publication 5193; presented at the International Conference on Supercomputing in Nuclear Applications, Mito City, Japan, 12–16 March.

Nelson W. R., Hirayama H. and Rogers D. W. O. (1985) The EGS4 Code System, Report SLAC-265.

Nishina Y. (1929) Die Polarisation der Comptonstrueuung nach der Diracschen Theorie des Elektrons. *Z. Phys.* **52,** 869.

Ohkawa T. and Hashimoto H. (1984) On the polarization mixing of X-rays: quantum theory of interference of white X-rays. *Phys. Stat. Sol.* **A85,** 335.

Olekhnovich N. M. (1969) The polarization factor in X-ray scattering, taking into account monochromator extinction. *Kristallograpy* **14,** 261; English translation. in *Sov. Phys.-Crystallogr.* **14,** 203 (1969).

Olsen H. (1968) Polarization effects in scattering and radiation processes. In *Applications of Quantum Electrodynamics, Springer Tracts in Modern Physics*, Vol. 44, Chap. 4, p. 106. Springer, Berlin.

Olsen H. and Maximon L. C. (1958) Electron and photon polarization in Bremsstrahlung and pair production. *Phys. Rev.* **110,** 589.

Olsen H. and Maximon L. C. (1959) Photon and electron polarization in high-energy Bremsstrahlung and pair production with screening. *Phys. Rev.* **114,** 887.

O'Rourke R. C. (1952) Multiple Compton scattering of low energy gamma radiation. *Phys. Rev.* **85,** 881.

O'Rourke R. C. (1953) Multiple Compton scattering of low energy gamma radiation. *Phys. Rev.* **89,** 999.

Pitkanen T., Laundy D., Holt R. S. and Cooper M. J. (1986) The multiple scattering profile in gamma ray Compton studies. *Nucl. Instrum. Meth.* **A251,** 536.

Pomraning G. C. (1973) *The Equations of Radiation Hydrodynamics.* Pergamon Press, Oxford.

Press W. H., Flannery B. P., Teukolsky S. A. and Vetterling W. T. (1989) *Numerical Recipes in Pascal. The Art of Scientific Computing.* Cambridge University Press, Cambridge.

Prins M., Dries W., Lenglet W., Davies S. T. and Bowen K. (1985) Trace element analysis with synchrotron radiation at SRS Daresbury. *Nucl. Instrum. Meth.* **B10,** 299.

Ribberfors R. and Berggren K. F. (1982) Incoherent-X-ray-scattering functions and cross-sections $(d\sigma/d\Omega')_{incoh}$ by means of a pocket calculator. *Phys. Rev.* **A26,** 3325; (1984) Erratum, *Phys. Rev.* **A29,** 3451.

Ribberfors R. and Matscheko G. (1992) Measurements of high energy photon spectra of synchrotron radiation from a storage ring. *Nucl. Instrum. Meth.* **A314,** 605.

Rodgers E. (1936) Polarization of hard X-rays. *Phys. Rev.* **50,** 875.

Roentgen W. C. (1895) Ueber eine neue Art von Strahlen. *Sitzungber. der Wurzburger Physik.-Medic. Gesellsch.*, Jahrg.; reprinted in *Annln Phys. Chem* **64,** 1 (1898); English translation (by A. Stanton) On a new kind of rays. *Nature* **53,** 274 (1896); reprinted in *Science* 3, 227.

Rogers D. W. O. and Bielajew A. F. (1990) Monte Carlo techniques of electron and photon transport for radiation dosimetry. In *The Dosimetry of Ionizing Radiation*, Vol. 3, Chap. 5, p. 488. Academic Press, New York.

Rollason A. J., Felsteiner J., Bauer G. E. W. and Schneider J. R. (1987) Self-scattering in gamma ray sources used in Compton scattering experiments. *Nucl. Instrum. Meth.* **A256,** 532.

Roy S. C., Sarkar B., Kissel L. D. and Pratt R. W. (1986) Polarization effects in elastic photon–atom scattering. *Phys. Rev.* **A34,** 1178.

Sakai N., Shiotani N., Ito M., Itoh F., Kawata H., Amemiya Y., Ando M., Yamamoto S. and Kitamura H. (1989) Challenge to precise magnetic Compton-profile measurements. *Rev. Sci. Instrum.* **60,** 1666.

Salem S. I., Boehm F. and Lee P. L. (1977) Instrumental line width of a bent crystal spectrometer and measurement of the Kβ X-ray width. *Nucl. Instrum. Meth.* **140,** 511.

Salem S. I., Panossian S. L. and Krause R. A. (1974) Experimental *K* and *L* relative X-ray emission rates. *Atom. Data Nucl. Data Tables* **14,** 91.

Saloman E. B. and Hubbell J. H. (1987) Critical analysis of soft X-ray cross sections data. *Nucl. Instrum. Meth.* **A255,** 38.

Saloman E. B., Hubbell J. H. and Scofield J. H. (1988) X-ray attenuation cross-sections for energies 100 eV to 100 keV and elements $Z = 1$ to $Z = 92$. *Atom. Data Nucl. Data Tables* **38,** 1.

Sartori R. and Fernández J. E. (1992) Monte Carlo simulation of multiple scattering effects in energy dispersive X-ray spectrometry. *X-Ray Spectrom.* **21,** 299.

Schaupp D., Schumacher M., Smend F., Rullhusen P. and Hubbell J. H. (1983) Small-angle Rayleigh scattering of photons at high energies: Tabulation of relativistic HFS modified atomic form factors. *J. Phys. Chem. Ref. Data* **12,** 467.

Schopper H. (1958) Measurement of circular polarization of gamma-rays. *Nucl. Instrum. Meth.* **3,** 158.

Schülke W. (1989) Inelastic X-ray scattering. *Nucl. Instrum. Meth.* **A280,** 338.

Schutz G., Frahm R., Wienke R., Wilhelm W., Wagner W. and Kienle P. (1989) Spin-dependent *K*- and *L*-absorption measurements. *Rev. Sci. Instrum.* **60,** 1661.

Scofield J. H. (1969) Radiative decay rates of vacancies in the *K* and *L* shells. *Phys. Rev.* **179,** 9.

Scofield J. H. (1973) Theoretical photoionization cross-sections from 1 to 1500 keV, Lawrence Livermore National Laboratory Report UCRL-51326.

Scofield J. H. (1974) Exchange corrections of *K* X-ray emission rates. *Phys. Rev.* **A9,** 1041.

Scofield J. H. (1975) Radiative transitions. In *Atomic Inner Shell Processes*, Vol. I, p. 265. Academic Press, New York.

Scofield J. H. (1987) Status of atomic photoeffect cross-section data. *Trans. Am. Nucl. Soc.* **55,** 200.

Scofield J. H. (1990) Angular distribution of photoelectrons from polarized X-rays. *Phys. Scr.* **41,** 59.

Seltzer S. M. (1988a) An overview of ETRAN Monte Carlo methods. In *Monte Carlo Transport of Electrons and Photons*, Chap. 7, p. 153. Plenum Press, New York.

Seltzer S. M. (1988b) Applications of ETRAN Monte Carlo codes. In *Monte Carlo Transport of Electrons and Photons*, Chap. 9, p. 221. Plenum Press, New York.

Seltzer S. M. (1991) Electron–photon Monte Carlo calculations: The ETRAN code. *Appl. Radiat. Isot.* **42,** 917.

Sherman J. (1955) The theoretical derivation of fluorescent X-ray intensities from mixtures. *Spectrochim. Acta* **7,** 283.

Sherman J. (1959) Simplification of a formula in the correlation of fluorescent X-ray intensities from mixtures. *Spectrochim. Acta* **11,** 466.

Shiraiwa T. and Fujino N. (1966) Theoretical calculation of fluorescent X-ray intensities in fluorescent X-ray spectrochemical analysis. *Jap. J. Appl. Phys.* **5,** 886.

Siddons D. P., Hastings J. B., Faigel G., Berman L. E., Haustein P. E. and Grover J. R. (1989) Direct observation of polarization mixing in nuclear Bragg X-ray scattering of synchrotron radiation. *Phys. Rev. Lett.* **62,** 1384.

Simon T. and Daniel H. (1977) Measurement of the spin dependence of Rayleigh scattering. *Phys. Rev.* **A15,** 1015.

Singh M., Anand S. and Sood B. S. (1964) Influence of incoherent scattering on the polarization of elastic scattering of gamma-rays. *Curr. Sci.* **33,** 239.

Singh M., Anand S. and Sood B. S. (1965) Azimuthal variation of Compton scattering of polarized gamma rays. *Nucl. Phys.* **62,** 267.

Singh N., Mittal R., Allawadhi K. L. and Sood B. S. (1987) Measurement of $L_{l+\alpha}$, L_β and L_γ X-ray production cross-sections in some rare-earth elements by 10, 18, 26 and 33 keV photons. *J. Phys.* **B20,** 5639.

Singh S., Metha D., Kumar S., Garg M. L., Singh N., Mangal P. C. and Trehan P. N. (1989) Contribution due to excitation by scattered photons in measurements of *L* X-ray cross-sections. *X-Ray Spectrom.* **18,** 193.

Smith V. H. Jr, Thakkar A. J. and Chapman D. C. (1975) A new analytical approximation to atomic incoherent X-ray scattering intensities. *Acta Cryst.* **A31,** 391.

Somayajulu D. R. S. and Lakshminarayana V. (1968) Rayleigh scattering of polarized photons. *J. Phys.* **A1,** 228.

Somayajulu D. R. S., Rama Rao J. and Lakshminarayana V. (1968) Polarization of elastically scattered gamma rays. *N. Cimento* **54,** 281.

Sood B. S. (1958) Polarization of 0.411, 0.662 and 1.25 MeV gamma-rays elastically scattered by lead. *Proc. Roy. Soc. Lond.* **A247,** 375.

Sparks C. J., Raman S., Ricci E., Gentry R. V. and Krause M. O. (1978) Evidence against superheavy elements in Giant-Halo inculsions re-examined with synchrotron radiation. *Phys. Rev. Lett.* **40,** 507.

Sparks C. J., Raman S., Yakel H. L., Gentry R. V. and Krause M. O. (1977) Search with synchrotron radiation the superheavy elements in Giant-Halo inclusions. *Phys. Rev. Lett.* **38,** 205.

Spencer L. V. (1948) Polarization of Multiply Scattered Gamma Rays. Interim Report on NBS Contract with the U.S. Office of Naval Research (Diffusion of Radiation) (unpublished).

Spencer L. V. and Wolff C. (1953) Penetration and diffusion of hard X-rays: Polarization effects. *Phys. Rev.* **90,** 510.

Standing K. G. and Jovanovich J. V. (1962) The elastic scattering of Co-60 gamma Rays. *Can. J. Phys.* **40,** 622.

Starace A. F. (1982) Theory of atomic photoionization. In *Handbuch der Physik*, Vol. XXXI, p. 1. Springer, Berlin.

Stoev K. N. (1992) Theoretical calculation of secondary X-ray fluorescence due to Compton electrons. *J. Phys.* **D25,** 131.

Stokes G. G. (1852) On the composition and resolution of streams of polarized light from different sources. *Trans. Cambridge Phil. Soc.* **9,** 399.

Storm E. and Israel H. I. (1970) Photon cross-sections from 1 keV to 100 keV for elements $Z = 1$ to $Z = 100$. *Nucl. Data Tables* **A7,** 565.

Stroscio M. A. (1984) Generalization of the Klein–Nishina scattering amplitude for an electromagnetic field of general polarization. *Phys. Rev.* **A29,** 1691.

Tanner A. C. and Epstein I. R. (1976a) Multiple scattering in the Compton effect. I. Analytic treatment of angular distributions and total scattering probabilities. *Phys. Rev.* **A13,** 335.

Tanner A. C. and Epstein I. R. (1976b) Multiple scattering in the Compton effect. II. Analytic and numerical treatment of energy profiles. *Phys. Rev.* **A14,** 313.

Tanner A. C. and Epstein I. R. (1976c) Multiple scattering in the Compton effect. III. Monte Carlo calculations. *Phys. Rev.* **A14,** 328.

Tartari A, Fernández J. E., Casnati E., Baraldi C. and Felsteiner J. (1993) EDXRS modelling for *in vivo* trace element analysis by using the SHAPE code. *X-Ray Spectrom.* In press.

Tolhoek H. A. (1956) Electron polarization, theory and experiment. *Rev. Mod. Phys.* **28,** 277.

Trubey D. K., Berger M. J. and Hubbell J. H. (1989) Photon cross sections for ENDF/B-VI. In *Advances in Nuclear Computation and Radiation Shielding*. 9–13 April, Santa Fe (NM).

Tsai W.-y., DeRaad L. L. and Milton K. A. (1972) Compton scattering. II. Differential cross sections and left–right asymmetry. *Phys. Rev.* **D6,** 1428.

Tseng H. K. and Pratt R. H. (1973) Polarization correlations in atomic-field Bremsstrahlung. *Phys. Rev.* **A7,** 1502.

Tseng H. K. and Pratt R. H. (1974) Polarization correlations in atomic-field pair production. *Phys. Rev.* **A9,** 752.

Van de Hulst H. C. (1957) Polarized light and symmetry relations. *Light Scattering by Small Particles*, Chap. 5 Wiley, New York [(1981) Reprinted with corrections by Dover, New York].

Van Espen P., Nullens H. and Adams F. (1980) An in-depth study of energy dispersive X-ray spectra. *X-Ray Spectrom.* **9,** 126.

Veigele W. J. (1973) Photon cross-sections from 0.1 keV to 1 MeV for elements $Z = 1$ to $Z = 94$. *Atomic Data* **5,** 51.

Veigele W. J., Tracy P. T. and Henry E. M. (1966) Compton effect and electron binding. *Am. J. Phys.* **34,** 1116.

Vincent M. G. (1982) The polarization factor for a repeatedly reflected X-ray beam: special cases. *Acta Cryst.* **A38,** 510.

Vincent M. G. and Flack H. D. (1980a) On the polarization factor for crystal-monochromated X-radiation. I. Assessment of errors. *Acta Cryst.* **A36,** 610.

Vincent M. G. and Flack H. D. (1980b) On the polarization factor for crystal-monochromated X-radiation. II. A method for determining the polarization ratio for crystal monochromators. *Acta Cryst.* **A36,** 614.

Vincze L., Janssens K. and Adams F. (1993) A general Monte Carlo simulation of ED-XRF spectrometers. Part I: Unpolarized radiation, homogeneous samples. *Spectrochim. Acta* **B**. In press.

Wick G. C. (1951) Detection of gamma-ray polarization by pair production. *Phys. Rev.* **81,** 467.

Wielopolski L., Rosen J. F., Slatkin D. N., Zhang R., Kalef-Ezra J. A., Rothman J. C., Maryansky M. and Jenks S. T. (1989) *In vivo* measurement of cortical bone lead using polarized X rays. *Med. Phys.* **16,** 521.

Wightman A. (1948) Note on polarization effects in Compton scattering. *Phys. Rev.* **74,** 1813.

Williams B. G. (Ed.) (1977) *Compton Scattering: The Investigation of Electron Momentum Distributions*. McGraw-Hill, London.

Williams B. G., Pattison P. and Cooper M. J. (1974) The spectral distribution of multiple Compton scattering of X-rays. *Phil. Mag.* **30,** 307.

Williams R. A. and McNeill K. G. (1965) Polarization of elastically scattered 1.33-MeV photons. *Can. J. Phys.* **43,** 1078.

Wobrauschek P. and Aiginger H. (1983) X-Ray fluorescence analysis with a linear polarized beam after Bragg reflection from a flat or a curved single crystal. *X-Ray Spectrom.* **12,** 72.

Xu Z.-x. (1984) Polarized-photon structure function and asymmetry in photon photoproduction process. *Phys. Rev.* **D30,** 1440.

NOMENCLATURE

A	Atomic weight.
β	Ellipticity angle.
C	As a subindex denotes Compton scattering.
χ	Angle defining the orientation of the major axis of the ellipse on the polarization plane.
$\delta(x-a)$	Dirac δ-function.
δ_{n0}	Kronecker δ-function.
E	Energy of photons.
$\hat{\epsilon}_{\perp,\parallel}$	Perpendicular and parallel vectors (in the polarization plane) with respect to the scattering plane.
$\mathscr{E}$	Electric field vector.
$F(\lambda', \omega \cdot \omega', Z)$	Coherent atomic form factor for an atom with atomic number Z.
Γ_{λ_i}	Line emission probability of the line at λ_i into its own spectral series.
$f(\mathbf{r}, \omega, \lambda)$	Angular flux.
$f^{(n)}(z, \omega, \lambda)$	Angular flux of nth order, i.e. the angular flux due to n interactions in the medium.
h	Plank constant.
$\mathbb{H}(\omega, \lambda, \omega, \lambda')$	Matrix kernel rotated in the laboratory system.
η	$(=\cos\vartheta)$ Director cosine ω_z.
$\mathbf{I}^{(n)(S)}_{(a_1,\ldots,a_n)}$	nth order Stokes intensity vector, for a chain of n events $(a_1, \ldots, a_n)$.
$\mathbf{I}^{(n)(S)}_{(a_1,\ldots,a_n)i}$	Component i of the nth order Stokes intensity vector, for a chain of n events $(a_1, \ldots, a_n)$.
I_I, I_Q, I_U, I_V	Intensity components of the Stokes intensity vector.
$I_\perp, I_\parallel, I_U, I_V$	Intensity components of the intensity vector (set L).
I_0	Constant intensity of the source.
$\mathbf{I}^{(n)}(\omega, \lambda)$	Angular intensity of nth order.
$\mathscr{I}^{(n)}(\omega)$	Wavelength-integrated angular intensity of nth order.
$\mathbf{I}^{(S)(1)}_{(a)I}(\omega, \lambda)$	First-order intensity due to the interaction a.
$\mathbf{I}^{(S)(2)}_{(a,\ell)I}(\omega, \lambda)$	Second-order intensity (corresponding to the chain of interactions a and ℓ, in this order).
$\mathbf{I}^{(S)(2)}_{(a,\ell)I}(\omega, \lambda)\vert_{ij}$	Second-order intensity of the photons produced as a consequence of one interaction a on the atom Z_i followed of one interaction ℓ on the atom Z_j.
J_{λ_i}	Absorption-edge jump.
Ψ, Ψ'	Rotation angles.
$\hat{k}$	Propagation direction of the photons.
$\mathbb{k}_a(\omega, \lambda, \omega', \lambda')$	Interaction kernal describing the probability density (per unit path, per unit solid angle, per unit wavelength) that the process a can change the phase-space variables ω', λ' to ω, λ.
$\mathbb{k}_a(\omega, \lambda, \omega', \lambda')\vert_j$	"Mass" kernel for the interaction a with the specie of atoms Z_j.
$K_{KN}(\lambda, \lambda')$	Klein–Nishina factor.
$\mathbb{L}^{(S)}$	Rotation matrix in the Stokes (or L) system.
λ	Wavelength of the emitted photons.
λ_0	Wavelength of the monochromatic source beam.
λ_i	Wavelength of the characteristic line i.
λ_c	Compton wavelength.
μ	Total attenuation coefficient obtained by adding the attenuation coefficients for the dominating processes in the low energy γ-ray regime [see equation (3)].
μ_0	$(=\mu(\lambda_0))$.
μ_i	$(=\mu(\lambda_i))$.
$(\mu/\rho)_j$	Total mass attenuation coefficient for the single element j.
N	Avogadro's number.
ν	Frequency.
ω	Flight direction of the photons.
P	As a subindex denotes photoelectric effect.
P_a	Degree of polarization for the interaction a.
$Q_{\lambda_i}(\lambda)$	Radiative photoelectric attenuation coefficient for the emission of the line at λ_i.

Θ	Scattering angle.	σ	Scattering cofficient.
R	As a subindex denotes Rayleigh scattering.	sgn z	Sign function.
		$\mathscr{U}(x-a)$	Heavyside (unitary step) function.
r_0	Classical radius of the electron.	φ	Azimuthal angle.
$\mathscr{S}(\mathbf{r}, \omega, \lambda)$	Source term.	W_j	Weight fraction of element j in the sample.
$S(\lambda', \omega \cdot \omega', Z)$	Incoherent scattering function for an atom with atomic number Z.	Z	Atomic number.